IDEA

Innovations Deserving Exploratory Analysis Programs

NCHRP IDEA Program

Development of Small Specimen Geometry for Asphalt Mixture Performance Testing

Final Report for
NCHRP IDEA Project 181

Prepared by:
Cassie Castorena
Y. Richard Kim
Sonja Pape
Kangjin Lee
North Carolina State University

September 2017

TRB TRANSPORTATION RESEARCH BOARD
The National Academies of
SCIENCES · ENGINEERING · MEDICINE

Innovations Deserving Exploratory Analysis (IDEA) Programs Managed by the Transportation Research Board

This IDEA project was funded by the NCHRP IDEA Program.

The TRB currently manages the following three IDEA programs:

- The NCHRP IDEA Program, which focuses on advances in the design, construction, and maintenance of highway systems, is funded by American Association of State Highway and Transportation Officials (AASHTO) as part of the National Cooperative Highway Research Program (NCHRP).
- The Safety IDEA Program currently focuses on innovative approaches for improving railroad safety or performance. The program is currently funded by the Federal Railroad Administration (FRA). The program was previously jointly funded by the Federal Motor Carrier Safety Administration (FMCSA) and the FRA.
- The Transit IDEA Program, which supports development and testing of innovative concepts and methods for advancing transit practice, is funded by the Federal Transit Administration (FTA) as part of the Transit Cooperative Research Program (TCRP).

Management of the three IDEA programs is coordinated to promote the development and testing of innovative concepts, methods, and technologies.

For information on the IDEA programs, check the IDEA website (www.trb.org/idea). For questions, contact the IDEA programs office by telephone at (202) 334-3310.

IDEA Programs
Transportation Research Board
500 Fifth Street, NW
Washington, DC 20001

NCHRP IDEA PROGRAM COMMITTEE

CHAIR
DUANE BRAUTIGAM
Consultant

MEMBERS
ANNE ELLIS
Arizona DOT
ALLISON HARDT
Maryland State Highway Administration
JOE HORTON
California DOT
MAGDY MIKHAIL
Texas DOT
TOMMY NANTUNG
Indiana DOT
MARTIN PIETRUCHA
Pennsylvania State University
VALERIE SHUMAN
Shuman Consulting Group LLC
L.DAVID SUITS
North American Geosynthetics Society

FHWA LIAISON
DAVID KUEHN
Federal Highway Administration

AASHTO LIAISON
KEITH PLATTE
American Association of State Highway Transportation Officials

TRB LIAISON
RICHARD CUNARD
Transportation Research Board

COOPERATIVE RESEARCH PROGRAM STAFF
STEPHEN PARKER
Senior Program Officer

IDEA PROGRAMS STAFF
CHRISTOPHER HEDGES
Director, Cooperative Research Programs
Lori Sundstrom
Deputy Director, Cooperative Research Programs
INAM JAWED
Senior Program Officer
DEMISHA WILLIAMS
Senior Program Assistant

EXPERT REVIEW PANEL

MAGDY MIKHAIL, *Texas DOT*
DAVID MENSCHING, *FHWA*
BEN BOWERS, *Virginia Transportation Research Council*
STACY DIEFENDERFER, *Virginia Transportation Research Council*
JO DANIEL, *University of New Hampshire*

Development of Small Specimen Geometry for Asphalt Mixture Performance Testing

IDEA Program Final Report

NCHRP IDEA Project N-181

Prepared for the IDEA Program
Transportation Research Board
The National Academies

Cassie Castorena

North Carolina State University

September 25, 2017

EXECUTIVE SUMMARY

The use of small specimen geometries in Asphalt Mixture Performance Tester (AMPT) testing has been gaining attention in recent years to enable the testing of as-built pavement layers. In addition, small specimens offer a means to improve the efficiency of laboratory specimen fabrication, by allowing the extraction of multiple test specimens per gyratory-compacted sample. The objectives of this project were to develop equipment to enable small specimen testing in the AMPT, evaluate the effects of specimen geometry on dynamic modulus and direct tension fatigue tests and pavement performance prediction, and optimize the laboratory fabrication of small specimens extracted from gyratory-compacted specimens. Rigorous assessment of specimen geometry effects and optimization of specimen fabrication are required prior to standardizing the use of small specimen geometries. The development of commercially available equipment is also necessary to enable widespread adoption of the small specimen geometries. In this project, two small specimen geometries were evaluated for dynamic modulus and direct tension fatigue testing: 38-mm diameter by 110-mm tall cylindrical specimens and 25-mm by 50-mm by 110-mm prismatic specimens.

The two small specimen geometries were compared against the standard 100-mm diameter cylindrical specimens using five mixtures with nominal maximum aggregate size (NMAS) values ranging from 9.5-mm to 25.0-mm. With the exception of a 9.5-mm mixture, the dynamic modulus and phase angle mastercurves at low and intermediate temperatures acquired from the large and small specimen geometries are statistically equivalent for all of the mixtures evaluated. At high temperature, the small specimen dynamic modulus values are higher and the phase angle values are lower than those of the large specimens. Therefore it is recommended to limit small specimen testing to the temperatures outlined in AASHTO PP 61. The specimen-to-specimen variability for the large and small specimen dynamic modulus tests are comparable. The cyclic fatigue test results of the small and large specimens are very similar for the mixtures evaluated. Monotonic fatigue tension testing was attempted. The monotonic tests results are repeatable but differ from the cyclic testing results. Therefore, it is recommended that only cyclic testing be used for fatigue characterization. Pavement performance was predicted by the Pavement ME program and the FlexPAVE™ program using the small and large specimen test results. The pavement performance prediction results suggest that specimen geometry does not significantly affect pavement fatigue damage predictions, which indicates promise for the use of small specimen geometries in practice.

To optimize the laboratory fabrication of small specimens from gyratory-compacted samples, the effect of coring direction was analyzed. Laboratory small specimen testing focuses solely on the cylindrical samples because it is more difficult to extract the prismatic specimens from gyratory samples. Small cylindrical specimens were cored both horizontally and vertically from gyratory-compacted specimens that were fabricated using plant-produced loose mixtures. These specimens were subjected to dynamic modulus and cyclic fatigue testing. Coring small specimens vertically (i.e., parallel to the compaction direction) would follow the current practice for laboratory fabricated large specimen testing. However, pavements experience tension perpendicular to the direction of compaction and hence, the horizontal extraction of small specimens best mimics field conditions. All of horizontally extracted small specimens subjected to fatigue testing exhibited failure at the specimen ends, outside the range of the displacement transducers. The horizontal extraction of small specimens from gyratory-compacted samples infringes on the peripheral region of the gyratory sample that has relatively high air void content. The air void gradient leads to end failure in fatigue testing, which prevents failure detection. In addition, the dynamic modulus and the fatigue test results obtained from vertically and horizontally cored small specimens indicate that the effects of anisotropy on the performance test results are minimal.

To minimize the difference between fatigue and dynamic modulus test procedures, a single coring pattern is preferred. Therefore, vertical coring is recommended for obtaining small specimens from gyratory-compacted samples for both fatigue and dynamic modulus testing.

Large specimens are extracted from the inner 100-mm diameter of gyratory-compacted samples. Therefore, it is proposed that small specimens also be extracted from the inner 100-mm diameter of gyratory-compacted samples where the air void content is relatively uniform. Four small specimens can be cored vertically from the inner 100 mm of gyratory-compacted samples, which is hence, the proposed procedure for the laboratory fabrication of small specimens. It should also be noted that the extraction of four small specimens from a single gyratory-compacted sample is not possible when using horizontal coring. Therefore, the use of vertical coring also reduces the quantity of mixture required to prepare small test specimens.

The specimen-to-specimen variability of four plant-produced mixtures with varying NMAS was evaluated using the optimized extraction procedure. All specimens were tested regardless of the deviation from the target air void content. Small specimen performance test results generally demonstrate an increase in specimen-to-specimen variability with increasing NMAS, which is also observed in large specimen testing. The results show no clear linkage between the small specimen air void content and the performance test results within the observed specimen air void content range of ± 0.7% from the target. Therefore, it is recommended that initial small specimen provisional standards include an air void content tolerance of ± 0.7% from the target, to be refined upon future ruggedness testing.

TABLE OF CONTENTS

INTRODUCTION

The Asphalt Mixture Performance Tester (AMPT) was developed under the National Cooperative Highway Research Program (NCHRP) Project 9-29 to enable the practical performance characterization of asphalt mixtures (*1*). The dynamic modulus is a fundamental property that is required when characterizing the performance of asphalt mixtures, and serves as a key input for mechanistic-empirical pavement performance prediction frameworks, such as the Pavement ME program. Researchers for the NCHRP Project 9-19 devoted significant effort to developing a test protocol to determine the dynamic modulus values of asphalt mixtures (*2*). Their work was formalized in AASHTO T 342 (*3*) for measuring the dynamic modulus in all servohydraulic machines and was expanded upon in AASHTO TP 79 (*4*) for measuring the dynamic modulus specifically in the AMPT. The dynamic modulus test specimens specified in AASHTO TP 79 and AASHTO T 342 are cylindrical with 100-mm diameter and 150-mm height.

The fatigue damage characteristics of asphalt mixtures are also becoming key inputs to pavement performance prediction frameworks. The FlexPAVE™ program, (formerly the LVECD program), was recently developed under the Federal Highway Administration (FHWA)-sponsored Hot Mix Asphalt Performance-Related Specifications project, number DTFH61-08-H-00005 as a tool for the comprehensive pavement structural analysis to predict pavement rutting and cracking using mechanistic performance test results. The FlexPAVE™ program computes pavement responses and performance under moving loads using three-dimensional viscoelastic analysis. A key input to FlexPAVE™ is the Simplified Viscoelastic Continuum Damage (S-VECD) fatigue model, which is calibrated using uniaxial fatigue test results. Underwood et al. (*5*) developed a formalized procedure for AMPT uniaxial cyclic fatigue testing of asphalt mixtures that has been adopted as a provisional standard, AASHTO TP 107 (*6*). AASHTO TP 107 specifies the use of 100-mm diameter by 130-mm tall specimens in the AMPT.

Given that many asphalt pavement layers are less than 100-mm thick, the standard AMPT dynamic modulus and fatigue test geometries do not allow for the testing of many individual pavement layers within field cores. In addition, standard 6-inch (150-mm) diameter field cores cannot be used to obtain 150-mm tall dynamic modulus test specimens.

Kim et al. (*7*) developed a test protocol and analytical framework using 38-mm thick, 150-mm diameter specimens in indirect tension (IDT) to obtain the dynamic modulus values of field core specimens. Their work demonstrated that the IDT specimen results are equivalent to those obtained from the axial compression testing of standard sized specimens. However, testing in the IDT mode has two primary disadvantages: the stress state is biaxial, which complicates analysis and modeling, and the tests require a separate loading fixture.

These disadvantages led Kutay et al. (*8*) to propose the use of small, cylindrical specimens with 38-mm diameter for uniaxial dynamic modulus and fatigue testing. Kutay et al. (*8*) concluded that the dynamic modulus and fatigue testing of large and small specimens provided equivalent results. However, their evaluation was limited to 12.5-mm nominal maximum aggregate size (NMAS) mixtures.

Since Kutay's initial work, several other researchers have evaluated the use of small uniaxial specimens (*11-15*). Park (*11-13*) also evaluated 38-mm diameter small specimens and introduced an additional prismatic small specimen geometry with a minimum dimension of 25-mm to allow the testing of thin surface layers when 38-mm diameter specimens cannot be obtained. Park (*11*) developed a sample extraction procedure for the 38-mm diameter specimens from 6-in (150-mm) field cores, where two samples were extracted from each pavement layer. Two larger diameter samples cannot be extracted from a pavement layer in a standard, 6-in (150-mm) field core. Li and Gibson (*14*) evaluated laboratory-fabricated 38-mm diameter cylindrical specimens using the AMPT. Ten mixture types with NMAS values ranging from 4.75-mm to 19-mm were tested. Generally, Li and Gibson found good agreement between the dynamic modulus values and phase angles obtained from testing both large and small specimens. Some significant differences between the large and small specimen values were observed but it was difficult to infer which factors led to these differences (*14*). Bowers et al. (*15*) compared the dynamic modulus values of laboratory-fabricated small and large specimens for asphalt mixtures with NMAS values ranging from 9.5-mm to 25.0-mm. They evaluated small specimens and proposed that the 38-mm diameter geometry should be limited to 9.5-mm and 12.5-mm mixtures based on observed differences between the large and small specimen test results (*15*).

It should be noted that alternative small specimen geometries have been used for testing outside of the AMPT. Marasteanu et al. (*9*) and Zofka et al. (*10*) used very small, prismatic asphalt mixture specimens (127-mm by 12.7-

mm by 6.35-mm) in the bending beam rheometer (BBR) to characterize the creep compliance of asphalt mixtures at low temperature. As temperature decreases, the modulus of asphalt binder increases and becomes closer to that of aggregate. Consequently, the role of coarse aggregates is more significant at high temperature than low, which allows for using smaller specimens to characterize bulk asphalt mixture behavior at low temperature than high (*9,10*). For dynamic modulus and fatigue testing in the AMPT, conducted at intermediate and high temperatures, the difference in aggregate and binder properties is significantly different and requires the use of larger test specimens.

Although the initial trial results obtained from uniaxial small specimen testing are promising, further research is needed to more rigorously evaluate the effects of specimen geometry on the mechanical properties of asphalt concrete prior to the development of standard specifications for use in practice. Past efforts have focused on evaluating material-level differences between small and large specimen test results. However, material-level differences may become insignificant when incorporated into pavement structural analyses for performance predictions. Therefore, the sensitivity of performance predictions based on structural analyses to specimen geometry merits consideration when judging the practical significance of material-level differences.

While small specimens were initially developed to enable the testing of field cores, they also offer a significant opportunity to improve the efficiency of laboratory-fabricated uniaxial specimen testing. Multiple small specimens can be extracted from a single gyratory sample. The smaller sample size also reduces the time required for thermal equilibration, which minimizes testing time and improves efficiency. End platens must be affixed to specimens for cyclic fatigue testing. The attachment of end platens to small specimens is expedited by using quick setting steel putty epoxy which allows testing to be conducted after one hour of gluing compared to the 24 hours required for large specimen testing. Quick setting epoxy cannot be used in large specimen testing because it sets before it can be spread over the large specimen diameter. The amount of glue necessary for affixing the specimen to the end platens is also significantly reduced by the use of small specimens. However, there is a need to optimize the fabrication of small specimens from gyratory samples.

The laboratory small specimen fabrication procedures used in past studies have varied. Some researchers have extracted specimens vertically (*8, 11-14*) while others have extracted specimens horizontally from gyratory samples (*11, 15*). Coring small specimens vertically would follow the current practice for laboratory fabricated large specimen uniaxial testing. However, pavements experience tension perpendicular to the direction of compaction and hence, the horizontal extraction of small specimens best mimics field conditions. Bowers et al. (*15*) proposed that small specimens should be horizontally extracted from gyratory samples to best mimic specimens acquired from field cores. Park (*11*) evaluated the effect of anisotropy on small specimen test results by comparing 100-mm tall small specimens horizontally and vertically extracted from gyratory samples. Park (*11*) concluded that anisotropy effects were insignificant but his study was limited to a single mixture. The pattern used to vertically extract small specimens from gyratory samples has varied among past researchers. It is known that gyratory-compacted samples inherently contain higher air void contents at their peripheries than at the specimen center (*16*). Consequently, several past efforts have vertically extracted three small specimens from the inner 100-mm diameter of gyratory samples where large specimens are obtained in effort to avoid the peripheral air void gradients in gyratory samples (8, *11-13*). In contrast, Li and Gibson (*14*) extracted six small specimens vertically from each gyratory-compacted sample, using a center specimen surrounded by a concentric ring of five specimens. Li and Gibson (*14*) found that the outer ring of five specimens had similar bulk air voids but the center specimen had comparably lower air voids, which led them to adjust the coring pattern to a ring of five specimens closer to the center of the gyratory sample. Li and Gibson (*14*) and Bowers et al. (*15*) varied the height of small specimens tested. Li and Gibson (*14*) found the height of 110-mm to be optimal because standard AMPT gauges cannot be used with shorter specimens and taller specimens proved to be problematic.

This study sought to identify the mixture and test conditions for which small specimen testing can provide representative results of bulk asphalt mixture behavior and to identify the optimal small specimen extraction pattern from gyratory samples.

OBJECTIVES

The primary objectives of this project were to:

1. Develop equipment to enable small specimen testing in the AMPT.
2. Evaluate the effects of specimen geometry on dynamic modulus and direct tension fatigue tests and pavement performance prediction using mixtures with various NMAS values.

3. Optimize the laboratory fabrication of small specimens extracted from gyratory-compacted specimens.
4. Facilitate technology transfer efforts, including development of draft specifications for small specimen testing.

SCOPE OF WORK

Two small specimen geometries were considered within the scope of this project: a small cylindrical geometry consisting of 38 mm diameter specimens with 110 mm height and a small prismatic geometry consisting of 25 mm thick by 50 mm wide specimens with 110 mm height. Li and Gibson (*14*) established that 110 mm is the minimum specimen height that accommodates AMPT LVDTs, and that taller specimens are problematic. It should be noted that maintaining consistent cross-sections and ensuring that all sides are perpendicular is difficult when sawing prismatic small specimens. Therefore, the use of prismatic specimens is only proposed for field core testing of pavement layers where 38-mm diameter cylindrical specimens cannot be obtained. All test specimens were extracted from gyratory samples due to the inherent lack of uniformity in field cores.

This study developed the equipment necessary to enable small specimen testing in the AMPT and conducted an experimental program to inform the development standard procedures for small specimen testing of field cores and laboratory-fabricated samples.

The experimental work conducted in this study was broken into three phases:

I. Evaluation of specimen geometry effect on dynamic modulus and direct tension test results.
II. Effect of coring direction on small specimens extracted from gyratory-compacted samples.
III. Specimen-to-specimen variability investigation.

Phase I experiments evaluated the effects of specimen geometry on dynamic modulus and fatigue results using five plant-produced mixtures with varying NMAS values. In addition, pavement structural analysis was conducted using the FlexPAVE™ program to assess the practical implications of material-level differences. The goal of Phase I was to identify the mixture and test conditions for which small specimen testing can provide representative results of bulk asphalt mixture behavior.

Phase II of the experimental work evaluated the effect of small specimen coring direction on dynamic modulus and cyclic fatigue testing results. Coring small specimens vertically would follow the current practice for laboratory fabricated large specimen testing. However, pavements experience tension perpendicular to the direction of compaction and hence, the horizontal extraction of small specimens best mimics field conditions and also matches the extraction pattern used when testing field cores. Therefore, the performance test results and air void variation within small specimens that were cored both horizontally (i.e., perpendicular to the compaction direction) and vertically (i.e., parallel to the compaction direction) from gyratory-compacted specimens were evaluated. The goal of the second phase of the experimental program was to optimize the procedure for the extraction of small specimens from laboratory-prepared, gyratory-compacted specimens.

In Phase III, the dynamic modulus and cyclic fatigue sample-to-sample variability of small specimens extracted from gyratory-compacted samples using the optimized procedure was evaluated using four plant-produced mixtures with varying NMAS values. The results of Phase III were used to establish preliminary guidance on the air void tolerance for small specimen testing.

Based on the equipment developed and experimental results, draft AASHTO standards for the preparation of small specimens, AMPT dynamic modulus testing of small specimens, and the AMPT cyclic fatigue testing of small specimens were developed. The draft standards and findings have been disseminated to the asphalt pavement community via presentations and workshops.

EQUIPMENT FOR SMALL SPECIMEN TESTING IN THE AMPT

OVERVIEW

The equipment necessary to facilitate small specimen testing in the AMPT was developed in partnership with Instrotek, Inc., the North Carolina State University Precision Machine Shop, IPC Global, and Controls Group. The equipment developed to facilitate small specimen testing include:

1. Jig to hold either pavement cores or gyratory specimens during the coring of small specimens
2. End platens for tension and compression testing
3. Adapters to accommodate small specimens in AMPT
4. Gluing jig adapters to affix transducer mounting studs and end platens to small specimens

It should also be noted that the use of alternative displacement measurement techniques was considered to negate the need for linear variable displacement transformer (LVDTs). Initially, both LVDT and actuator displacement combined with machine compliance correction factor approaches were considered for displacement measurement. However, based on the efficiency of the spring-loaded LVDTs used in the AMPT, combined with the complexity of measuring machine compliance, the continued use of LVDTs is recommended. In addition to the equipment developed, Instrotek, Inc. developed calibration factors and associated procedures for bulk specific gravity of small specimens using the CoreLok. Note that that the Saturated Surface Dry (SSD) procedure for specific gravity measurement does not require adjustment for small specimens.

JIG FOR CORING SPECIMENS

Coring systems are not part of the AMPT package distributed by vendors. Therefore, an in-house coring system was developed for use in this study. A preliminary drawing of the coring system developed for this study to extract small cylindrical specimens from a gyratory sample or field core is shown in Figure 1. The coring system can also accommodate large specimen extraction. The specimen holder slides forwards and backwards to allow for coring from various types of samples and at varying positions, as shown for both large and small specimens in Figure 2. Drawings of the coring system are available from the authors upon request. The metal template shown in Figure 3 was developed to facilitate marking of the gyratory sample to determine precise locations for core extraction.

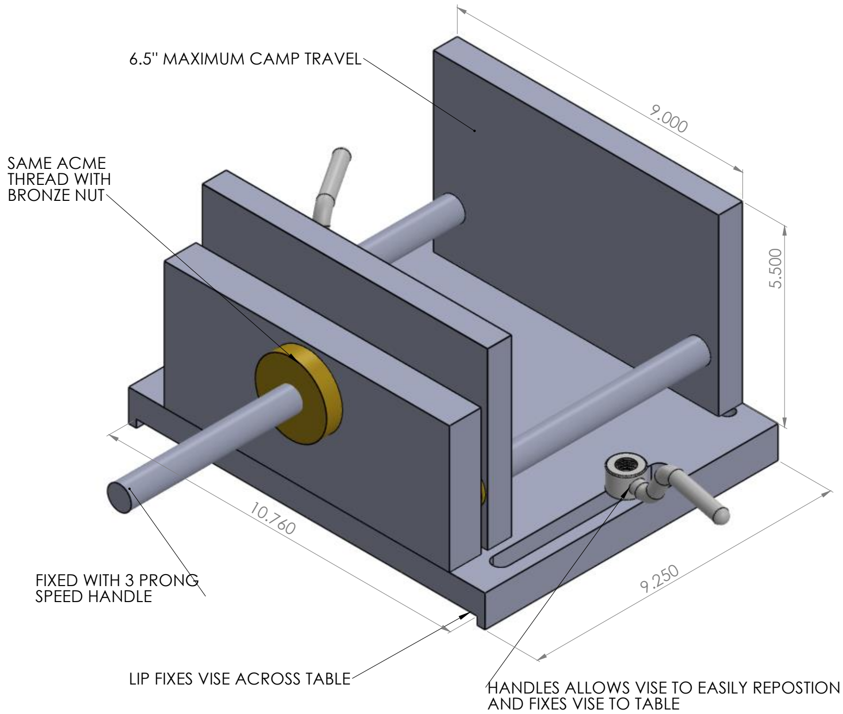

FIGURE 1 Preliminary graphic of coring jig design.

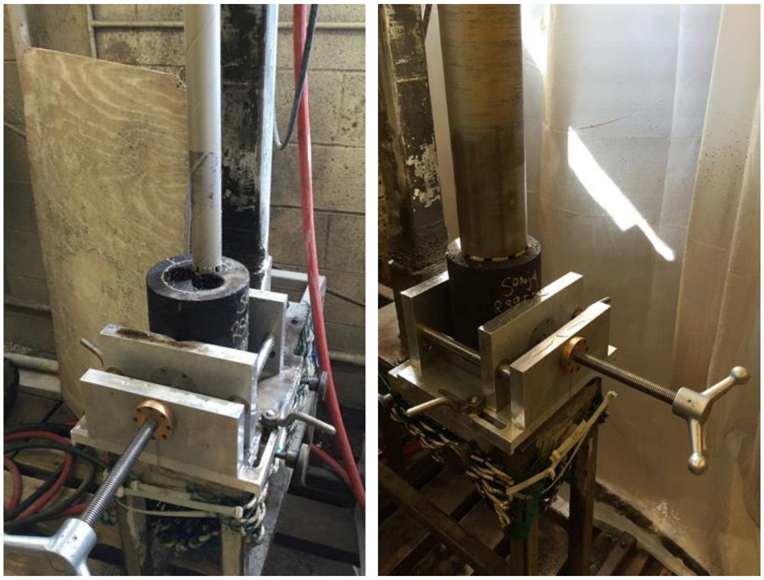

FIGURE 2 Coring jig aligned for small specimens (left) and large specimens (right).

FIGURE 3 Template used to mark gyratory specimen for extraction of small specimens.

END PLATENS AND ADAPTERS

The research team worked with Instrotek, Inc., (former U.S. distributor of the AMPT for IPC, Global), to design small specimen compression end platens for both small cylindrical specimens and small prismatic specimens. The compression end plates for dynamic modulus are very similar to their larger counterpart for standard testing as shown in Figure 4. Note that the base for small specimen testing had to be the same size as the standard base to use the centering ring on the AMPT actuator. Also, note that the lower small specimen platen does not have the vent for confining pressure that is on the large specimens, because confined testing was beyond the scope of this work. Small specimen platens for compression testing are commercially available from IPC Global.

FIGURE 4 Dynamic modulus setup comparison.

Designing end platens for tension testing was a greater challenge because the holes for attaching the tension platens in the AMPT are widely spaced to accommodate large specimens as shown in Figure 4. Initially, a wide solid platen, similar to the large specimen platen but with a small gluing platform, was evaluated. However, it was determined that the broad size and weight of the platens damaged small specimens. Therefore, smaller endplates were designed with adapters to allow for attaching the small endplates to the AMPT. The small specimen endplates and adapter are shown in Figure 4. It can be seen that the small specimen has identical platens on each end, and is sitting on the lower adapter. An upper adapter would also be needed in the AMPT. Small specimen platens and adapters for tension testing will be made commercially available from IPC Global.

FIGURE 5 Fatigue platen setup comparison with adapter for small specimen.

GLUING JIGS

Specimen deformation is measured by sensors during dynamic modulus and cyclic fatigue tests, which are attached to glued gauge points. IPC Global currently produces adapters for affixing gauge points to small specimens using their gauge point fixing jig. A photo of the IPC Global gauge point fixing jig with small specimen adapters is shown in Figure 6.

FIGURE 6 Gauge point fixing jig with small specimen adapters.

The attachment of the end platens to the sample is critical to the preparation of fatigue test specimens. In addition to developing the small specimen end platens for tension testing, adapters were developed to attach the end platens to small specimens using the commercially available IPC Global tension platen fixing jig. The tension platen fixing jig with adapters is shown in Figure 7. The set of adapters includes a lengthened centering arm with a smaller notch to center the small specimen in the jig, a revised top plate which holds small end platens centered, and a step which centers and raises the small specimen to the appropriate position.

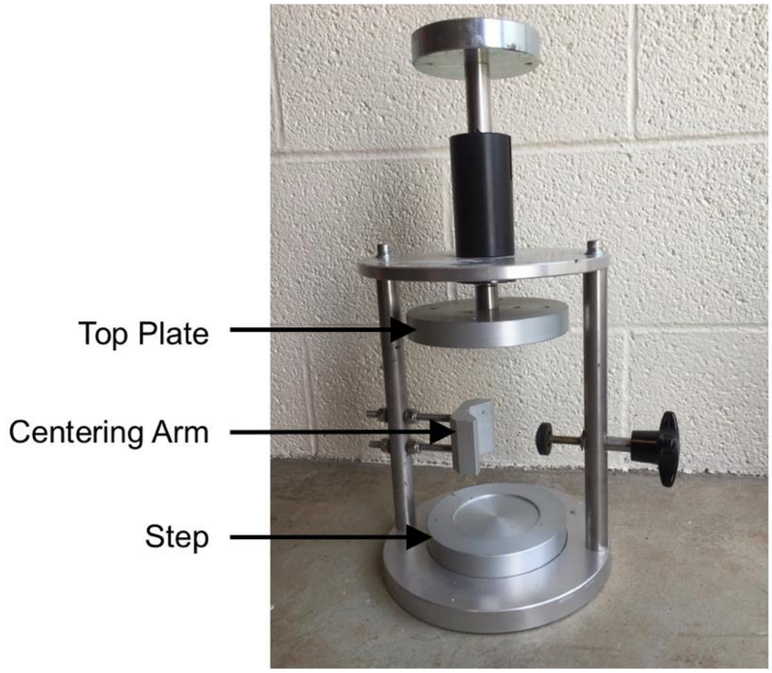

FIGURE 7 AMPT tension platen fixing jig with small specimen adapters.

EXPERIMENTAL PLAN

PHASE I: EVALUATION OF SPECIMEN GEOMETRY EFFECT ON DYNAMIC MODULUS AND DIRECT TENSION TEST RESULTS

Overview

In this phase of work, the dynamic modulus and fatigue results of the two small specimen geometries were compared to the large specimen geometry for mixtures of varying NMAS values. All specimens were extracted vertically from gyratory-compacted samples within inner 100-mm diameter from which large specimens are acquired to best isolate the influence of specimen geometry on test results. Two types of fatigue tests were considered: cyclic and monotonic. Cyclic fatigue testing of large specimens is accepted as a provisional standard (AASHTO TP 107). Monotonic fatigue testing is advantageous over cyclic testing because failure occurs within several minutes of the onset of loading (*5*, *17*). However, the load cell capacity of the AMPT prohibits uniaxial monotonic fatigue testing of large specimens and therefore, use is limited. However, the reduced cross sectional area of small specimens enables monotonic fatigue testing of small specimens within the load cell capacity of the AMPT. Therefore, monotonic fatigue testing of small specimens was tried to determine if equivalent results could be obtained to cyclic testing.

Materials

Table 1 summarizes the materials employed to evaluate the effects of specimen geometry on dynamic modulus and fatigue test results. Five plant-produced loose mixes composed of various NMAS values, binder types, and reclaimed asphalt pavement (RAP) contents were investigated. All of the mixtures evaluated are typical North Carolina mixtures, except for the 12.5-mm mixture, which was sourced from Virginia. State-assigned mixture designations are used throughout this report. The North Carolina Department of Transportation (NCDOT) mixture designations correspond to the mixture names given in Table 1. The R indicates that the mixture contains RAP, the second letter indicates surface (S), fine surface (SF), intermediate (I) or base (B) mixture, followed by the NMAS and a letter designation according to expected traffic (A for light traffic, to D for heaviest traffic). The Virginia mixture is a surface mix (SM), and the PG 64-22 binder grade is denoted in the trailing letter (A), due to different state nomenclature.

TABLE 1 Mixtures Used to Evaluate Geometry Effects

Mixture Name	NMAS (mm)	Binder Grade	Binder Content (%)	RAP Content (%)	Recycled Binder Ratio	VMA (%)	VFA (%)	# Design Gyrations (N_{ini}/N_{des})
RB25.0B	25.0	PG 64-22	4.2	30	0.28	13.6	71.5	7/65
RI19.0B	19.0	PG 64-22	4.4	20	0.23	14.5	71.5	7/65
SM12.5A	12.5	PG 64-22	5.3	30	*	*	*	*
RSF9.5A	9.5	PG 64-22	6.0	30	0.27	17.0	75.3	6/50
RS9.5D	9.5	PG 76-22	5.4	20	0.17	15.8	75.0	8/100

*Limited information was available for the SM12.5A mixture

Specimen Fabrication

All specimens were vertically extracted from gyratory specimens which were compacted to a height of 178 mm. Small specimens were cored within the inner portion of specimens (100-mm diameter) from which large specimens were acquired to further minimize variability between large and small specimens as shown in Figure 8. The air void contents of all the small and large specimens were measured. All cored and cut test specimens had air void contents in the range of 4.0% ± 0.5%. The target air void content of 4% was selected under the assumption that fatigue cracking accumulates primarily late in a pavement's service life after significant densification has occurred.

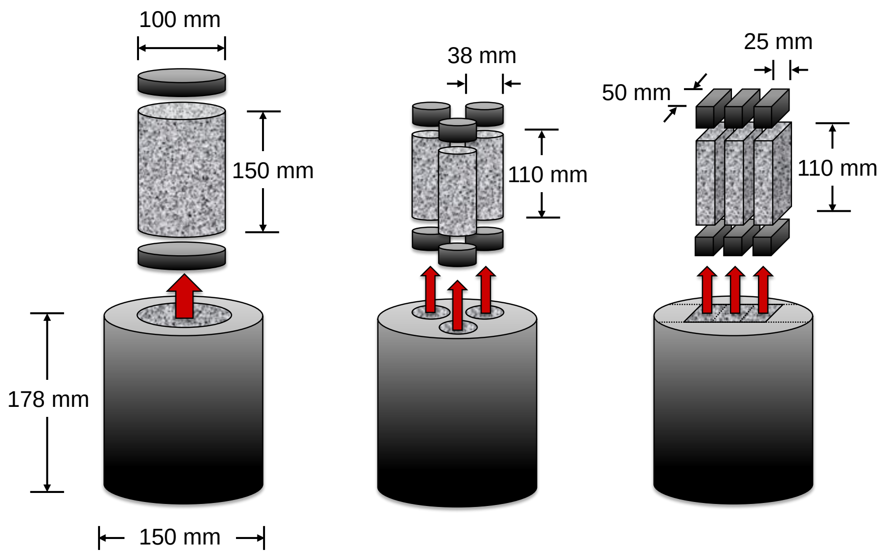

FIGURE 8 Test specimen extraction from gyratory specimens for evaluation of specimen geometry (prior to optimization).

Experiments

The experiments conducted to evaluate the effect of specimen geometry on performance test results are detailed in Table 2. Note that only the vertical core tests detailed in Table 2 were used for Phase I of the experimental plan to evaluate specimen geometry effects. The horizontal tests were used to evaluate anisotropy in Phase II, discussed in a later section of the report. Dynamic modulus testing was conducted on all mixtures. Fatigue testing was initially limited to the RSF9.5A and RB25.0B mixtures because they represent the two extreme NMAS mixtures. Due to unsuccessful large specimen fatigue testing of testing the RB25.0B mixture, the RI19.0B mixture was also subjected to fatigue testing. Both cyclic and monotonic fatigue tests were considered for small specimen testing of the RSF9.5A and RI19.0B mixtures. Recall that prism testing is only proposed for field core testing of pavement layers that do not allow for the extraction of 38-mm cylindrical specimens. The 9.5 NMAS mixtures are the only mixtures evaluated that would likely be placed in thin lifts where 38-mm cylindrical specimens could not be obtained. Prism testing was limited to the RSF9.5A mixture due to limited material quantity of the RS9.5D mixture.

TABLE 2 Experimental Plan to Specimen Evaluate Geometry Effects

Mixture Name	Geometries Tested			Vertical Cores			Horizontal Cores**	
	Large Cylinder	Small Cylinder	Small Prisms	Dynamic Modulus	Cyclic Fatigue	Monotonic Fatigue*	Dynamic Modulus	Cyclic Fatigue
RB25.0B	X	X		X	X			
RI19.0B	X	X		X	X	X	X	X
SM12.5A	X	X		X				
RSF9.5A	X	X	X	X	X	X		
RS9.5D	X	X		X			X	

*Monotonic fatigue testing was only conducted on small specimens

**Horizontal testing was only conducted small cylindrical specimens

Test Methods

Within Phase I, dynamic modulus tests were conducted in a modified Simple Performance Tester (SPT), the precursor to the AMPT. The SPT was designed for compression testing only and therefore, could not be used for fatigue testing. An MTS servo-hydraulic test system was used for fatigue testing in Phase I of the experimental work. Performance testing within the MTS and SPT used four loose-core linear variable differential transformers (LVDTs) mounted onto the specimen surface at 90° radial intervals with a 70-mm gauge length centered on the specimen to measure the deformations. The use of four LVDTs allows for comparison of the LVDTs placed on opposite sides of a specimen, allowing for direct evaluation of eccentricity and was therefore, thought to be most appropriate when performing initial tests. A maximum of three standard, AMPT spring-loaded LVDTs can be attached to small specimens due to the large size of the mounting clamps, which is why loose-core LVDTs were used. An in-house data acquisition system was used to obtain measurements of load and on-specimen displacement because the standard dynamic modulus software only allows for the acquisition of data from three LVDTs. It is not anticipated that the use of testing equipment other than the AMPT will affect the findings of the comparison between the performance test results of different testing geometries. A single instrument was used to evaluate each test method, irrespective of test geometry to mitigate the potential influence of machine bias. In addition, statistical analyses were conducted to infer the significance of differences between the results of different test geometries, thereby accounting for the influence of specimen-to-specimen variability when interpreting findings. It should be noted that an AMPT, with the standard software and equipment, was used when evaluating the specimen-to-specimen variability of the optimized small specimen fabrication procedure in Phase III of the experimental program.

Dynamic modulus tests in Phase I were conducted at 4, 20, 40, and 54°C, with frequencies of 25, 10, 5, 1, 0.5, and 0.1 Hz applied at each temperature. The modified SPT Polytetrafluoroethylene sheets, cut to fit the loading platens, were used to reduce friction between the specimen and the loading platens. The target average strain in the gauges was 62 με for both small and large specimens, with an allowable range of 50-75 με. Note that the target average strain herein is lower than the specification in AASHTO TP 79. Based work by Underwood and Kim (*18*), use of this strain range limits nonlinear effects and minimizes the potential for aggregate mobilization at high temperature. Large specimen dimensions were 100 mm diameter by 150 mm, following AASHTO PP 60 (*19*). Small specimens, (both prisms and cylinders), were tested using the same loading frequencies and temperatures as large specimens. For both large and small specimens, three replicates were conducted for each testing condition. Once the dynamic modulus and phase angle values were computed for each temperature and loading frequency, dynamic modulus and phase angle mastercurves were produced by means of the time-temperature superposition principle.

Cyclic fatigue tests were conducted in an MTS servo-hydraulic test system, in accordance with AASHTO TP 107, which specifies constant crosshead displacement amplitude loading at a frequency of 10 Hz and a test temperature of 18°C for the mixtures evaluated (*6*). Simplified Viscoelastic Continuum Damage S-VECD analysis was used to develop damage characteristic curves (i.e., C versus S curves) and the pseudo strain energy-based so-called G^R failure criterion. To obtain the damage characteristic curves and failure criterion curves, the fatigue tests were conducted at three different crosshead displacement amplitudes for both the large and small specimens.

Monotonic fatigue tests were conducted using several different strain rates and temperatures due to the lack of a standard test method. The initial strain rate used was selected to match the reduced strain rate proposed by

Underwood et al. (*5*) to minimize the effects of viscoplasticity, and the initial temperature was 18°C to match the cyclic fatigue testing. Based on the observed results, additional monotonic fatigue test results were conducted at 10°C in an effort to further minimize possible interference from viscoplasticity. Rigorous viscoelastic continuum damage (VECD) analysis was used to analyze monotonic fatigue test results, because the S-VECD protocol applies only to cyclic tests.

A problem that arises in both large and small specimen fatigue testing is failure at the specimen end, outside of the range of LVDTs, which prevents failure detection during testing. In some instances, "end failure" is caused by adhesion loss between the glue used to affix the specimen to end platens and the specimen, which can be minimized or prevented by proper cleaning of end platens and the use of appropriate adhesives. Adhesive end failure was not observed in this project. For the purposes of this work, end failures are exclusively referring to failures that occur in the asphalt mixture but not entirely between the gauges. An example of an end failure and a middle failure (i.e., acceptable failure) are shown in Figure 9(a) and (b), respectively.

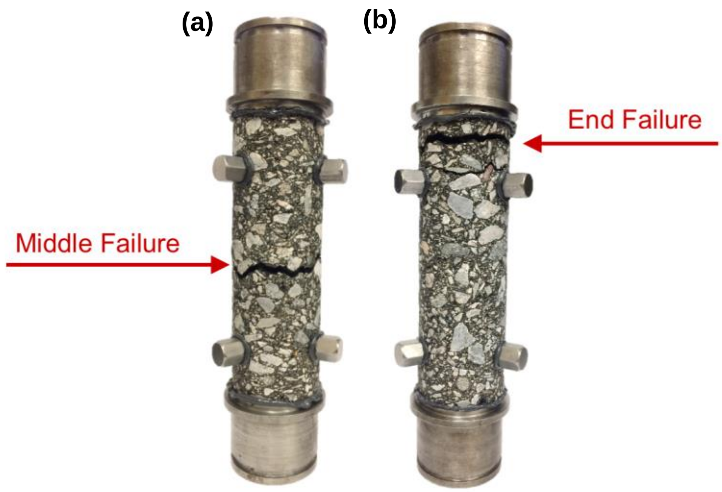

FIGURE 9 Photographs of cyclic fatigue specimen failures.

Performance Prediction

The effects of the specimen geometries on the fatigue performance were evaluated at the pavement level using Pavement ME and FlexPAVE™. For all mixtures and specimen geometries evaluated, dynamic modulus results were used within the Pavement ME program to predict bottom-up fatigue cracking and permanent deformation in pavements. The dynamic modulus and cyclic fatigue test results were used within the FlexPAVE™ program to predict fatigue performance in pavements, using the two mixtures for which complete fatigue characterization was acquired: RSF9.5A and RI19.0B. There are significant differences between the two pavement prediction programs. The FlexPAVE™ program computes pavement responses and performance under moving loads using three-dimensional viscoelastic analysis. In contrast, Pavement ME uses non-moving loads within a layered linear elastic analysis.

PHASE II: EFFECT OF CORING DIRECTION ON SMALL SPECIMENS EXTRACTED FROM GYRATORY-COMPACTED SAMPLES

Overview

The effect of coring direction on small specimen performance test results was evaluated to guide identification of the optimal small specimen extraction pattern from gyratory-compacted samples. The vertically cored specimen dynamic modulus and cyclic fatigue test results from Phase I were compared to the results of small, cylindrical specimens horizontally cored from gyratory-compacted samples. In addition, the air void variation within small specimens that were cored both horizontally and vertically from gyratory-compacted specimens was studied.

Materials

The RI19.0B, RS9.5D, and SM12.5A materials detailed in Table 1 were also used to study the effect of coring direction, leveraging the results of vertically cored specimens from Phase I. The RI19.0B and RS9.5D mixtures were selected to cover a broad range of NMAS values when evaluating the effect of coring direction on performance test results. Recall that the fatigue testing of the RB25.0B mixture proved to be problematic for both large and small vertical cores. The SM12.5A mixture was used to analyze the distribution of air voids within horizontally and vertically extracted small specimens due to exhaustion of the RI19.0B mixture from the preparation of performance test specimens.

Specimen Fabrication

Initial gyratory samples used to horizontally extract small specimens were 120-mm tall because taller gyratory samples are expected to have greater radial air void gradients (*16*). However, it was found that the specimens were extracted too close to the ends of the gyratory specimen which made obtaining uniform air void contents between the small specimens obtained from a single gyratory sample difficult. Therefore, the gyratory sample height was increased to 140-mm in an effort to core samples from the inner region of gyratory samples where there is a more uniform air void content.

Initially, four cores were extracted from each gyratory sample as illustrated in Figure 10 (a) to maximize the efficiency of specimen fabrication. However, extracting two cores at the same height from the gyratory sample led to regions of high air voids at the specimen ends which led to end failure in the cyclic fatigue tests conducted on the RI19.0B mixture. Therefore, the extraction pattern was adjusted to a two-core pattern, with one sample taken from each lift in an effort to extract specimens further away from the edges of the gyratory sample as shown in Figure 10 (b). Cyclic fatigue tests were also conducted using the two-core pattern using the RI19.0B mixtures. In addition, the two-core pattern was used when preparing dynamic modulus and air void analysis specimens. All of the small specimens evaluated had total air void contents within the range of 4.0±0.5%.

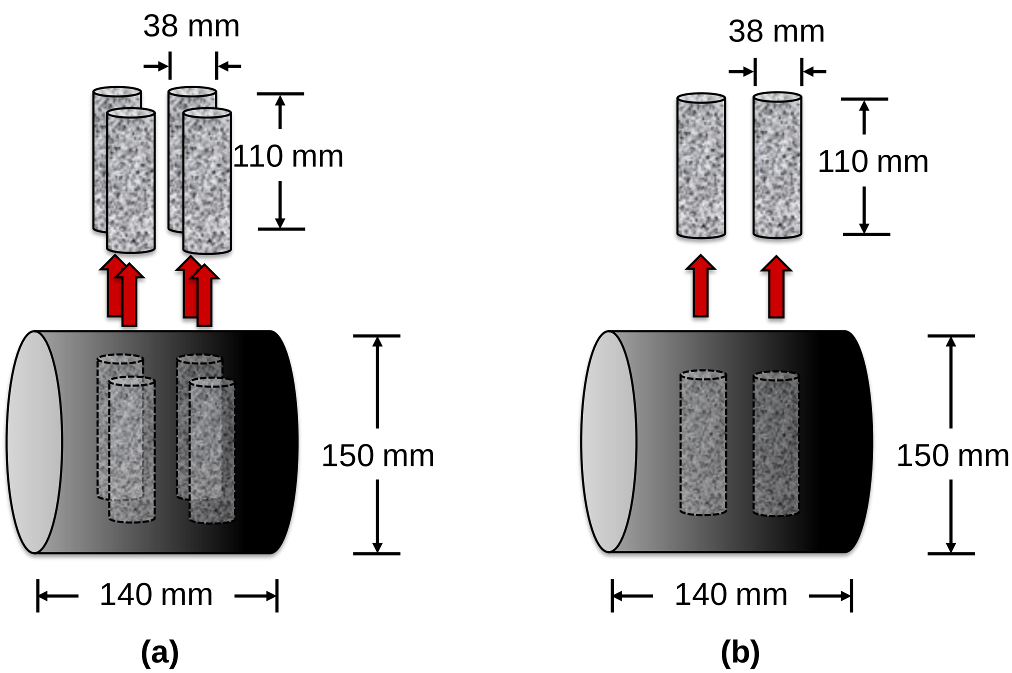

FIGURE 10 Depiction of horizontal extraction of (a) four small specimens and (b) two small specimens from a gyratory-compacted sample.

Experiments

The experiments conducted on horizontal cores are detailed in Table 2. The RI19.0B mixture was used for both for dynamic modulus and cyclic fatigue testing of horizontally extracted small specimens because it was the largest

NMAS mixture where successful fatigue test results were acquired in the previous phase of work. Dynamic modulus was also conducted horizontal cores prepared using the RS9.5D mixture. While fatigue testing of horizontally extracted small RS9.5D specimens was also initially planned, fatigue testing of horizontal cores was aborted based on the results of the RI19.0B mixture. The dynamic modulus results of each mixture were input into Pavement ME for comparison with the vertically cored specimen results from Phase I.

Air Void Analysis

An air void analysis was conducted using the SM12.5A mixture to determine whether there was a difference in the general trends in air void distribution within the horizontally extracted specimens and the vertically extracted specimens. Small test specimens that were horizontally and vertically extracted from gyratory samples were sawn into four sections of equal height along their length. The air void content of each individual sample section was measured using the Corelok method, specifically calibrated for the partial samples, to infer the horizontal and vertical air void in gyratory samples.

Test Methods

Dynamic modulus and fatigue testing was conducted on horizontal cores using the same equipment and test parameters as those used in Phase I. However, based on the observed difference in large and small specimen dynamic modulus test results at 54°C, the use of test data at 54°C was aborted. Note that Bowers et al. (*15*) also recommended that small specimen testing at 54°C be avoided. Pavement ME analysis was conducted using the horizontally extracted small specimen dynamic modulus results and compared to Phase I analyses.

PHASE III: SPECIMEN-TO-SPECIMEN VARIABILITY INVESTIGATION

Overview

To develop a uniform small specimen fabrication procedure for performance testing, the vertical extraction of small specimens from gyratory-compacted samples is required because the results of Phase II demonstrate that cyclic fatigue testing cannot be conducted on specimens horizontally extracted from gyratory-compacted samples without inducing end failure. Large specimens are extracted from the inner 100 mm of gyratory specimens. Thus, it was expected that small specimens extracted from the inner 100 mm of the gyratory samples would have sufficiently uniform air voids for performance testing. It was found that four small specimens can be cored vertically from the inner 100 mm of gyratory-compacted samples. Therefore, the extraction of four small specimens from the inner 100 mm of 178-mm tall gyratory-compacted samples is the proposed small specimen laboratory fabrication procedure as shown in Figure 11.

An analysis of the specimen-to-specimen variability in dynamic modulus and cyclic fatigue test results was conducted using the optimized specimen extraction procedure. There will inevitably be variation in the air void content among small specimens extracted from a given gyratory sample. Within Phase III, specimens were tested regardless of whether or not they met the target air void content to establish preliminary guidance on the acceptable air void tolerance range for small specimen testing, to be refined upon future ruggedness testing.

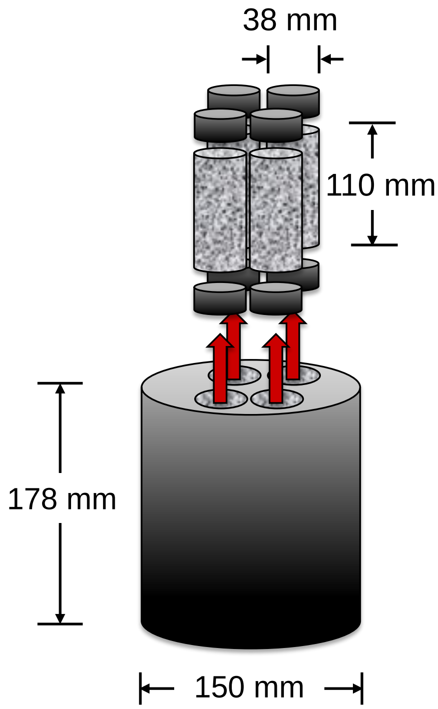

FIGURE 11 Depiction of final recommended vertical small specimen extraction procedure.

Materials

To evaluate specimen-to-specimen variability, small specimens were fabricated using the optimized procedure using four plant-produced loose mixes with varying NMAS. The mixtures used to evaluate sample-to-sample variability using the optimized procedure are detailed in Table 3. Note that the RI19.0B-2 mixture is different than the RI19.0B mixture included in Table 1. The RI19.0B mixture used when evaluating specimen geometry effects and the effect of coring direction was exhausted which necessitated the use of the new RI19.0B-2 mixture for this phase of the experimental work. The two 19.0-mm mixtures share the same mixture designation, but the test results indicate that the performance of the two mixtures differ significantly.

TABLE 3 Asphalt Mixtures for Specimen-to-Specimen Variability Study

Mixture Name	NMAS (mm)	Binder Grade	Binder Content (%)	RAP Content (%)	Recycled Binder Ratio	VMA (%)	VFA (%)	# Design Gyrations (N_{ini}/N_{des})
RS9.5D	9.5	PG 76-22	5.4	20	0.17	15.8	75.0	8/100
SM12.5A	12.5	PG 64-22	5.3	30	*	*	*	*
RI19.0B-2	19.0	PG 64-22	4.5	40	0.38	14.0	73.0	7/65
RB25.0B	25.0	PG 64-22	4.2	30	0.28	13.6	71.5	7/65

*Limited information was available for the SM12.5A mixture

Specimen Fabrication

Gyratory Sample Fabrication

It is important to minimize the variability in the air void content of small specimens extracted from a given gyratory sample. Within Phase I, 36.5% (19/52) of the initial small specimens produced fell outside of the accepted the widely-accepted tolerance of ±0.5% variability from the target air void content, which was 4.0% for the Phase I experiments. During the initial effort, specimens were fabricated with no particular control of the way the loose mixture was poured into the gyratory mold. When the loose mixture is not evenly distributed within the mold, the mixture will densify non-uniformly under compaction. Thus, small specimens from different sides of the gyratory sample can have dramatically different air void contents.

It was found that pouring the loose mixture directly to the center of the gyratory mold, using the Superpave transfer device, greatly reduces small specimen air void variability within gyratory-compacted samples. Therefore, in the specimen-to-specimen variability analysis, the loose mixture was poured into the center of the gyratory mold to fabricate samples. When the loose mixture was poured to the center of the mold, only 18.8% (9/48) of small specimens produced fell outside of the widely accepted air void tolerance of ±0.5%. This suggests a significant improvement in the air void uniformity by charging the center of the gyratory mold. However, adhering to the current standard for air void tolerance would still result in the loss of some of small samples produced.

For small specimens, determining the appropriate gyratory sample mass to achieve the target air void content at the specified gyratory height is not as straightforward as for large specimens. In large specimen testing, a trial sample mass can be determined using the recommended procedure in Appendix X1 of AASHTO PP 60 (*19*). In the AASHTO PP 60 procedure, one trial gyratory sample is compacted at the calculated trial mass. One large test specimen is extracted from the trial gyratory sample, and the air void content is measured and compared to the target. If the target air void content is not met, an adjustment calculation is performed and a second trial gyratory sample is compacted to verify the target air void content is met.

The AASHTO PP 60 method for determining gyratory sample mass can be adapted for small specimens. Three options for specimen extraction procedures to determine the gyratory sample mass to achieve target air void contents in small specimens are shown in Figure 12. The first option, shown in Figure 12 (a), is to core only one small specimen from the trial gyratory sample. However, due to the variation in air void contents between small specimens extracted from a single gyratory sample, evaluating a single small specimen may not provide representative results. The second option is to core all of the small specimens from the gyratory sample, as shown in Figure 12 (b), and measure their air void contents. However, this procedure is time-consuming due to the larger number of specimens, and thus is not ideal. The third option is to core a large specimen, as shown in Figure 12 (c), and assume that the small specimens will have similar air void contents to the large specimen because they are acquired from the same region. In Phase I, the procedure depicted in Figure 12 (c) was used successfully to determine the appropriate gyratory sample mass for each mixture for both large and small specimens.

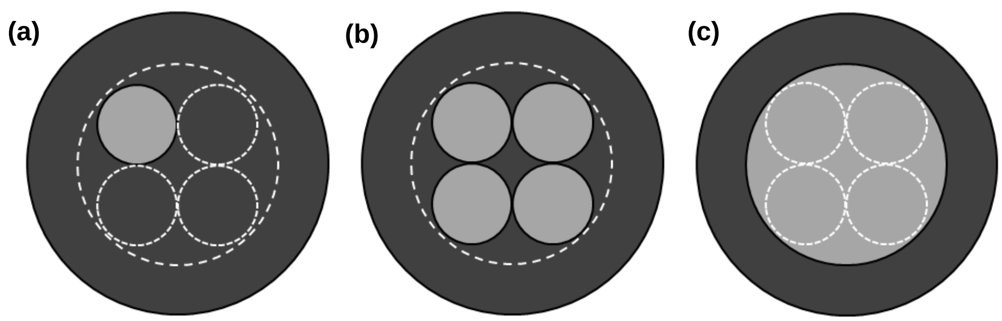

FIGURE 12 Options for extracting trial specimens to determine the gyratory sample mass to achieve a target air voids

An alternative method for determining the appropriate gyratory sample mass to achieve a target air void content using large specimens is included in Appendix X1 of the draft standard “Preparation of Small Cylindrical Performance Test Specimens Using the Superpave Gyratory Compactor (SGC) and Field Cores” in the Appendix A. This procedure is similar to the AASHTO PP 60 procedure, but three gyratory samples are compacted: the first at the mass determined using the same formula in the AASHTO PP 60 procedure and the other two at ± 100 g of the first. The procedure in AASHTO PP 60 is ideal when limited material is available because only one trial gyratory sample is compacted at a time (*19*). However, if determining a trial mass in a timely manner is of greater importance, and sufficient material is available to compact three trial specimens, the procedure in the draft standard may be more appropriate because if the initial trial mass from the AASHTO PP 60 procedure is not correct, an additional gyratory sample must be fabricated and evaluated.

Test Specimen Fabrication

For each mixture evaluated, three gyratory samples were compacted to the target air void content, with special attention given to the direction of pouring the material into the mold, to minimize air void variation between specimens. The Superpave transfer device was held to the right-hand side of the gyratory mold, with the operator standing at the red arrow in Figure 13. The operator focused on pouring material directly into the center of the mold, rather than allowing it to run down the side. The operator marked the side of the mold facing them and then kept that direction forward during coring. The sample labeling system includes a number, which indicates the specific gyratory sample, and two letter Front/Back and Left/Right designation to indicate the location of the core, as shown in Figure 13, to track any patterns of variance depending on the material pouring. All gyratory-compacted samples were prepared with a diameter of 150 mm diameter and height of 178 mm.

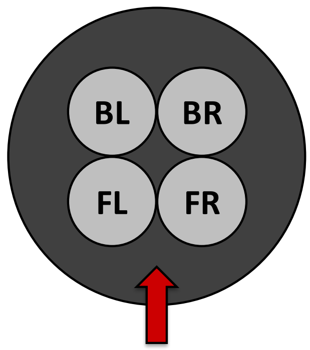

FIGURE 13 Sample extraction pattern for four vertically cored specimens.

For the specimen-to-specimen variability study, all the small specimens extracted from gyratory samples were tested regardless of air void content. The purpose of testing all specimens was to evaluate the sensitivity of performance test results to the air void content to provide preliminary into whether small specifications should adhere to the standard of accepting only ±0.5% from the target or if the range of acceptance can be broadened. The target air void contents were increased slightly for the NMAS values larger than 9.5-mm from the previous set of experiments. Because the RB25.0B demonstrated a high propensity for end failure at 4.0±0.5% air voids used during the evaluation of specimen geometry effects, the SM12.5A and RI19.0B target air void contents were increased to 4.5% and the RB25.0B was increased to 5.0%. One of the gyratory samples produced for each mixture was used to obtain dynamic modulus test specimens and the remaining two gyratory samples were used to obtain cyclic fatigue test specimens.

One of the three gyratory samples was selected for dynamic modulus testing and the other two were used for cyclic fatigue testing. Three replicate dynamic modulus tests were conducted using, in most cases, the specimens closest to the average air void content. All eight small test specimens extracted from the two remaining gyratory samples were subjected to cyclic fatigue testing, regardless of whether the air void content was within ±0.5% of the target, to evaluate whether specimens outside of this range warrant rejection.

Experiments

The experimental plan for the evaluation of specimen-to-specimen variability is shown in Table 4. Each mixture was subjected to dynamic modulus and cyclic fatigue. Test specimen average air void contents and ranges are shown in Table 4. Note that while the RS9.5D has very low variance in air voids, but the remaining three mixtures have similar variation, which is only slightly higher than the standard accepted tolerance of ±0.5%.

TABLE 4 Experimental Plan for Evaluation of Specimen-to-Specimen Variability

Mixture Name	Dynamic Modulus	Cyclic Fatigue	Air Void Contents (%)
RS9.5D	X	X	3.8±0.3%
SM12.5A	X	X	4.6±0.6%
RI19.0B-2	X	X	4.3±0.7%
RB25.0B	X	X	4.7±0.7%

Test Methods

Phase III testing was conducted using a standard AMPT to allow for the evaluation of variability expected from the standard test equipment. Dynamic modulus tests were conducted at 4, 20, and 40°C, with frequencies of 25, 10, 5, 1, 0.5, and 0.1 Hz applied at each temperature. Testing was not conducted at 54°C because it was found that small specimens cannot be used to measure bulk mixture behavior at 54°C. Testing was conducted using the three, standard "spring-loaded" LVDTs spaced at 120° intervals, and the standard AMPT data acquisition system.

Cyclic fatigue tests were conducted in accordance with AASHTO TP 107. Initially, per AASHTO TP 107, tests were conducted at three displacement amplitudes to target fatigue lives varying from 1,000 to 10,000 cycles to failure (*6*). Tests conducted to evaluate specimen-to-specimen variability on the RI19.0B-2 and RB25.0B materials were all performed with a target fatigue life of 10,000 cycles for the test specimens from the first gyratory specimen and 20,000 cycles to failure for the test specimens from second gyratory sample to provide a more direct assessment of specimen-to-specimen variability. In this phase of the work, a new fatigue failure criterion, D^R, was used to evaluate mixtures. The D^R criterion is equal to the average reduction in pseudo stiffness (i.e., C) up to failure. The D^R value is calculated as the summation of $(1 - C)$, illustrated in Figure 14, divided by the fatigue life (number of cycles to failure) for individual test replicates. D^R is a material constant that is independent of mode of loading, temperature, and stress/strain amplitude. Note that the calculation of D^R is in arithmetic scale rather than in log-log scale. Consequently, D^R results are not as affected by test variability as the G^R failure criterion.

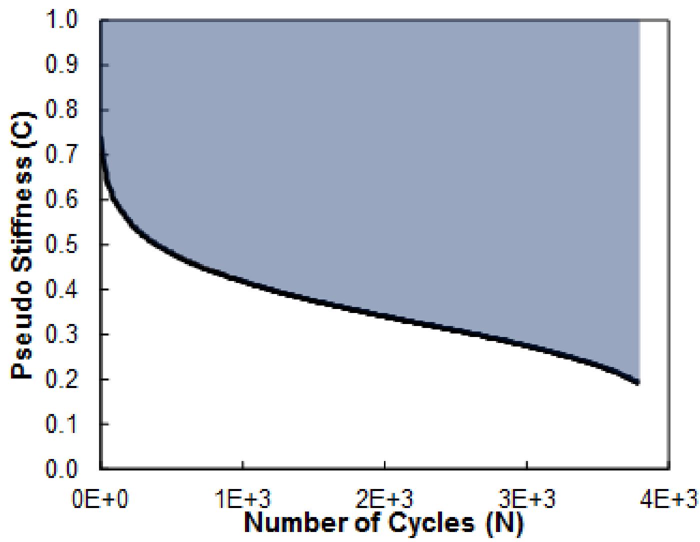

FIGURE 14 Illustration of summation of (1-*C*).

RESULTS

EFFECT OF SPECIMEN GEOMETRY

Dynamic Modulus Test Results

Figure 15 presents the individual sample dynamic modulus mastercurves, phase angle mastercurves, and time-temperature shift factor results obtained from the experiments conducted to evaluate the effect of specimen geometry. A reference temperature of 5°C was used to construct the mastercurves. Generally, good agreement is visually observed between the dynamic modulus values and phase angles of the large and small specimens at the high and intermediate reduced frequencies (low and intermediate temperatures). At low reduced frequency (high temperature), the small specimen dynamic moduli appear slightly higher and the phase angles appear slightly lower than the large specimen values. The time-temperature shift factors appear to be unaffected by the specimen geometry.

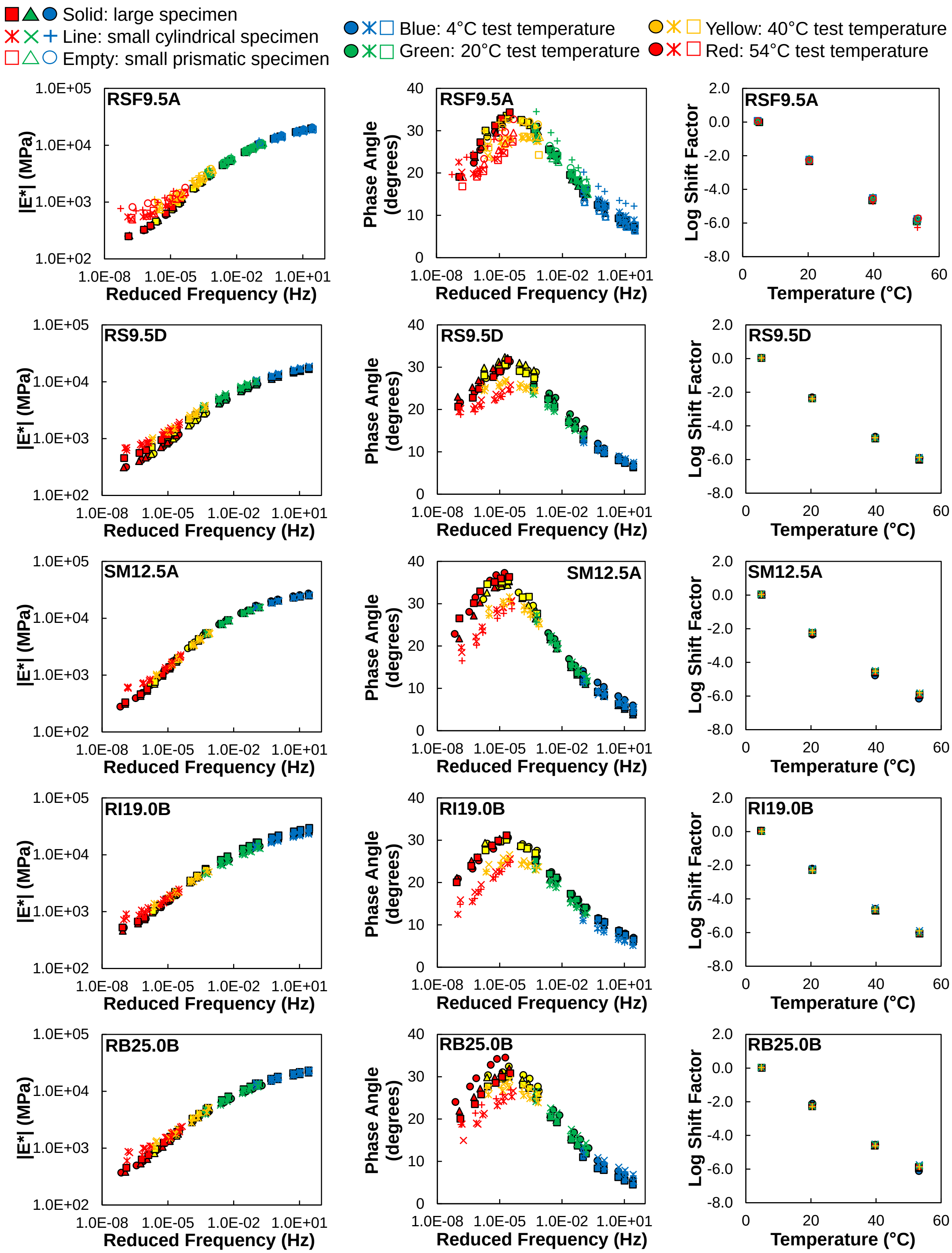

FIGURE 15 Dynamic modulus test results for evaluation of sample geometry.

To evaluate the results statistically, dynamic modulus values were acquired at the AASHTO T 342 (*3*) standard test temperatures and frequencies from the dynamic modulus mastercurve of each replicate specimen. To determine the significance of differences between the sample geometries, a two-tailed Student's t-Test with equal variance was conducted. To verify equal variance, f-Tests were conducted and equal variance was verified at a confidence of 95%. The p-value results of the Student's t-Test are shown in Table 5. Results that indicate significant differences between the geometries at a 95% confidence level are highlighted yellow, and those that indicate significant differences at a 98% confidence level are highlighted green.

Generally, no statistical difference exists between the dynamic modulus values of the large and small specimens at the low and intermediate temperatures with the exception of the RS9.5D mixture. The RS9.5D mixture exhibits significant differences between the specimen geometries at low temperature (4.4°C). At high temperature, the small specimen dynamic moduli values are consistently, significantly higher than the large specimen values with the exception of the RSF9.5A mixture. The RSF9.5A mixture small specimen dynamic modulus results exhibited higher variability than the other mixtures evaluated, which means that the detection of a significant difference between two geometries requires a very large difference between average values.

TABLE 5 Student's t-Test p-value Results for Evaluation of Sample Geometry

Temperature (°C)	Frequency (Hz)	RB25.0B	RI19.0B	SM12.5A	RS9.5D	RSF9.5A		
		Large/ Small	Large/ Small	Large/ Small	Large/ Small	Large/ Small	Small/ Prism	Large/ Prism
4.4	25	0.430	0.189	0.268	0.003	0.875	0.629	0.579
	10	0.497	0.169	0.252	0.004	0.878	0.618	0.560
	5	0.558	0.155	0.232	0.006	0.883	0.614	0.547
	1	0.725	0.127	0.157	0.015	0.912	0.627	0.532
	0.5	0.802	0.117	0.119	0.023	0.933	0.645	0.536
	0.1	0.970	0.104	0.053	0.045	0.994	0.723	0.586
21.1	25	0.699	0.071	0.335	0.063	0.823	0.695	0.411
	10	0.612	0.065	0.401	0.074	0.796	0.762	0.371
	5	0.563	0.063	0.454	0.078	0.759	0.823	0.334
	1	0.531	0.074	0.608	0.069	0.616	0.974	0.306
	0.5	0.568	0.093	0.729	0.060	0.543	0.969	0.305
	0.1	0.860	0.291	0.689	0.037	0.382	0.888	0.240
37.8	25	0.888	0.256	0.316	0.041	0.420	0.254	0.078
	10	0.685	0.633	0.202	0.030	0.322	0.340	0.081
	5	0.505	0.777	0.121	0.023	0.264	0.420	0.078
	1	0.176	0.055	0.020	0.012	0.170	0.609	0.067
	0.5	0.105	0.021	0.008	0.009	0.142	0.672	0.063
	0.1	0.038	0.006	0.001	0.006	0.099	0.761	0.059
54.4	25	0.060	0.034	0.014	0.008	0.192	0.112	0.064
	10	0.037	0.017	0.005	0.006	0.134	0.229	0.062
	5	0.026	0.012	0.002	0.005	0.106	0.330	0.062
	1	0.015	0.007	0.000	0.003	0.071	0.527	0.062
	0.5	0.013	0.007	0.000	0.003	0.063	0.587	0.063
	0.1	0.011	0.006	0.000	0.003	0.051	0.678	0.068

The specimen-to-specimen variability of different test specimen geometries was evaluated by determining the coefficient of variation (COV) for the AASHTO T 342 (*3*) standard test temperatures and frequencies. Figure 16 shows the COV of dynamic moduli results for each mixture and test geometry. Three replicate specimens were used for each calculation of COV. In addition, Figure 16 (a) shows the average COV values for each test geometry, based on all of the mixtures evaluated. The average COV values for the large and small cylindrical specimens are comparable at all test temperatures and frequencies. The COV requirements by AASHTO TP 79 (*4*) vary with mixture properties, allowing for higher COV at higher temperatures as the asphalt binder softens. However, according to Witczak (*20*) and Pellinen (*21*, *22*), COV values of 11 to 15% are typical for large specimens. In testing below 54°C, no COV value higher than 15% is observed at all, and the COV value is generally below 11%, thus indicating acceptable variability for the small specimens.

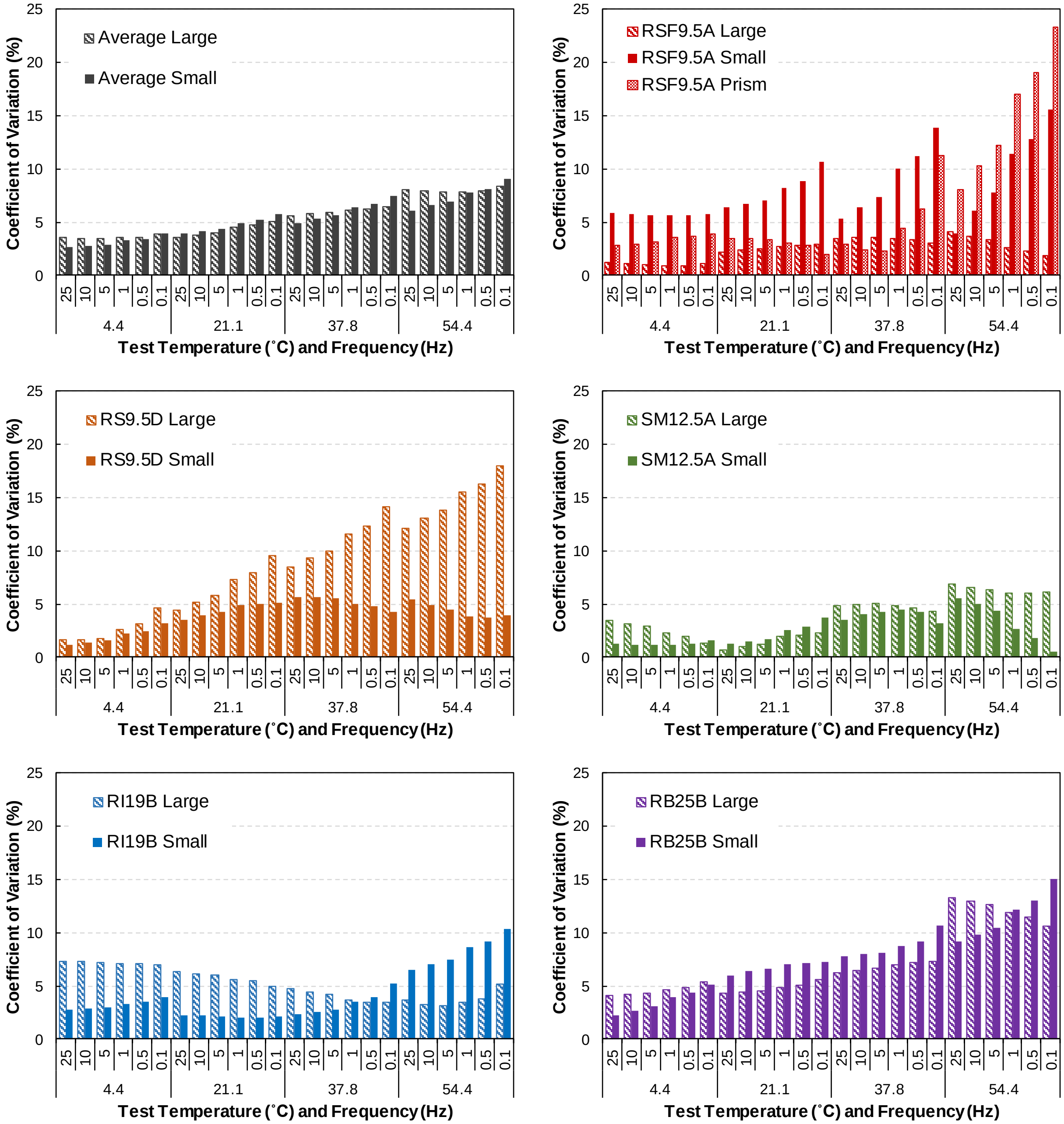

FIGURE 16 Coefficient of variation for dynamic modulus with respect to test temperature and frequency.

The dynamic modulus test results highlight the limitations of using small specimens. The dynamic modulus test results of the small and large specimens generally differ significantly at 54°C whereas the majority of the mixtures evaluated demonstrated statistically equivalent dynamic modulus results at low and intermediate temperatures. Additionally, at low and intermediate temperatures, COV values are less than 15%, indicating that specimen-to-specimen variability is within the generally accepted range. Therefore, it is recommended to limit small specimen testing to the temperatures outlined in AASHTO PP 61, which specifies three test temperatures with the highest temperature selected as a function of the Performance Grade (PG). The highest temperature specified by AASHTO PP 61 ranges between 35°C and 45°C for different asphalt binder PG grades. As will be shown within the pavement performance prediction analyses conducted, the observed difference in the mastercurve at high temperature does not significantly affect pavement fatigue performance predictions.

Fatigue Test Results

Three of the five mixtures subjected to dynamic modulus testing were subjected also to cyclic fatigue testing; these three mixtures were the RSF9.5A, RI19.0B, and RB25.0B mixtures. The S-VECD model was used to derive damage characteristic curves and a failure criterion for performance predictions. Damage characteristic curves represent the relationship between material integrity (C) and damage (S). According to the time-temperature superposition principle with growing damage, the damage characteristic curve should be independent of loading and temperature history. This allows the derivation of a model to predict fatigue damage evolution under any loading and temperature history of interest, using limited test results. The failure criterion is defined as the relationship between the average rate of pseudo strain energy release up to failure (G^R) and fatigue life (N_f). This failure criterion is unique to loading and temperature history and allows the prediction of when failure will occur in damage evolution predictions. Monotonic fatigue testing was conducted on the RSF9.5A and RI19.0B mixtures. Results were used to generate C versus S curves. However, the failure criterion only applies to cyclic test results. Results for individual mixtures follow.

RSF9.5A – 9.5-mm NMAS, PG64-22 binder

Figure 17 presents the damage characteristic curves generated from the cyclic fatigue test data for the RSF9.5A mixture. Each curve corresponds to an individual test specimen. The majority of the test results for all specimen geometries are in good agreement. However, two of small specimen test results demonstrate outlier behavior. These specimens contained broken coarse aggregate particles in the failed surface. In a large specimen, a few broken coarse aggregate particles would be insignificant because they would constitute only a small portion of the specimen cross-section. However, in small specimens the coverage of the cross-sectional area can be significant, which is illustrated in Figure 18. A broken aggregate with a diameter of 12.7 mm on the failure surface comprises only 1.6% of the large specimen failure surface but 11.2% of the small specimen failure surface.

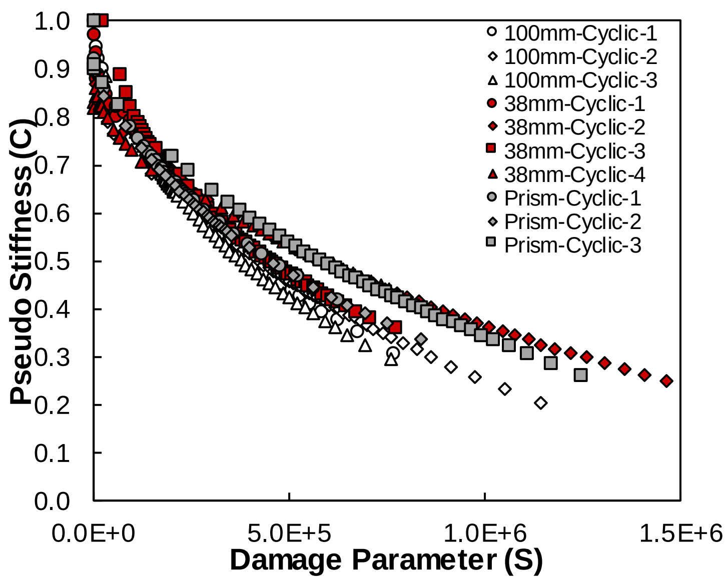

FIGURE 17 RSF9.5A cyclic damage characteristic curves.

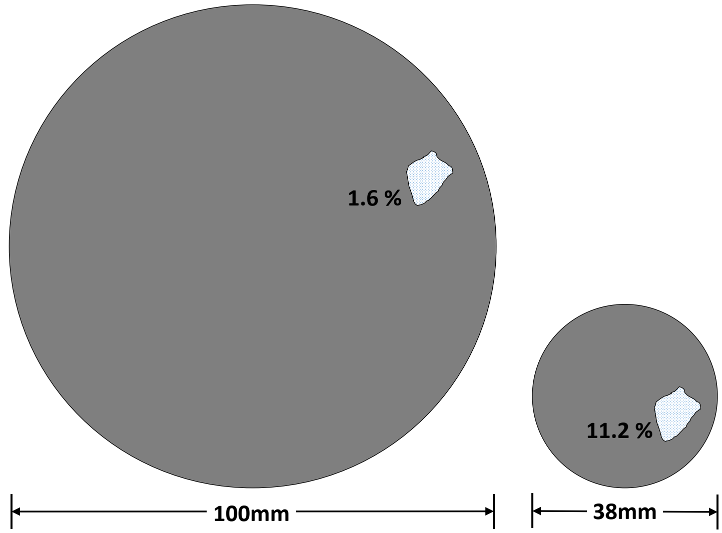

FIGURE 18 Illustration of effects of a 12.7 mm aggregate on large and small specimen failure surfaces.

For the specimens where the damage characteristic curves aligned, G^R failure criteria analysis was conducted. Results are shown in Figure 19. All the data points fall on a single curve, indicating good agreement among the test results for the differing specimen geometries.

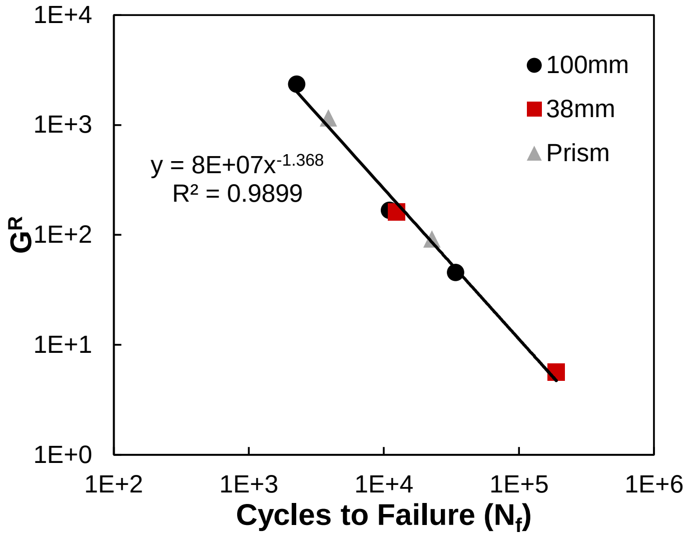

FIGURE 19 RSF9.5A fatigue failure criteria results.

Figure 20 presents the damage characteristic curves generated from both the cyclic fatigue test data and monotonic fatigue test data for the RSF9.5A mixture. Small cylinder and prism specimens were initially subjected to monotonic fatigue testing at 18ºC to match the cyclic tests. The strain rate used was selected to match the reduced strain rate proposed by Underwood et al. (*5*) to minimize the effects of viscoplasticity. However, as shown in Figure 20, monotonic fatigue test results conducted at 18ºC differ from cyclic test results. Therefore, additional monotonic fatigue test results were conducted at 10ºC in an effort to further minimize possible interference from viscoplasticity. While all monotonic fatigue test results are in good agreement, there is a significant difference between monotonic and cyclic damage characteristic curves. It is speculated that these trends are the result of differences in the failure mechanisms induced by monotonic and cyclic tests. Monotonic fatigue test specimens exhibited evidence of brittle failure whereas cyclic test specimens exhibited evidence of ductile failure. The failure surfaces of monotonic fatigue test specimens were relatively flat and many specimens demonstrated evidence of aggregate breakage. Cyclic test specimens exhibited irregular failure surfaces and less aggregate breakage, which is more indicative of ductile failure.

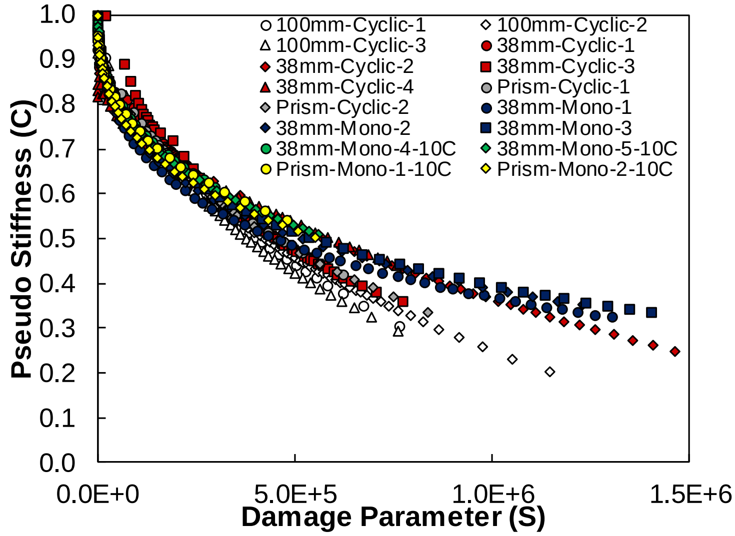

FIGURE 20 RSF9.5A damage characteristic curves from all modes of loading.

RI19.0B – 19.0-mm NMAS, PG 64-22 binder

Figure 21 presents the damage characteristic curves results for the RI19.0B mixture. Results demonstrate good agreement between large and small specimen cyclic test results. However, it should be noted that, although four small specimen tests were conducted, two tests resulted in failure at the specimen edge, outside the range of the LVDTs and with less than 500 cycles to failure. These results are excluded from based on requirements of AASHTO TP 107 (*6*). Failure at the specimen ends may have resulted from damage localization near large aggregate particles situated near the specimen edge. Only limited monotonic fatigue testing was conducted using the RI19.0B mixture based on results of the RSF9.5A mixture which indicated a lack of promise for the use of monotonic fatigue testing. The damage characteristic curve from the monotonic fatigue test deviates from the cyclic test curves. Therefore, it is recommended that only cyclic testing be used for fatigue characterization.

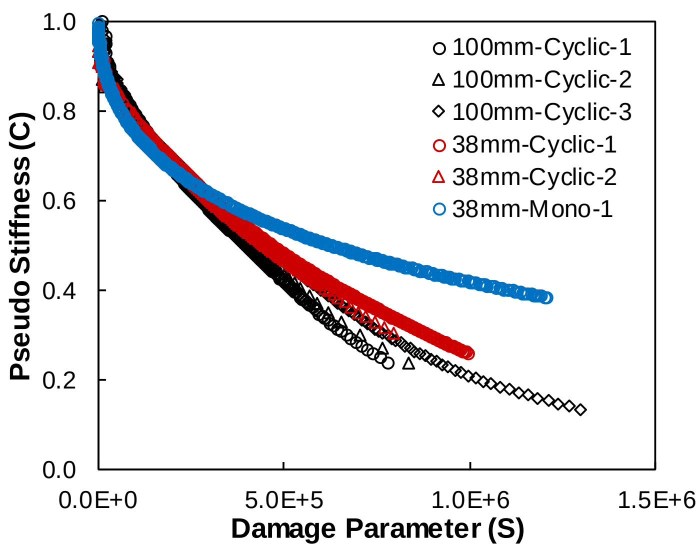

FIGURE 21 RI19.0B damage characteristic curves.

Figure 22 presents the G^R failure criteria results of the RI19.0B mixture. The results demonstrate good agreement between the large and small specimen test results.

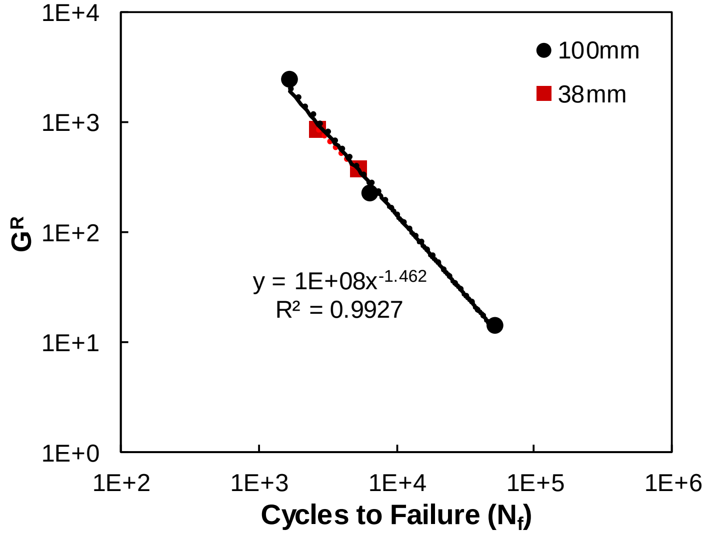

FIGURE 22 RI19.0B fatigue failure criteria results.

RB25.0B – 25.0-mm NMAS, PG 64-22 binder

Figure 23 presents the damage characteristic curves results for the RB25.0B mixture. The large specimen testing for this mixture was the leading concern. Six of the eight large specimens failed at the specimen ends, where the LVDTs could not capture the failure, which is an unreasonably high failure rate. Although end failure was less problematic in the small specimens, the small specimen test results demonstrated high variability and poor agreement with the large specimen test results. It should be noted that the RB25.0B mixture was compacted to achieve 4% air voids, which may be an unrealistic compaction state for a base course. A possible air void gradient in the test specimens could be responsible for the high occurrence of end failure and high variability. In addition, failure was observed due to damage localization at the boundary of the aggregate particles and at aggregate particles that were broken during the specimen fabrication. Failure at the boundary of large aggregate particles may have contributed to the high variability in the small specimen test results. Therefore, in the experiments to evaluate specimen-to-specimen variability, further analysis of the RB25.0B mixture was conducted at 5.0% air voids, to evaluate whether using a more realistic compaction effort would allow for fatigue characterization of the RB25.0B mixture.

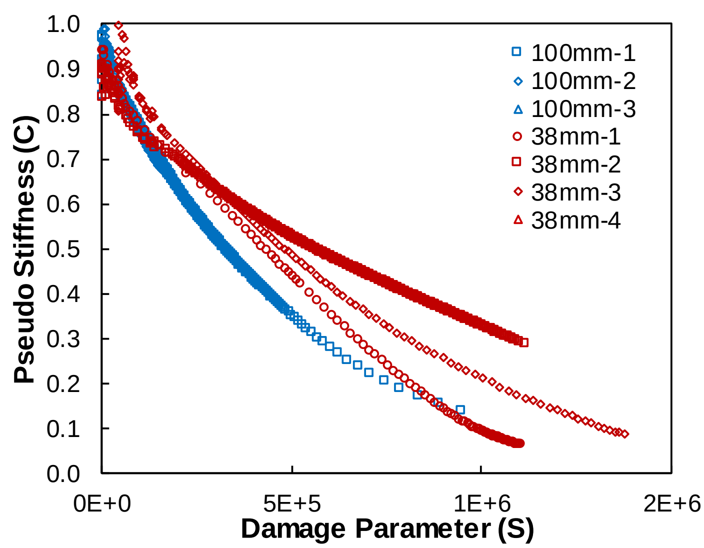

FIGURE 23 RB25.0B C versus S fatigue results.

Implications of Specimen Geometry on Pavement Performance Prediction

To further evaluate the significance of observed differences in large and small specimen test results, pavement performance predictions were conducted in Pavement ME and FlexPAVE™. For the Pavement ME program, all the tested mixtures and specimen geometries were evaluated by varying the dynamic modulus of the asphalt layer, holding all other inputs constant. Due to a lack of specific binder information, binder data for a typical PG 64-22 binder was used because binder test data is required for analysis when using measured asphalt mixture dynamic modulus values. The pavement structure evaluated was a 4-in asphalt concrete layer over a 6-in aggregate base and a semi-infinite subgrade. The climate station was selected as the Raleigh/Durham Airport because the mixtures were sourced from Raleigh, NC and the surrounding area. The traffic input for Pavement ME analyses was 1,000 annual average daily truck traffic with no growth. All other traffic information was left as default. The structure and traffic input values were chosen such that the fatigue damage growth would be apparent in the analysis, and close to the default failure threshold within a performance prediction range of 20 years. The results of the bottom-up fatigue cracking and permanent deformation predictions at 20 years are shown in Table 6. The percent difference of each small specimen geometry compared to the large specimen geometry was calculated. The comparison in the pavement bottom-up fatigue cracking and permanent deformation severity using the small specimen results are within 5% of the predictions using the large specimen results with the exception of the RSF9.5A small cylinders. The predicted distress severities using the RSF9.5A small cylindrical specimen dynamic modulus results are still within 10% of the predictions using the large specimen results.

TABLE 6 Pavement ME Results to Evaluate the Effect of Specimen Geometry

Mixture	Geometry	Fatigue Cracking (% lane area)	Percent Difference - Fatigue	Permanent Deformation (in)	Percent Difference - Permanent Deformation
RSF9.5A	Large	25.43	---	0.90	---
	Small	23.64	7.0	0.82	8.9
	Prism	25.24	0.7	0.88	2.2
RS9.5D	Large	26.51	---	0.91	---
	Small	25.66	3.2	0.88	3.3
SM12.5A	Large	22.69	---	0.79	---
	Small	22.86	0.7	0.79	0.0
RI19.0B	Large	23.83	---	0.80	---
	Small	23.61	0.9	0.82	2.5
RB25.0B	Large	24.00	---	0.83	---
	Small	23.88	0.5	0.83	0.0

FlexPAVE™ analysis was only conducted using the RSF9.5A and RI19.0B mixtures because they were the only mixtures with complete cyclic fatigue characterization. A simple pavement structure was considered: a 10-cm asphalt concrete layer over a 20-cm aggregate base and 380-cm subgrade. The location selected for the Enhanced Integrated Climatic Model (EICM) data was Raleigh, NC. The traffic input for this structure was 3,500 daily equivalent single-axle loads with no growth. These structure and traffic input values were chosen such that the fatigue damage growth would be apparent in the analysis within a performance prediction range of 20 years. Figure 24 shows the predicted distribution of damage within a cross-section of the asphalt concrete pavement layer after one, 10, and 20 years of traffic loading moving from left to right. The wheel path is directly above the region of damage localization. Figure 24 shows no noticeable difference in the distribution of damage predicted from the large and small specimen test results for both the RSF9.5A mixture and the RI19.0B mixture.

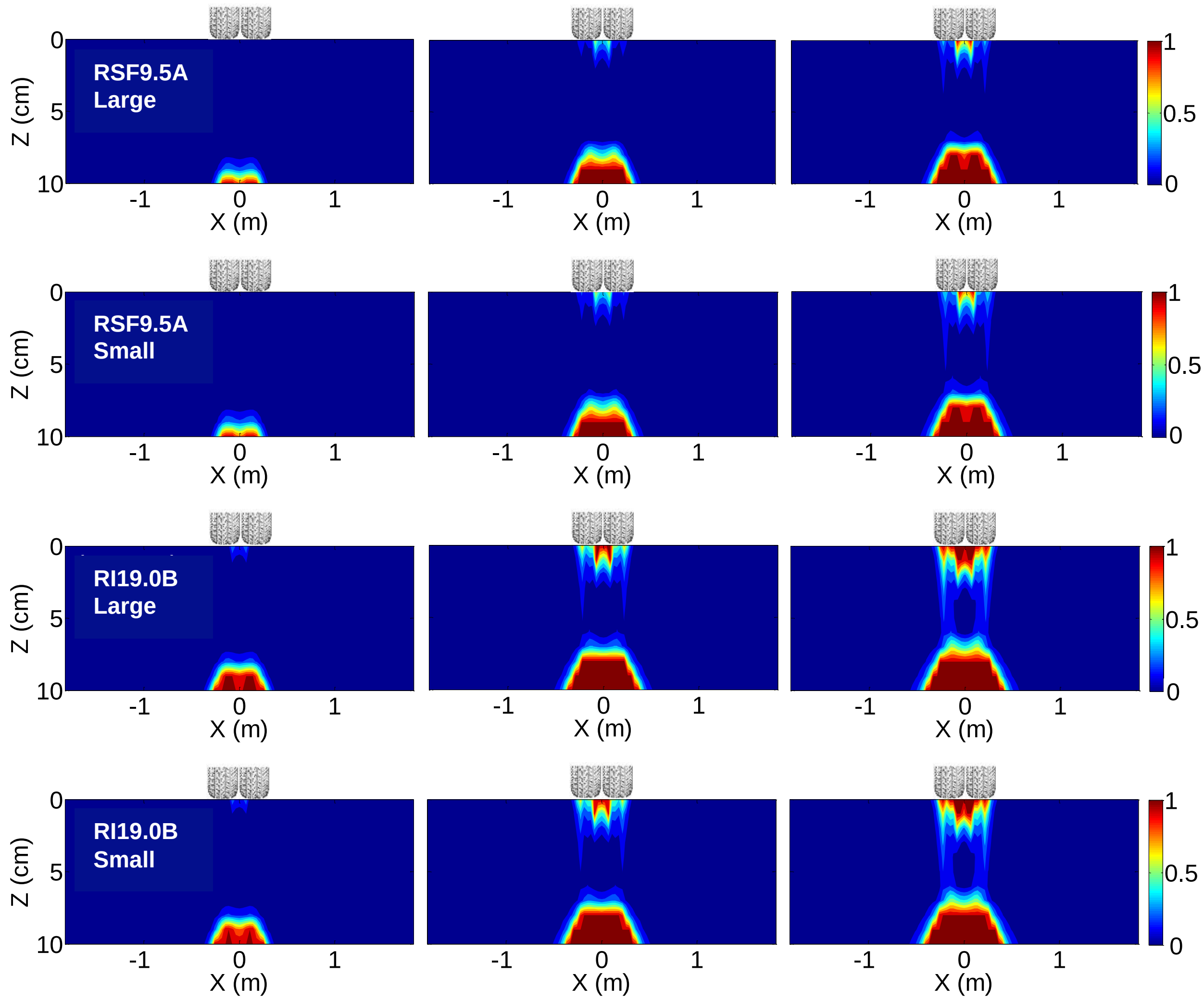

FIGURE 24 FlexPAVE™ damage contours for 9.5-mm and 19-mm mixtures after 1, 10, and 20 years.

To further compare the results of the fatigue cracking predictions, the fatigue damage area as a function of time was computed for each case. The fatigue damage area is defined as the ratio of the damaged cross-sectional area (i.e., the area that experiences fatigue failure) to the total cross-sectional area. Figure 25 presents the results. The difference between the large and small specimen test results for the RI19.0B mixture is slightly greater than that for the RSF9.5A mixture. However, the overall results indicate good agreement between the predictions from the large and small specimens.

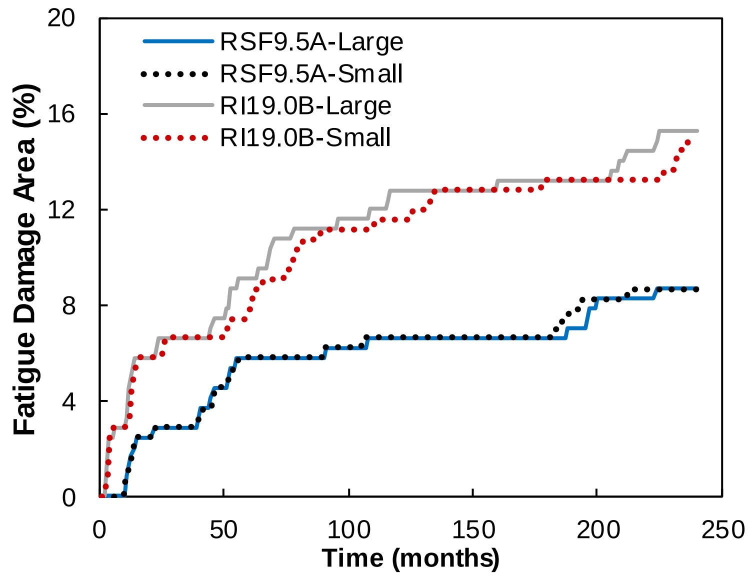

FIGURE 25 Comparison of fatigue damage areas for both large and small specimen test results for each mixture.

In summary, the performance prediction results from both the Pavement ME and FlexPAVE™ programs indicate that the differences in the material-level performance test results between small and large cylindrical specimens do not lead to significant differences in pavement performance predictions.

EFFECT OF SMALL SPECIMEN EXTRACTION DIRECTION

Dynamic Modulus Test Results

Figure 26 presents the comparison of dynamic modulus mastercurves obtained from horizontally and vertically extracted specimens for the RS9.5D and RI19.0B mixtures. Good agreement is visually observed for the dynamic modulus of horizontally and vertically extracted small specimens of the RS9.5D mixture, shown in Figure 26 (a) and (b). In Figure 26 (c) and (d) it is visually apparent that the RI19.0B mixture small specimens extracted vertically exhibit slightly higher average dynamic moduli at high reduced frequencies and phase angle values at low reduced frequency compared to the horizontally extracted small specimens.

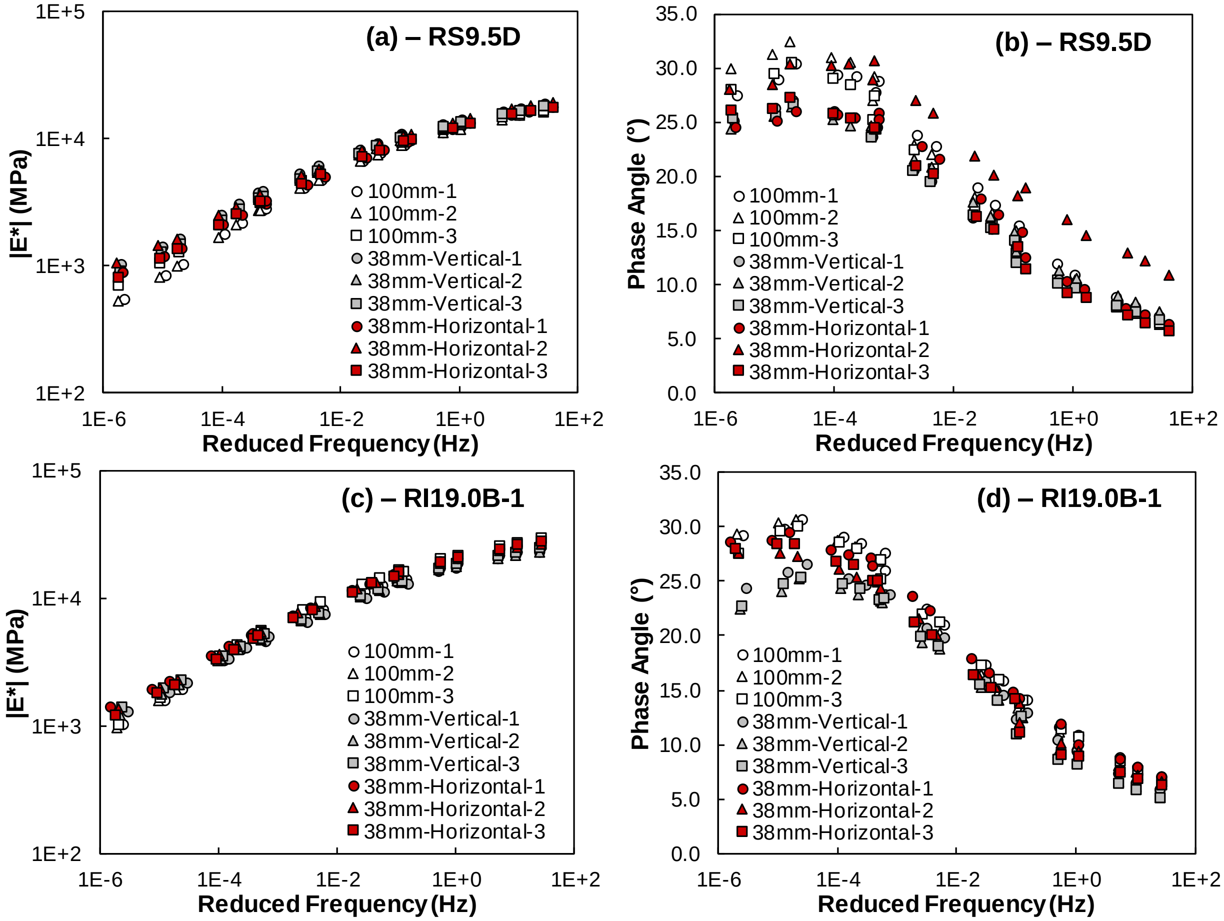

FIGURE 26 Dynamic modulus and phase angle mastercurves for small specimens extracted vertically and horizontally.

TABLE 7 presents the p-value results of the Student's t-test used to determine if observed differences are significant between the horizontally and vertically extracted samples. Results that indicate significant differences between the geometries at a 95% confidence level are highlighted yellow, and those that indicate significant differences at a 98% confidence level are highlighted green. For the RS9.5D mixture, the small specimens dynamic modulus results obtained from vertically and horizontally extracted specimens are statistically equivalent. In contrast, for the RI19.0B, there is a statistically significant difference between the dynamic modulus results of the small specimens vertically and horizontally extracted at low and intermediate temperature. However, the horizontally extracted small specimen dynamic modulus results are statistically equivalent to the larger specimens that are vertically extracted, indicating anisotropy effects are negligible.

TABLE 7 Student's t-Test p-value Results for Evaluation of Coring Direction

Temperature (°C)	Frequency (Hz)	RI19.0B			RS9.5D		
		Large/Vert.	Vert./Horiz.	Large/Horiz.	Large/Vert.	Vert./Horiz.	Large/Horiz.
4.4	25	0.189	0.004	0.437	0.003	0.527	0.022
	10	0.169	0.004	0.445	0.004	0.743	0.027
	5	0.155	0.004	0.453	0.006	0.946	0.034
	1	0.127	0.004	0.476	0.015	0.598	0.075
	0.5	0.117	0.004	0.486	0.023	0.461	0.110
	0.1	0.104	0.004	0.498	0.045	0.289	0.230
21.1	25	0.071	0.009	0.668	0.063	0.235	0.225
	10	0.065	0.013	0.564	0.074	0.202	0.288
	5	0.063	0.018	0.505	0.078	0.191	0.312
	1	0.074	0.063	0.471	0.069	0.191	0.276
	0.5	0.093	0.117	0.517	0.060	0.199	0.235
	0.1	0.291	0.379	0.854	0.037	0.230	0.136
37.8	25	0.256	0.168	0.933	0.041	0.226	0.129
	10	0.633	0.312	0.636	0.030	0.243	0.094
	5	0.777	0.459	0.396	0.023	0.258	0.073
	1	0.055	0.860	0.069	0.012	0.296	0.042
	0.5	0.021	0.973	0.026	0.009	0.312	0.034
	0.1	0.006	0.676	0.003	0.006	0.343	0.024

Pavement ME was used to further evaluate the significance of the effect of coring direction using the results of Phase I complemented with analysis using the horizontal core test results. The pavement structure, material, and traffic inputs were consistent with the analysis conducted in Phase I with the exception that the dynamic modulus results of the horizontally extracted specimen results were used for the asphalt layer. The Pavement ME predictions of bottom-up fatigue cracking and permanent deformation are shown in Table 8. The result indicate negligible differences in the predicted bottom-up fatigue cracking severity and permanent deformation, further validating that anisotropy effects are insignificant.

TABLE 8 Pavement ME Results to Evaluate the Effect of Small Specimen Extraction Direction

Mixture	Geometry	Fatigue Cracking (% lane area)	Percent Difference - Fatigue	Permanent Deformation (in)	Percent Difference - Permanent Deformation
RS9.5D	Horizontal	25.72	---	0.89	---
	Vertical	25.66	0.2	0.88	1.1
	Large	26.51	3.1	0.91	2.2
RI19.0B	Horizontal	23.73	---	0.79	---
	Vertical	23.61	0.5	0.82	3.8
	Large	23.83	0.4	0.80	1.3

Cyclic Fatigue Test Results

Seven horizontally extracted RI19.0B small specimens were subjected to cyclic fatigue testing. All of the horizontally extracted specimens failed at the specimen end. Photographs of four of the horizontally extracted RI19.0B small specimens after cyclic fatigue testing are shown in Figure 27. The photos show the failure locations of the tested specimens, demonstrating failure outside of the gauge points. Fatigue failure outside the range of the gauge points prohibits failure detection by the LVDTs as previously discussed. The occurrence of end failure was speculated to be caused by a relatively high air void content at the edge of small, horizontally extracted specimens. Regions of higher air voids will be more susceptible to fatigue, which explains the observed end failure. The use of shorter, horizontally extracted specimens to avoid the peripheral region of the gyratory sample is prohibited by the length of the AMPT LVDTs.

FIGURE 27 Photographs of horizontally cored RI19.0B small specimens after cyclic fatigue testing.

While ultimate fatigue failure cannot be captured when end failure occurs, data prior to failure can still be analyzed to generate damage characteristic curves. Thus, damage characteristic curves were developed for both test results corresponding to horizontally and vertically extracted test specimens. However, the data quality for two of the horizontally extracted specimens was poor, which prohibited analysis. Figure 28 presents the damage characteristic curves for horizontally and vertically extracted small specimen test results. The results demonstrate good agreement, suggesting that anisotropy effects are negligible. The finding that anisotropy does not affect dynamic modulus or cyclic fatigue test results suggests that coring specimens vertically for laboratory fabricated samples and horizontally for field core samples is acceptable.

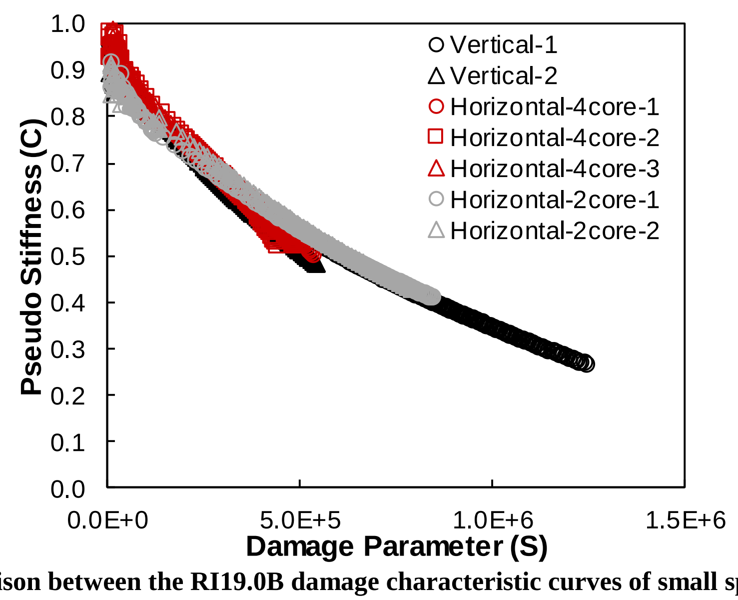

FIGURE 28 Comparison between the RI19.0B damage characteristic curves of small specimens extracted vertically and horizontally from gyratory samples.

Air Void Analysis

An analysis of the air void distribution within horizontally and vertically extracted small specimens was conducted to better understand the observed occurrence of end failure in horizontally extracted specimen cyclic fatigue test results. Each test specimen was given a unique identifier based on the gyratory sample it was extracted from. Each test specimen was sliced into four parts for which bulk air void content were measured.

Figure 29 (a) presents the results of the air void tests conducted on horizontally extracted small specimens from the SM12.5A mixture. The horizontal graph axis corresponds to the section of the test specimen from which the air void content was measured, which is detailed the schematic shown in Figure 29 (b). The number in the title of each data series (e.g., the 1 in 1-T) corresponds to the gyratory sample. Thus, analysis was conducted on small specimens extracted from three different gyratory samples. The T versus B included in the title of the data series indicated if the small specimen was extracted from the top or bottom portion of the gyratory sample, respectively. The results demonstrate variability in air void content within test specimens, indicating a spread of up to 2.1% within a single test specimen. All of the test specimens evaluated exhibited the highest air void content at their end (i.e., location #1 or #4 on the x-axis), which explains the end failure results in fatigue testing because regions with higher air voids will be more susceptible to fatigue. With the exception of one specimen, the decrease in air void content from the section with the highest air void content to the neighboring section is greater than 0.5%, indicating a significant gradient in air void content based on the typical acceptance tolerance for the variability in the bulk air void content of test specimens for performance testing (*3*, *4*, *6*).

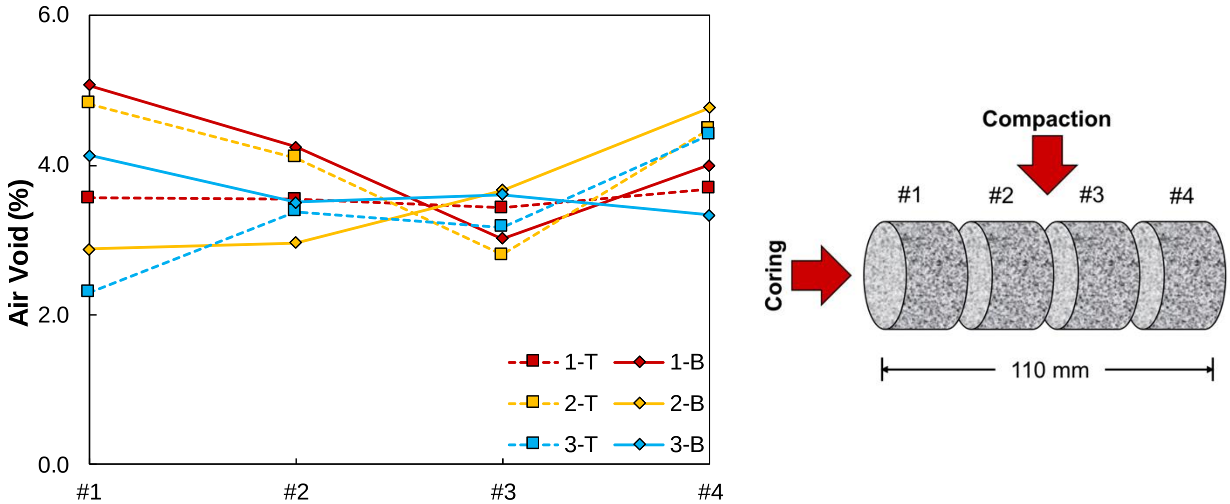

FIGURE 29 (a) Air void analysis results and (b) schematic of sample locations for the horizontally extracted specimens.

Figure 30 (a) presents the results of the air voids analysis conducted on vertically extracted small specimens from the SM12.5A mixture. The horizontal graph axis corresponds to the section of the test specimen from which the air void content was measured, which is detailed the schematic shown in Figure 30 (b). The first number in the title of each data series (e.g., the 1 in 1-2) corresponds to the gyratory sample. Thus, analysis was conducted on small specimens extracted from three different gyratory samples. The second number in the title of each data series (e.g., the 2 in 1-2) corresponds to the specimen number extracted from a specific gyratory. Three small specimens were extracted from the inner 100-mm diameter of gyratory samples. Results demonstrate some variability in air voids within test specimens with a maximum span of 2.9%. Three out of the nine specimens evaluated exhibited the highest air void content within a middle section of the sample. In addition, three out of the six specimens with highest air voids at the end exhibited less than 0.5% air void content difference between the section with the highest air void content and a neighboring section. Based on current standards for bulk air void tolerance variability of performance test specimens, it is not anticipated that ±0.5% air voids may result in significant differences in performance. Thus, the air void content results suggest a considerably higher probability of failure within the middle portion of the specimen in fatigue test results when small specimens are vertically cored, which corroborates fatigue testing findings.

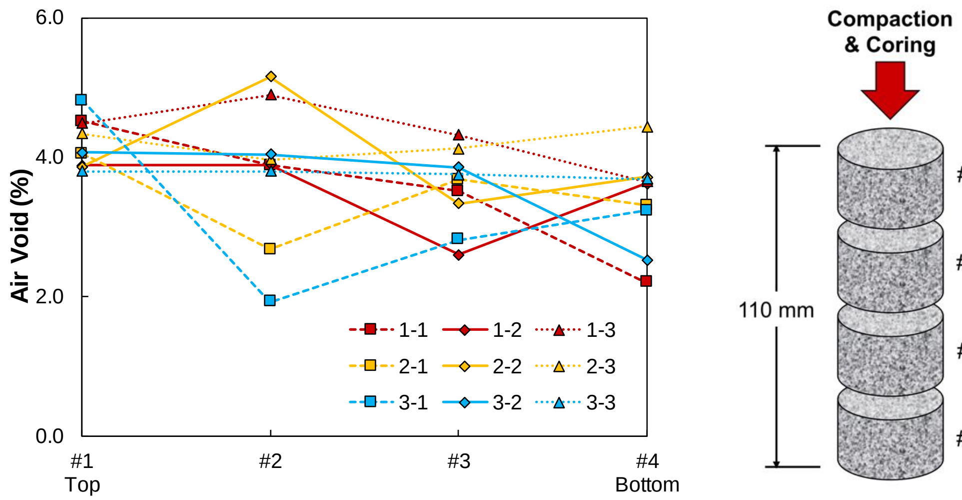

FIGURE 30 (a) Air void analysis results and (b) schematic of sample locations for the vertically extracted specimens.

Summary

Based on the results presented, anisotropy does not significantly impact dynamic modulus and cyclic fatigue test results. While fatigue testing of horizontal cores is problematic due to the peripheral air void gradient in gyratory samples, reliable dynamic modulus testing of both horizontal and vertical cores is possible. However, the vertical extraction of small specimens from gyratory-compacted samples is the recommended procedure for the laboratory fabrication of both fatigue and dynamic modulus specimens for consistency. Large specimens are extracted from the inner 100 mm of gyratory-compacted samples. Therefore, it is expected that air void content is relatively uniform within this region. It is possible to vertically extract four small specimens from the inner 100 mm of a gyratory-compacted procedure, which is therefore the recommended procedure. It should also be noted that a maximum of three, vertically stacked, horizontal cores have been extracted per gyratory-compacted (*15*). However, the extraction of three horizontal cores requires a gyratory-compacted sample height of 200 mm, which is not possible with all gyratory samples, including the one used herein. Given this constraint, the horizontal extraction of two small specimens per gyratory sample would be practical for standardization. Thus, the use of vertical coring significantly reduces the quantity of material required for fabricating small specimens compared to horizontal coring. While horizontal coring is not recommended for routine laboratory specimen fabrication, it could still merit value in forensic investigations where laboratory-fabricated and field core samples are compared.

The extraction of four small specimens per gyratory-compacted sample suggests a significant opportunity to improve the efficiency of specimen fabrication compared to large specimen testing where only one test specimen is acquired per gyratory-compacted sample. The small specimen size and air void content variability may lead to increased specimen-to-specimen variability in performance test results warrant further investigation. Therefore, the specimen-to-specimen variability of small specimens fabricated using the optimized approach was evaluated.

SPECIMEN-TO-SPECIMEN VARIABILITY ANALYSIS

Dynamic Modulus Test Results

The dynamic modulus test results of the specimen-to-specimen variability analysis (i.e., Phase III) for each mixture

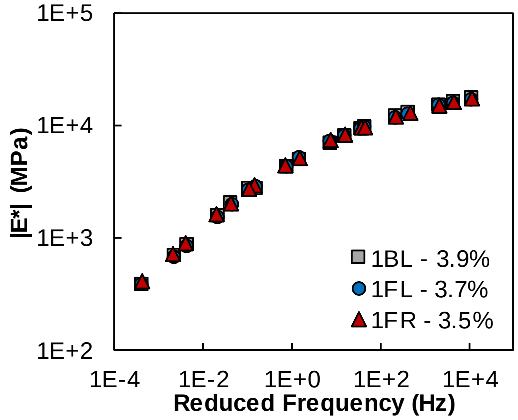

are shown in

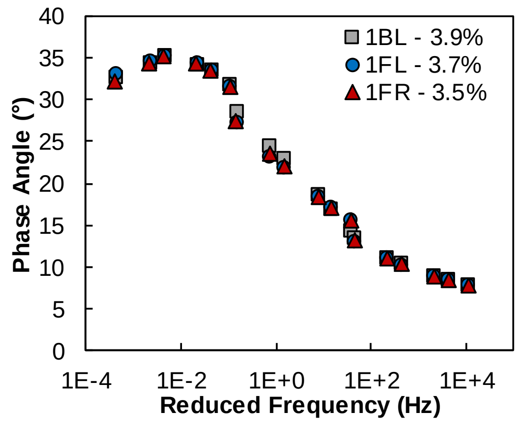

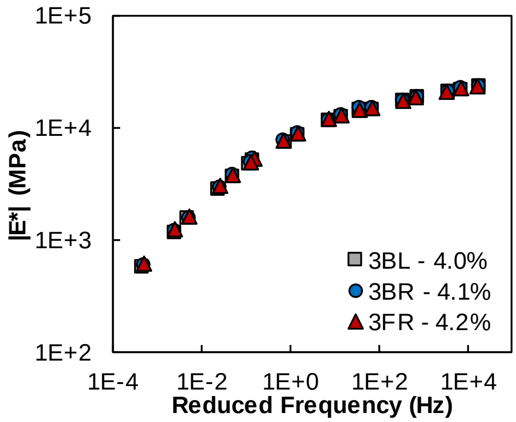

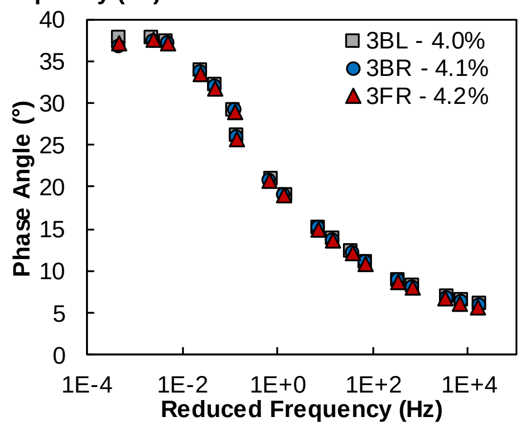

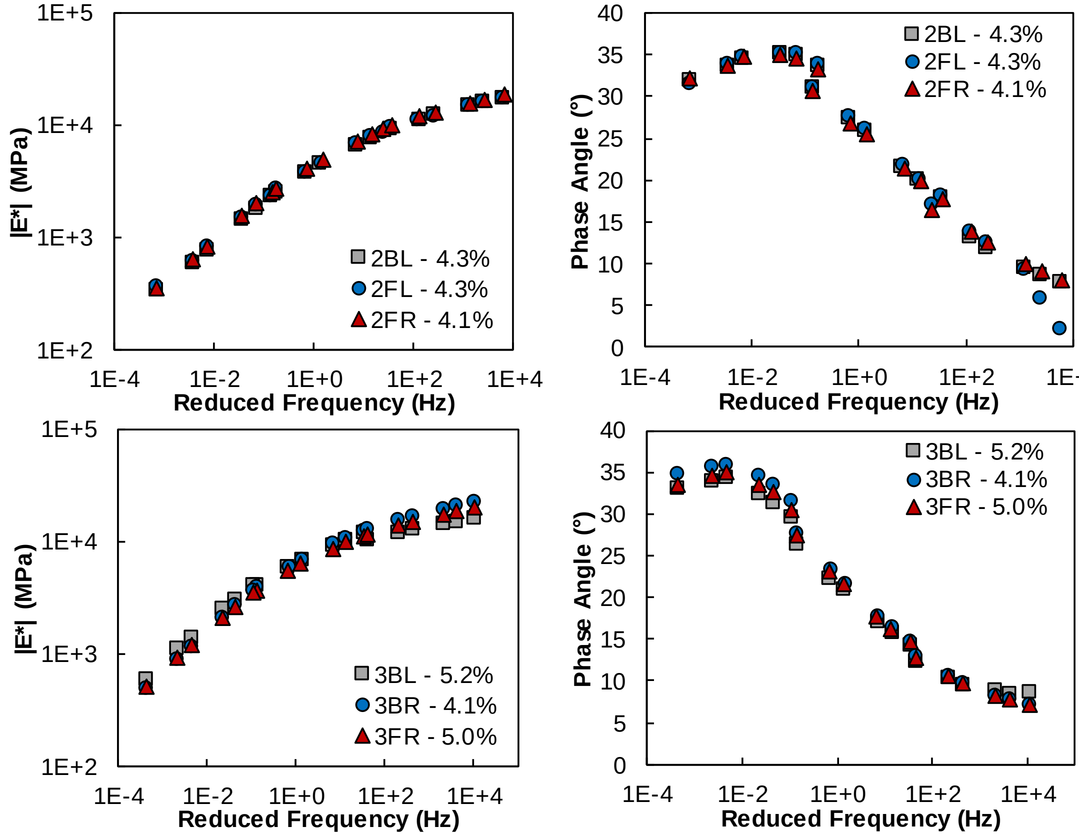

FIGURE 31. The legends within the results indicates the location from which the core was acquired and the air void content of the specimen. Results indicate very low specimen-to-specimen variability for all mixtures with the exception of the RB25.0B mixture. Note that the AMPT dynamic modulus specification, AASHTO TP 79, places repeatability requirements on test results that are NMAS dependent, suggesting an increase in specimen-to-specimen variability in dynamic modulus test results is also expected in large specimen testing (*4*). The relatively high variability observed in the RB25.0B mixture dynamic modulus test results could be caused by its relatively large NMAS or its relatively large specimen-to-specimen variability in air void content. The air void contents of the test specimens for the RS9.5D, SM12.5A, and RI19.0B-2 mixtures had a maximum range of 0.4% whereas the air void contents of the RB25.0B specimens had a considerably higher span of 1.2%.

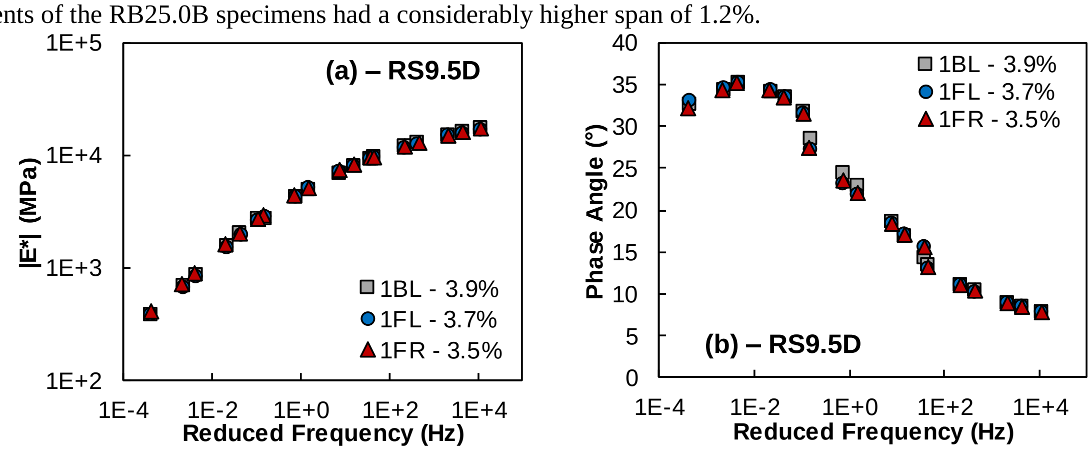

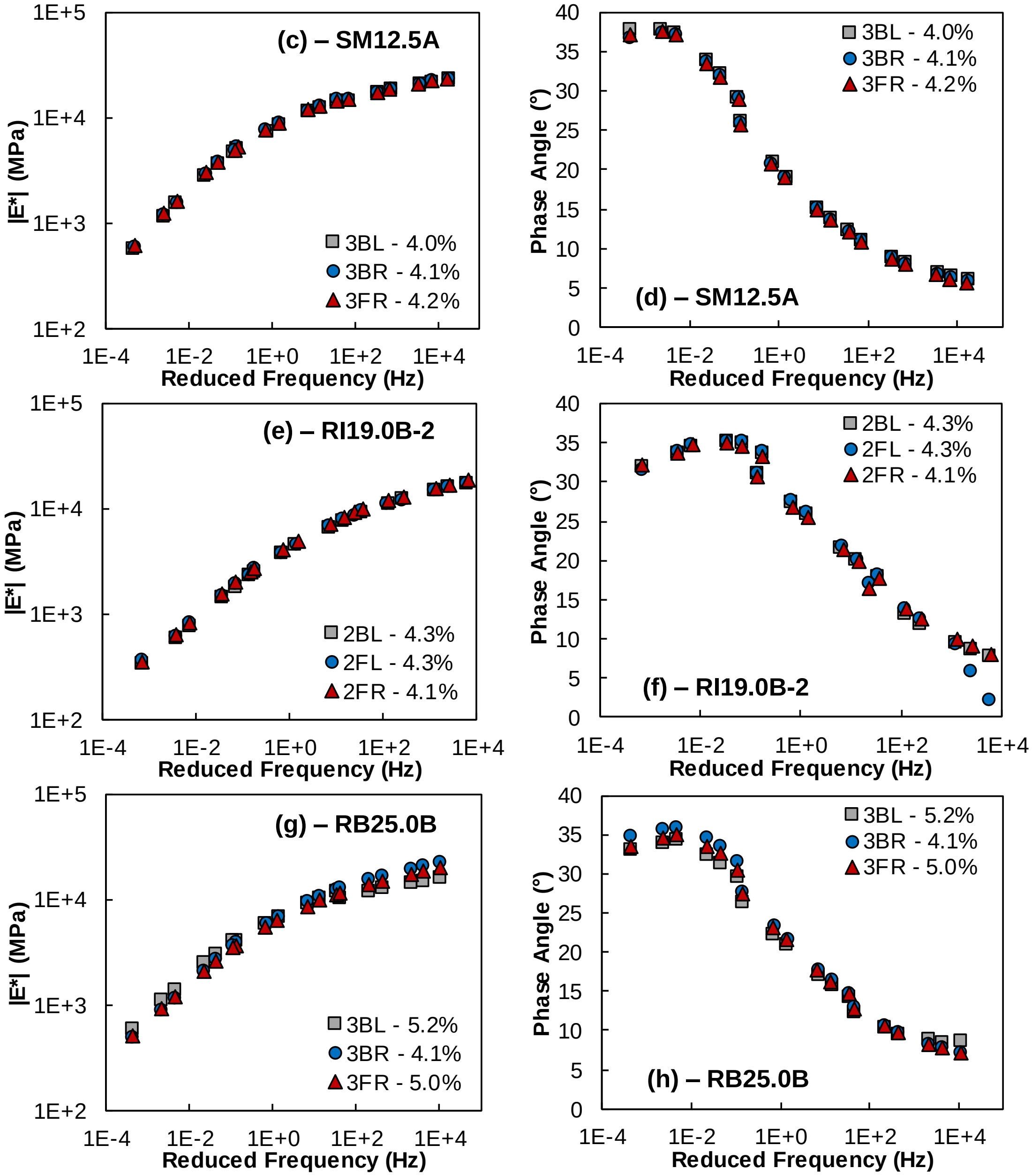

FIGURE 31 Dynamic modulus and phase angle mastercurves for sample-to-sample variability analysis.

Cyclic Fatigue Test Results

The fatigue damage characteristic curves and D^R failure criteria results for each mixture evaluated within the specimen-to-specimen variability study are shown in Figure 32. The end failure rate of the cyclic fatigue tests on each mixture is shown in Table 9. Recall that the D^R failure criterion is equal to the summation of $(1 - C)$ up to the point of failure divided by the number of cycles to failure for a given specimen (*13*). Thus, variability in test replicates can be visually observed in the cross plot of the summation of $(1 - C)$ up to the point of failure versus the number of cycles to failure. If there is low variability in the D^R values of test replicates, data points align to form a line that passes through the origin. Outliers and variability in the data can be observed by the deviation of data points from a best fit line of the summation of $(1 - C)$ up to the point of failure versus the number of cycles to failure. The legends within the results indicates the location from which the core was acquired and the air void content of the specimen.

Generally, the results demonstrate good agreement between the damage characteristic curves with an increase in variability with increasing mixture NMAS. Similarly, the failure criteria plots indicate generally low scatter with a small increase in scatter with increasing mixture NMAS. A low incidence of end failure was observed for all mixtures with no clear relationship to mixture NMAS. Note that the faded damage characteristic curves and corresponding failure criteria in Figure 32 correspond to irregular failures, including end failure and the presence of large voids or broken coarse aggregates on the failure surface. Generally, irregular failures corresponds to outlier behavior. It should be noted that while eight fatigue tests were conducted on each mixture, two data files were lost to corruption and thus, the results could not be included in Figure 32. It should also be noted that the plant operator who provided the RI19.0B-2 mixture indicated that the mixture was of poor quality, which likely contributed to the observed scatter in the results.

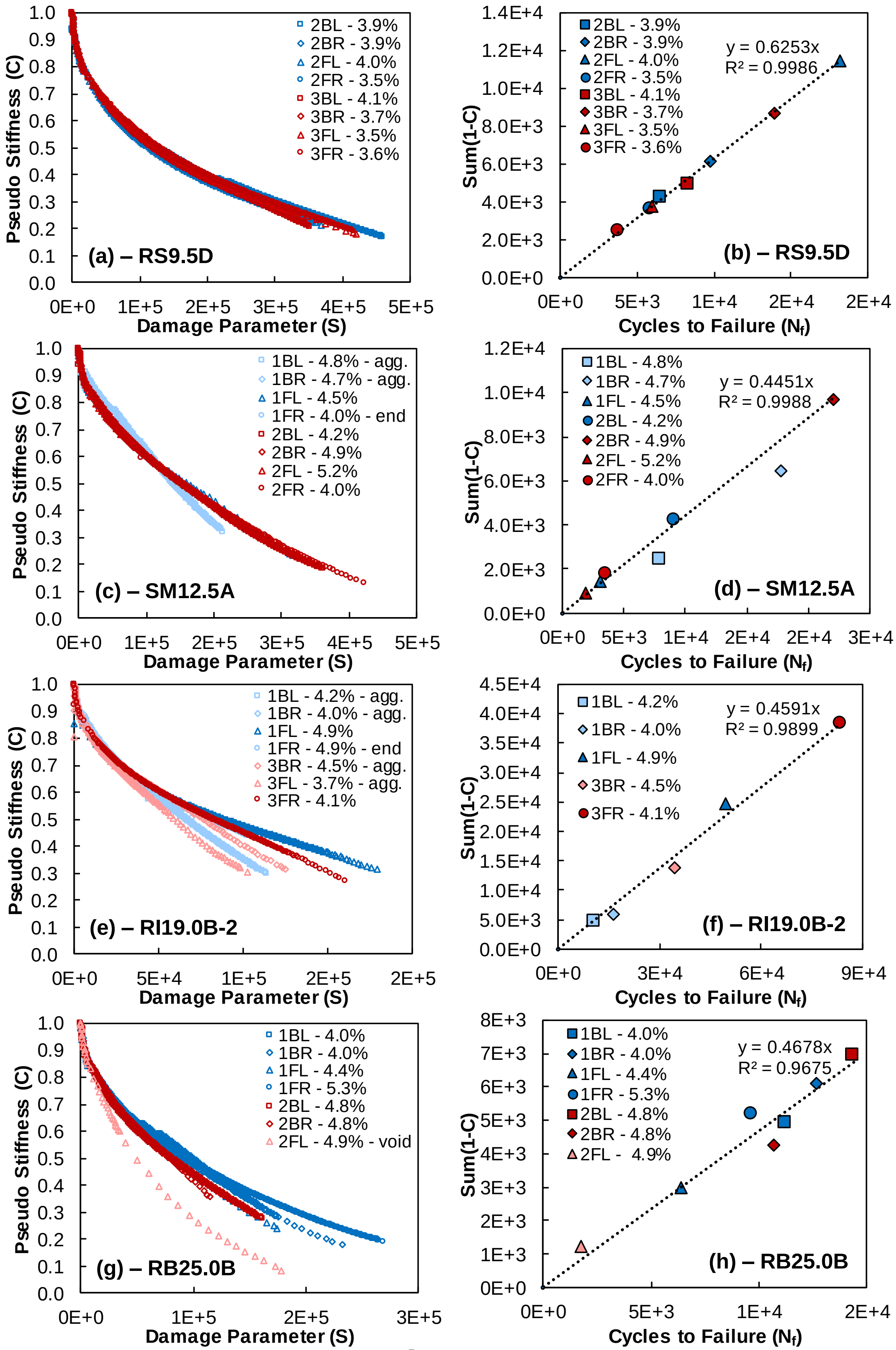

FIGURE 32 Damage characteristic curves and D^R failure criteria for sample-to-sample variability analysis.

TABLE 9 Cyclic Fatigue End Failure Rate

Mixture	End Failure Rate
RS9.5D	0/8
SM12.5A	1/8
RI19.0B-2	2/8
RB25.0B	0/8

Summary of Sample-to-Sample Variability Results

The results presented suggest that the vertical extraction of four small specimens from the inner 100-mm of gyratory samples is acceptable for the laboratory production of small specimens. It is apparent that specimen-to-specimen variability is generally higher for the 19.0-mm and 25.0-mm mixtures, compared to mixtures with smaller NMAS. The current dynamic modulus specification (AASHTO TP 79) places repeatability requirements on test results that are NMAS dependent. Thus, it is recommended that the same criterion be adopted for small specimen testing, which will force the testing of sufficient replicates to obtain reliable results. AASHTO TP 107 does not currently contain provisions for repeatability. Development of a parameter to quantify variability in fatigue testing is underway, but outside of the scope of this project. There was no clear relationship between the small specimen air void content and the performance test results within the observed specimen air void content range of ± 0.7%. Therefore, it is recommended that initial small specimen provisional standards include an air void content tolerance of ± 0.7%, to be refined upon ruggedness testing.

TECHNOLOGY TRANSFER EFFORTS

Several efforts to facilitate technology transfer have been undertaken. The research team participated in an AMPT User's Group meeting at the 2017 Transportation Research Board (TRB) Annual Meeting led by the Federal Highway Administration (FHWA). The research team discussed their small specimen geometry findings and answered questions from the audience.

In addition, the research team hosted a hands-on training workshop financially supported through the Performance Related Specification (PRS) project sponsored by the FHWA. The hands-on workshop was a two-day program where representatives from several agencies (FHWA, Maine Department of Transportation (DOT), Missouri DOT, North Carolina DOT, Oklahoma DOT, and the Western Federal Lands) were given training in small specimen fabrication, testing, and data analysis. The development of small specimen ancillary devices and testing platens was commenced with IPC Global, and their parent company Controls Group. Prototypes were provided by IPC Global for the workshop such that participants could gain hands-on experience with the commercially available equipment. IPC Global also implemented adjustments to the seating load for small specimen cyclic fatigue testing within their software per recommendations by the research team, which is available from IPC Global upon request for users with cyclic fatigue testing equipment. In addition, an Excel-based template, Flex-MAT™, has been developed that automates the analysis of small specimen performance test results and will be distributed by the FHWA to further aid in the technology transfer.

Draft AASHTO standards for the 38-mm diameter small cylindrical geometry are included in the Appendices of this report, including specimen fabrication and testing procedures for both dynamic modulus and cyclic fatigue. The draft standards have been developed in coordination with FHWA and were presented to the FHWA Expert Task Group in May 2017 for feedback before submission to AASHTO.

CONCLUSIONS AND RECOMMENDATIONS

The following summarizes the primary findings and recommendations:

- Small and large specimens generally have equivalent dynamic moduli at high and intermediate reduced frequency (i.e., low and intermediate temperature). At low reduced frequency (i.e., high temperature), small specimen dynamic moduli are typically statistically higher than large specimens. Therefore it is recommended to limit small specimen testing to the temperatures outlined in AASHTO PP 61.
- Analysis of dynamic modulus coefficients of variation indicates similar specimen-to-specimen repeatability in large and small specimen results. Therefore, it is recommended that the same specimen-to-specimen

variability requirements of large specimen testing be adopted initially, to be refined upon ruggedness testing.

- Results of cyclic direct tension testing indicate small specimens provide equivalent results to large specimens, given that small specimens do not experience significant aggregate breakage during testing.
- Small specimen monotonic fatigue test results coupled with VECD analysis produced damage characteristic curves which differed from cyclic tests. It was observed that monotonic fatigue testing led to more brittle failure than cyclic tests which is speculated to be the source of the differences in damage characteristic curves. Therefore, monotonic testing is not recommended for the fatigue characterization of asphalt mixtures.
- Pavement ME and FlexPAVE™ analyses indicate that use of small specimen results does not significantly influence pavement fatigue or permanent deformation prediction, indicating small specimen testing can be used for pavement performance prediction.
- The use of prismatic specimens does not influence dynamic modulus or direct tension test results compared to small cylindrical specimens. Fabrication of small prisms is more challenging than fabrication of small cylinders, therefore, small prisms should only be used when testing field cores with thin layers that prohibit extraction of 38-mm diameter cylinders.
- The horizontal extraction of small specimens from gyratory-compacted samples infringes on the peripheral region of the gyratory sample that has relatively high air void content. The air void gradient leads to end failure in fatigue testing, which prevents failure detection. This problem is alleviated by vertical coring.
- Anisotropy does not impact dynamic modulus test results and damage characteristic curves developed from cyclic fatigue test results. Due to the problems associated with horizontally extracted small specimen cyclic fatigue testing and insignificance of anisotropy, it is recommended that all small specimens be vertically extracted from gyratory-compacted samples for uniformity.
- The proposed laboratory small specimen fabrication procedure is to vertically core four specimens within the inner 100-mm diameter of gyratory-compacted samples.
- It is recommended that future research be conducted to investigate the differences between specimens taken from field cores and laboratory-compacted specimens. The findings pertaining to anisotropy were limited to gyratory compaction in this study.
- There was no clear relationship between the small specimen air void content and the performance test results within the observed specimen air void content range of ± 0.7%. Therefore, it is recommended that initial small specimen provisional standards include an air void content tolerance of ± 0.7%, to be refined upon ruggedness testing.
- It is recommended that the findings of this study be verified by the testing of additional materials with a broader set of characteristics (e.g., modifiers, high RAP contents, Reclaimed Asphalt Shingles (RAS)).

ACKNOWLEDGMENTS

Many thanks to our reviewers, Dave Mensching, Jo Sias Daniel, Stacey Diefenderfer, and Ben Bowers, whose feedback improved this report immensely. The FHWA assisted with the draft specifications, and organized the opportunities for technology transfer. Instrotek Inc., IPC Global, Controls Group, and the North Carolina State Precision Machine Shop are all due recognition for all their patience working to repeatedly improve the small specimen preparation and testing equipment. The North Carolina Department of Transportation provided support in acquiring materials, and the use of their AMPT for Phase III of this work. Asphalt materials were sourced primarily from the Fred Smith Company, with additional materials from the Carolina Sunrock Group. Thanks are also due to Farhad Yousefi Rad and Michael Elwardany for assisting in the initial designs of equipment, and David Wang for running the Pavement ME simulations.

REFERENCES

1. Bonaquist, R. *NCHRP Report 614: Refining the Simple Performance Tester for Use in Routine Practice*. Transportation Research Board of the National Academies, Washington, D.C., 2008.
2. Witczak, M. W., K. Kaloush, T. Peillinen, M. El-Basyouny, and H. Von Quintus. *NCHRP Report 465: Simple Performance Test for Superpave Mix Design*. Transportation Research Board of the National Academies, Washington, D.C., 2002.

3. American Association of State Highway and Transportation Officials. *Determining Dynamic Modulus of Hot Mix Asphalt (HMA),* AASHTO T 342, Washington D.C., 2015.
4. American Association of State Highway and Transportation Officials. *Determining the Dynamic Modulus and Flow Number of Asphalt Mixtures Using the Asphalt Mixture Performance Tester (AMPT),* AASHTO TP 79, Washington D.C., 2015.
5. Underwood, B. S., Y. R. Kim, and M. N. Guddati. Improved Calculation Method of Damage Parameter in Viscoelastic Continuum Damage Model. *International Journal of Pavement Engineering*, Vol. 11, No. 6, 2010, pp. 459-476.
6. American Association of State Highway and Transportation Officials. *Determining the Damage Characteristic Curve of Asphalt Concrete from Direct Tension Cyclic Fatigue Tests*, AASHTO TP 107, Washington D.C., 2015.
7. Kim, Y. R., Y. Seo, M. King, and M. Momen. Dynamic Modulus Testing of Asphalt Concrete in Indirect Tension Mode. *Transportation Research Record: Journal of the Transportation Research Board*, No. 1891, Transportation Research Board of the National Academies, Washington, D.C., 2004, pp. 163-173.
8. Kutay, M. E., N. Gibson, J. Youtcheff, and R. Dongre. Use of Small Samples to Predict Fatigue Lives of Field Cores: Newly Developed Formulation Based on Viscoelastic Continuum Damage Theory. *Transportation Research Record: Journal of the Transportation Research Board*, No. 2127, Transportation Research Board of the National Academies, Washington, D.C., 2009, pp. 90-97.
9. Marasteanu, M., A. C. Falchetto, M. Turos and J.-L. Le. *Development of a Simple Test to Determine the Low Temperature Strength of Asphalt Mixtures and Binders: IDEA Program Final Report, NCHRP IDEA 151.* Transportation Research Board of the National Academies, Washington, D.C., 2012.
10. Zofka, A., M. O. Marasteanu, and M. Turos. Determination of Asphalt Mixture Creep Compliance at Low Temperatures by Using Thin Beam Specimens. *Transportation Research Record: Journal of the Transportation Research Board,* No. 2057, Transportation Research Board of the National Academies, Washington, D.C., 2008, pp. 134–139.
11. Park, H. *Investigation of Primary Causes of Cracking in Asphalt Concrete*. Ph.D. dissertation, North Carolina State University, Raleigh, NC, 2013.
12. Park, H., and Y. R. Kim. Investigation into top-down cracking of asphalt pavements in North Carolina. *Transportation Research Record: Journal of the Transportation Research Board*, No. 2368, Transportation Research Board of the National Academies, Washington, D.C., 2013, pp. 45-55.
13. Park, H., M. Eslaminia and Y. R. Kim. Mechanistic evaluation of cracking in in-service asphalt pavements. *Materials and Structures*, Vol. 47, No. 8, 2014, pp. 1339–1358.
14. Li, X. and N. H. Gibson. Using Small Scale Specimens for AMPT Dynamic Modulus and Fatigue Tests. *Journal of the Association of Asphalt Paving Technologists*, Vol. 82, 2013, pp. 579-616.
15. Bowers, B. F., B. K. Diefenderfer, and S. D. Diefenderfer. Evaluation of Dynamic Modulus in Asphalt Paving Mixtures Utilizing Small-Scale Specimen Geometries. *Journal of the Association of Asphalt Paving Technologists*, Vol. 84, 2015, pp. 497-526.
16. Chehab, G.R., E. O'Quinn, and Y. R. Kim. Specimen Geometry Study for Direct Tension Test Based on Mechanical Tests and Air Void Variation in Asphalt Concrete Specimens Compacted by Superpave Gyratory Compactor. *Transportation Research Record: Journal of the Transportation Research Board*, No. 1723, Transportation Research Board of the National Academies, Washington, D.C., 2000, pp. 125-132.
17. Daniel, J. S. and Y. R. Kim. Development of a Simplified Fatigue Test and Analysis Procedure Using a Viscoelastic, Continuum Damage Model. *Journal of the Association of Asphalt Paving Technologists*, Vol. 71, 2002, pp. 619-650.
18. Underwood, B. S., and Y. R. Kim. Comprehensive Evaluation of Small Strain Viscoelastic Behavior of Asphalt Concrete. *Journal of Testing and Evaluation*, Vol. 40, No. 4, 2012, pp. 622-632.
19. American Association of State Highway and Transportation Officials. *Determining Dynamic Modulus of Hot Mix Asphalt (HMA),* AASHTO T 342, Washington D.C., 2015.
20. Witczak, M. W., "Draft Test Method DM-1 Standard Test method for Dynamic Modulus of Asphalt Concrete Mixtures," Superpave Support and Performance Models Management, NCHRP

9-19, Arizona State University, Tempe, AZ, 2002.
21. Pellinen, T. K., “Investigation of the Use of Dynamic Modulus as an Indicator of Hot-Mix Asphalt Performance,” Doctoral dissertation, Arizona State University, Tempe, AZ, 2001.
22. Pellinen, T. K., Xiao, S., and Raval, B.S. "Dynamic Modulus Testing of Thin Pavement Cores," Journal of ASTM International, Vol. 3, No. 4, 2006, pp. 1-14.

APPENDIX A

Standard Method of Practice for

Preparation of Small Cylindrical Performance Test Specimens Using the Superpave Gyratory Compactor (SGC) and Field Cores

AASHTO Designation: PP XX-XX

AASHTO
THE VOICE OF TRANSPORTATION

American Association of State Highway and Transportation Officials
444 North Capitol Street N.W., Suite 249
Washington, D.C. 20001

Standard Method of Test for

Preparation of Small Cylindrical Performance Test Specimens Using the Superpave Gyratory Compactor (SGC) or Field Cores

AASHTO Designation: PP XX-XX

AASHTO
THE VOICE OF TRANSPORTATION

1. SCOPE

1.1. This practice covers the use of a Superpave gyratory compactor (SGC) or field cores to prepare 38-mm-diameter by 110-mm-height performance test specimens for use in a variety of axial compression and tension performance tests. This practice is intended for dense-graded asphalt mixtures with nominal maximum aggregate sizes up to 25.0 mm.

1.2. *This standard may involve hazardous material, operations, and equipment. This standard does not purport to address all safety problems associated with its use. It is the responsibility of the user of this procedure to establish appropriate safety and health practices and to determine the applicability of regulatory limitations prior to use.*

2. REFERENCED DOCUMENTS

2.1. *AASHTO Standards*:

- R 30, Mixture Conditioning of Hot Mix Asphalt
- T 166, Bulk Specific Gravity (G_{mb}) of Compacted Hot Mix Asphalt (HMA) Using Saturated Surface Dry Specimens
- T 209, Theoretical Maximum Specific Gravity (G_{mm}) and Density of Hot Mix Asphalt (HMA)
- T 269, Percent Air Voids in Compacted Dense and Open Asphalt Mixtures
- T 312, Preparing and Determining the Density of Asphalt Mixture Specimens by Means of the Superpave Gyratory Compactor
- T 342, Determining the Dynamic Modulus of Hot Mix Asphalt (HMA)
- TP XX, Determining the Dynamic Modulus for Asphalt Mixtures Using Small Specimens in the Asphalt Mixture Performance Tester (AMPT)
- TP XX, Determining the Damage Characteristic Curve and Analysis Parameters Using Small Specimens in the Asphalt Mixture Performance Tester (AMPT) Cyclic Fatigue Test

2.2. *ASTM Standard*:

- D3549/D3549M, Standard Test Method for Thickness or Height of Compacted Bituminous Paving Mixture Specimens

3. TERMINOLOGY

3.1. *SGC specimen*—a 150-mm-diameter by 180-mm-tall (minimum) cylindrical specimen prepared in an SGC meeting the requirements of T 312.

3.2. *38-mm test specimen*—a 38-mm-diameter by 110-mm-tall cylindrical specimen that is cored and sawed from an SGC specimen.

3.3. *end perpendicularity*—the degree to which an end surface departs from being perpendicular to the axis of the cylindrical test specimen. This configuration is measured using a precision square with the beam touching the cylinder parallel to its axis (or prisms) and the blade touching the highest point on the end of the cylinder (or prism). The distance between the blade of the square and the lowest pint on the end of the cylinder is checked with 1.0-mm-diameter wire or feeler gauges.

3.4. *end planeness*—maximum departure of the specimen end from a plane. This dimension is checked using a straightedge and 0.5-mm-diameter wire or feeler gauges.

4. SUMMARY OF PRACTICE

4.1. This practice presents methods for extracting 38-mm-diameter by 110-mm-tall cylindrical test specimens from SGC specimens and field cores for use in a variety of axial compression and tension performance tests.

5. SIGNIFICANCE AND USE

5.1. This practice should be used to prepare specimens for TP XX (|E*|) and TP XX (fatigue).

5.2. This practice may also be used to prepare specimens for other tests requiring 38-mm-diameter by 110-mm-height cylindrical test specimens.

6. APPARATUS

6.1. *Superpave Gyratory Compactor*—Meeting the requirements of T 312 and capable of preparing 150-mm-diameter specimens that are a height of at least 180 mm.

6.2. *Mixture Preparation Equipment*—Balances, ovens, thermometers, mixer, pans, and other miscellaneous equipment needed to prepare SGC specimens in accordance with T 312, perform bulk specific gravity (G_{mb}) measurements in accordance with T 166, and perform maximum specific gravity (G_{mm}) measurements in accordance with T 209.

6.3. *Core Drill*—An air- or water-cooled, diamond-bit core drill capable of cutting cores to a nominal diameter of 38-mm and meeting the dimensional requirements of Section 9.5.4. The core drill shall be equipped with a fixture for holding the SGC specimens or field cores from which the test specimens are being extracted.

Note 1—Core drills with fixed and adjustable rotational speed have been used successfully to prepare specimens meeting the dimensional tolerances given in Section 9.5.4. Rotational speeds from 450 to 750 rpm have been used.

Note 2—Core drills with automatic and manual feed rate have been used successfully to prepare specimens meeting the dimensional tolerances given in Section 9.5.4.

6.4. *Masonry Saw*—An air- or water-cooled, diamond-bladed masonry saw capable of cutting specimens to a nominal length of 110 mm and meeting the tolerances for end perpendicularity and end flatness given in Section 9.5.4.

Note 3—Heavy duty tile saws with good stability have been found effective for sawing 38-mm-diameter specimens. Larger masonry saws may not produce specimens meeting the dimensional tolerances. Saws require a fixture to securely hold the specimen during sawing and to control the feed rate.

6.5. *Square*—Precision square with 8-in. beam and 12-in. blade. McMaster Carr Pro-Value Square, Catalog Number 2278A21 or equivalent.

6.6. *1.0-mm Diameter Carbon Steel Wire*—0.039-in. (1-mm) diameter carbon steel wire, McMaster Carr Catalog Number 8907K42 or equivalent.

6.7. *0.5-mm Diameter Carbon Steel Wire*—0.020-in. (0.5-mm) diameter carbon steel wire, McMaster Carr Catalog Number 8907K21 or equivalent.

6.8. *Feeler Gauges*—Tapered-leaf feeler gauges in 0.05-mm increments.

6.9. *Metal Ruler*—Capable of measuring 150-mm-long (nominal) specimens to the nearest 1 mm.

6.10. *Calipers*—Capable of measuring 100-mm-diameter (nominal) specimens to the nearest 0.1 mm.

7. HAZARDS

7.1. This practice and associated standards involve handling of hot asphalt binder, aggregates, and HMA. It also includes the use of sawing and coring machinery. Use standard safety precautions, equipment, and clothing when handling hot materials and operating machinery.

8. STANDARDIZATION

8.1. Items associated with this practice that require calibration or verification are included in the AASHTO standards referenced in Section 2. Refer to the pertinent section of the referenced standards for information concerning calibration or verification.

9. PROCEDURE A – FABRICATION FROM GYRATORY SPECIMENS

9.1. *Asphalt Mixture Preparation:*

9.1.1. Prepare asphalt mixture for each SGC specimen in accordance with T 312 and prepare a companion test specimen for maximum specific gravity (G_{mm}) in accordance with T 209.

9.1.2. The mass of asphalt mixture needed for each specimen will depend on the SGC specimen height, the G_{mm} of the mixture, the nominal maximum aggregate size, gradation (coarse or fine), and target air void content of the test specimens.

Note 4—Appendix X1 describes one procedure for determining the mass of asphalt mixture required to reach a specified test specimen target air void content.

9.1.3. Perform conditioning on the asphalt mixture for the test specimens and companion G_{mm} sample in accordance with R 30.

9.2. *SGC Specimen Compaction:*

9.2.1. Compact the SGC specimens to a height of 180 mm or higher, in accordance with T 312, carefully following the exceptions noted.

9.2.2. Pour the mixture into the center of the mold to minimize air void variation between samples. Pouring material down the sides of the mold will result in lower air voids on that side of the mold.

9.2.3. Charge the mold in two equal lifts, and rod the sample 20 times after each lift, to minimize vertical air void variance.

9.3. *Long-Term Conditioning (optional):*

9.3.1. If it is desired to simulate long-term aging, condition the SGC specimen in accordance with R 30.

9.3.2. To obtain accurate volumetric measurements on the long-term-conditioned specimens, also condition a sample of short-term-conditioned loose asphalt mixture meeting the sample size requirements of T 209 in accordance with R 30.

9.4. *SGC Specimen Density and Air Voids (Optional):*

9.4.1. Determine the G_{mm} of the asphalt mixture in accordance with T 209. If long-term conditioning has been used, determine the G_{mm} on the long-term-conditioned loose asphalt mixture. Record the G_{mm} of the mixture.

9.4.2. Determine G_{mb} of the SGC specimen in accordance with T 166. Record the G_{mb} of the SGC specimen.

9.4.3. Compute the air void content of the SGC specimen in accordance with T 269. Record the air void content of the SGC specimen.

Note 5—Section 9.4 is optional because acceptance of the test specimen for mechanical property testing is based on the air void content of the test specimen, not the SGC specimen. However, monitoring SGC specimen density can identify improperly prepared specimens early in the specimen fabrication process. Information on SGC specimen air voids and test specimen air voids will also assist the laboratory in establishing potentially more precise methods than Appendix X1 for preparing test specimens to a target air void content

9.5. *Test Specimen Preparation:*

9.5.1. Prepare the gyratory specimen by marking the location(s) where the cores will be taken. All cores must be taken within the inner 100 mm of the gyratory specimen. As many as four 38-mm diameter cores can be extracted from one gyratory specimen, as shown by the gray circles in Figure 1. The optimal lines to mark to extract four gyratory specimens are shown in white in Figure 1.

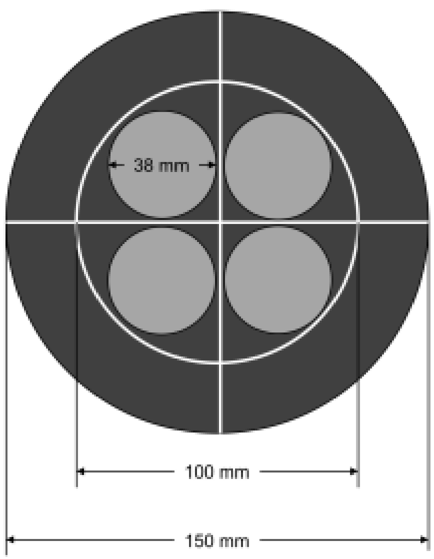

Figure 1-Graphic of a marked gyratory specimen

9.5.2. Drill a core of nominal diameter of 38 mm from the SGC specimen. Both the SGC specimen and the drill shall be adequately supported to ensure that the resulting core is cylindrical with sides that are smooth, parallel, and meet the tolerances on specimen diameter given in Table 1.

9.5.3. Saw the ends of the core to obtain a test specimen of a nominal height of 110 mm. Both the core and the saw shall be adequately supported to ensure that the resulting test specimen meets the tolerances given in Table 1 for height, end flatness, and end perpendicularity.

Note 6—With most equipment, it is better to perform the coring before the sawing. However, these operations may be performed in either order as long as the dimensional tolerances in Table 1 are satisfied.

9.5.4. Test specimens shall meet the dimensional tolerances given in Table 1.

Table 1—Test Specimen Dimensional Tolerances

Item	Specification	Method Reference
Average diameter	36 to 40 mm	9.5.4.1
Standard deviation of diameter	[illegible]	9.5.4.1
Height	107.5 to 112.5 mm	9.5.4.2
End flatness	[illegible]	9.5.4.3
End perpendicularity	[illegible]	9.5.4.4

9.5.4.1. Using calipers, measure the diameter at the center and third points of the test specimen along axes that are 90 degrees apart. Record each of the six measurements to the nearest 0.1 mm. Calculate the average and the standard deviation of the six measurements. Reject specimens not meeting the average and the standard deviation requirements given in Table 1. The average diameter, reported to the nearest 0.1 mm, shall be used in all material property calculations.

9.5.4.2. Measure the height of the test specimen in accordance with ASTM D3549/D3549M. Reject specimens with an average height outside the height tolerance listed in Table 1. Record the average height.

9.5.4.3. Using the blade of the precision square as a straightedge, check the flatness of each end at three locations approximately 120 degrees apart. At each location, place the blade of the precision square across the diameter of the specimens and check the maximum departure of the specimen from the blade using the 0.5-mm-diameter carbon steel wire or feeler gauge. Reject specimens if the 0.5-mm-diameter carbon steel wire fits between the blade and the specimen at any location.

9.5.4.4. Check the perpendicularity of each end of the specimen using the precision square and the 1.0 mm carbon steel wire at two locations approximately 90 degrees apart. Place the precision square on a table with the beam in contact with the table and the blade extending vertically. Place the long axis of the specimen on the beam such that the blade is in contact with the end of the specimen. Check the maximum departure of the specimen from the blade using the 1.0-mm-diameter carbon steel wire or feeler gauge. Reject any specimens if the 1.0-mm-diameter carbon steel wire fits between the blade and the specimen at any location.

9.6. *Test Specimen Density and Air Voids:*

9.6.1. Determine the G_{mm} of the asphalt mixture in accordance with T 209. If long-term conditioning has been used, determine the G_{mm} on the long-term-conditioned loose asphalt mixture. Record the G_{mm} of the mixture.

9.6.2. Determine G_{mb} of the test specimen in accordance with T 166. Record the G_{mb} of the SGC specimen.

Note 7—When wet-coring and sawing methods are used, measure the immersed mass, followed by the surface-dry mass followed by the dry mass, to minimize drying time and expedite the specimen fabrication process.

9.6.3. Compute the air void content of the SGC specimen in accordance with T 269. Record the air void content of the SGC specimen.

9.7. *Test Specimen Storage:*

9.7.1. Mark the test specimen with a unique identification number.

9.7.2. Store the test specimen, until tested, on its end on a flat shelf in a room with the temperature controlled between 15 and 27ºC.

Note 8—Definitive research concerning the effects of test specimen aging on various mechanical property tests has not been completed. Some users enclose specimens in plastic wrap, or minimize specimen storage time to two weeks, or both.

10. PROCEDURE B – FABRICATION FROM FIELD CORES

10.1. *Field Core Preparation:*

10.1.1. Obtain sufficient field cores for all testing and additional cores to provide sufficient material to conduct the maximum specific gravity (G_{mm}) test in accordance with T 209.

10.1.2. Mark the direction of traffic on the field core before coring in the field, if possible. Otherwise evaluate the field core and select the most probable direction of traffic.

10.1.3. Reduce the size of the field core, if needed, using the saw to make the field core a geometry which can be held stable by the fixture for coring and is suitable for extracting one or more specimens perpendicular to the direction of traffic. Before cutting, mark the direction of traffic on all sections of the field core.

10.2. *Test Specimen Preparation:*

10.2.1. Prepare the field core by marking where the cores will be taken. Two 38-mm diameter cores can be extracted from one 6-inch diameter field core, as shown by the gray rectangles in Figure 2. Additional samples may be extracted from larger field cores, provided the samples are all extracted perpendicular to the direction of traffic.

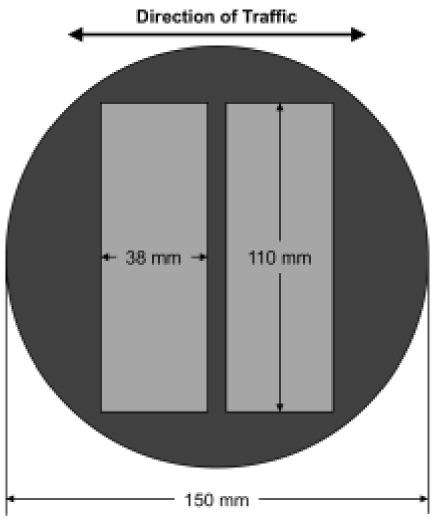

Figure 1-Graphic of samples extracted from a 6-inch field core

10.2.2. Drill a core of nominal diameter of 38 mm from the SGC specimen. Both the field core and the drill shall be adequately supported to ensure that the resulting core is cylindrical with sides that are smooth, parallel, and meet the tolerances on specimen diameter given in Table 1.

10.2.3. Saw the ends of the core to obtain a test specimen of a nominal height of 110 mm. Both the core and the saw shall be adequately supported to ensure that the resulting test specimen meets the tolerances given in Table 1 for height, end flatness, and end perpendicularity.

Note 9—With most equipment, it is better to perform the coring before the sawing. However, these operations may be performed in either order as long as the dimensional tolerances in Table 2 are satisfied.

10.2.4. Test specimens shall meet the dimensional tolerances given in Table 1.

10.3. *Test Specimen Density and Air Voids:*

10.3.1. Procure sufficient material from separate field cores to determine the G_{mm} of the asphalt mixture in accordance with T 209.

10.3.2. Determine G_{mb} of the SGC specimen in accordance with T 166. Record the G_{mb} of the SGC specimen.

Note 10—When wet-coring and sawing methods are used, measure the immersed mass, followed by the surface-dry mass followed by the dry mass, to minimize drying time and expedite the specimen fabrication process.

10.3.3. Compute the air void content of the SGC specimen in accordance with T 269. Record the air void content of the SGC specimen

10.4. *Test Specimen Storage:*

10.4.1. Mark the test specimen with a unique identification number.

10.4.2. Store the test specimen, until tested, on its end on a flat shelf in a room with the temperature controlled between 15 and 27ºC.

Note 11—Definitive research concerning the effects of test specimen aging on various mechanical property tests has not been completed. Some users enclose specimens in plastic wrap, or minimize specimen storage time to two weeks, or both.

11. REPORTING

11.1. *Report the following information:*

11.1.1. Unique test specimen identification number;

11.1.2. Mixture design data including design compaction level and air void content, asphalt binder type and grade, binder content, binder specific gravities, aggregate types and specific gravities, aggregate consensus properties, and G_{mm};

11.1.3. Type of conditioning used;

11.1.4. G_{mm} for the conditioned specimens;

11.1.5. SGC specimen target height (optional);

11.1.6. SGC specimen G_{mb} (optional);

11.1.7. SGC specimen air void content (optional);

11.1.8. Test specimen average height;

11.1.9. Test specimen average diameter;

11.1.10. Test specimen G_{mb};

11.1.11. Test specimen air void content;

11.1.12. Test specimen end flatness for each end;

11.1.13. Test specimen end perpendicularity for each end; and

11.1.14. Remarks concerning deviations from this standard practice.

12. KEYWORDS

12.1. Gyratory compaction; performance test specimens

APPENDIXES

(Nonmandatory Information)

X1. METHOD FOR ACHIEVING A TARGET AIR VOID CONTENT

X1.1. *Purpose:*

X1.1.1. This appendix presents a procedure for estimating the mass of asphalt mixture required to produce test specimens at a target air void content. It was developed to avoid compacting repeat trial specimens. A trial and error method which may use less material is available in PP 60 Appendix X1.

X1.1.2. This procedure can be used with either plant-produced or laboratory-prepared asphalt mixtures.

X1.2. *Summary:*

X1.2.1. An estimate of the mass of mixture required is made knowing the maximum specific gravity of the mixture, G_{mm}, and the volume of the gyratory specimen.

X1.2.2. Three trial specimens are compacted to the target height, one at the target mass and the other two at the target mass ±100 grams. 100-mm diameter by 150-mm height specimens are extracted from each of the gyratory specimens.

X1.2.3. The air void contents of the trial specimens are measured and used to develop a relationship between gyratory specimen mass and test specimen air voids.

X1.3. *Procedure:*

X1.3.1. Measure the maximum specific gravity, G_{mm}, of the mixture in accordance with T 209.

X1.3.2. Calculate the mass of the mixture required for a gyratory specimen of target height, H, using Equation X1.1:

$$\text{Mass} = \left[\frac{100-(Va_t+F)}{100}\right] * G_{mm} * 176.7147 * H \quad (X1.1)$$

where:

Mass = estimated mass of mixture to prepare a test specimen to the target air voids, g

Va_t = target air void content for the test specimen, percent by volume

G_{mm} = maximum specific gravity for the mixture

H = height of the gyratory specimen, cm

F = air void adjustment factor: 1.0 for fine-graded; 1.5 for coarse-graded

X1.3.3. Using the estimated mass from Equation X1.1, prepare three trial gyratory specimens at the target mass and ±100 grams. Extract 100-mm diameter by 150-mm height specimens from each of the gyratory specimens.

X1.3.4. Measure the bulk specific gravity of the trial test specimens and calculate the air void content of the trial test specimens in accordance with Section 9.6.

X1.3.5. Prepare a plot of the gyratory specimen mass against the test specimen air void content. Fit a line to the three points as shown in Figure X1.1.

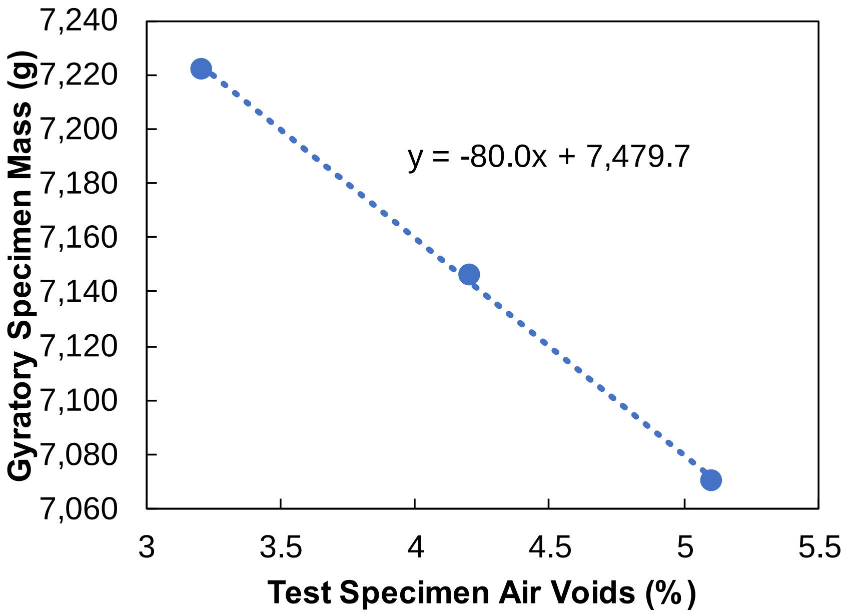

Figure X1.1-Example of Air Void Relationship Plot with Fitted Line and Equation

X1.3.6. Use the fitted line to determine the mass needed for the specific target air voids.

X1.3.7. This procedure does require three specimens, but it avoids the repeat compaction which may be needed in a trial-and-error procedure.

APPENDIX B

Standard Method of Test for

Determining the Dynamic Modulus for Asphalt Mixtures Using Small Specimens in the Asphalt Mixture Performance Tester (AMPT)

AASHTO Designation: TP XX-XX

AASHTO
THE VOICE OF TRANSPORTATION

American Association of State Highway and Transportation Officials
444 North Capitol Street N.W., Suite 249
Washington, D.C. 20001

Standard Method of Test for

Determining the Dynamic Modulus for Asphalt Mixtures Using Small Specimens in the Asphalt Mixture Performance Tester (AMPT)

AASHTO Designation: TP XX-XX

AASHTO
THE VOICE OF TRANSPORTATION

1. SCOPE

1.1. This standard describes test methods for measuring the dynamic modulus and flow number for hot mix asphalt (HMA) using the Asphalt Mixture Performance Tester (AMPT). This practice is intended for dense-graded mixtures with nominal-maximum aggregate sizes up to 25.0 mm.

1.2. *This standard may involve hazardous material, operations, and equipment. This standard does not purport to address all safety problems associated with its use. It is the responsibility of the user of this procedure to establish appropriate safety and health practices and to determine the applicability of regulatory limitations prior to use.*

2. REFERENCED DOCUMENTS

2.1. *AASHTO Standards*:

- PP XX, Preparation of 38-mm Diameter Cylindrical Performance Test Specimens Using the Superpave Gyratory Compactor (SGC)
- TP 79, Determining the Dynamic Modulus and Flow Number for Asphalt Mixtures Using the Asphalt Mixture Performance Tester (AMPT)

2.2. *Other Document*:

- NCHRP Report 629, *Equipment Specifications for the Simple Performance Test System, Appendix E*, October 16, 2007

3. TERMINOLOGY

3.1. *dynamic modulus,* |E*|—the absolute value of the complex modulus calculated by dividing the peak-to-peak stress by the peak-to-peak strain for a material subjected to a sinusoidal loading.

3.2. *phase angle, δ*—the angle in degrees between a sinusoidally applied stress and the resulting strain in a controlled stress test.

4. SUMMARY OF METHOD

4.1. This test method describes the procedure for measuring the dynamic modulus of HMA. A test specimen at a specific test temperature is subjected to a controlled sinusoidal (haversine) compressive stress of various frequencies. The applied stresses and resulting axial strains are measured as a function of time and used to calculate the dynamic modulus and phase angle.

5. SIGNIFICANCE AND USE

5.1. The dynamic modulus is a performance-related property that can be used for mixture evaluation and for characterizing the stiffness of HMA for mechanistic-empirical pavement design.

6. APPARATUS

6.1. *Specimen Fabrication Equipment*—For fabricating dynamic modulus test specimens as described in PP XX.

6.2. *Dynamic Modulus Test System*—Meeting the requirements of the equipment specification for the Simple Performance Test (SPT) System, Version 3.0.

6.3. *Conditioning Chamber*—An environmental chamber for conditioning the test specimens to the desired testing temperature. The environmental chamber shall be capable of controlling the temperature of the specimen over a temperature range from 4 to 60°C to an accuracy of ±0.5°C. The chamber shall be large enough to accommodate the number of specimens to be tested plus a “dummy” specimen with a temperature sensor mounted in the center for temperature verification.

6.4. *Teflon Sheet*—0.25 mm thick, to be used as a friction reducer between the specimen and the loading platens in the dynamic modulus test.

7. HAZARDS

7.1. This practice and associated standards involve handling of hot asphalt binder, aggregates, and HMA. It also includes the use of sawing and coring machinery and servo-hydraulic testing equipment. Use standard safety precautions, equipment, and clothing when handling hot materials and operating machinery.

8. STANDARDIZATION

8.1. Verification with Proving Ring:

8.1.1. Verify the normal operation of the AMPT weekly or at the beginning of a new testing program using the manufacturer-provided proving ring. Perform a dynamic modulus test on the proving ring using a target strain of 100 microstrain at 1.0 Hz. The dynamic modulus of the proving ring should be within ±3 percent of the value obtained on the proving ring for the same testing conditions during the last calibration.

8.2. *Calibration:*

8.2.1. The following systems on the AMPT shall be calibrated annually, when the AMPT system is moved, or when any of its components are changed:

- Load Measuring System
- Actuator Displacement Measuring System
- Specimen-Mounted Deformation Measuring System
- Confining Pressure Measuring System
- Temperature Measuring System

Methods for calibration of each of these systems are available in AASHTO TP 79, Annex B.

---

9. PROCEDURE

9.1. *Test Specimen Fabrication:*

9.1.1. Testing shall be performed on 38-mm diameter by 110-mm tall small test specimens fabricated in accordance with PP XX.

9.1.2. Prepare three test specimens at the target air void content ±0.5 percent and with the aging condition in accordance with PP XX.
Note 1—The coefficient of variation for properly conducted dynamic modulus tests is approximately 13 percent. The coefficient of variation of the mean dynamic modulus for tests on multiple specimens is given in Table 1.

9.2. *Test Specimen Instrumentation (Standard Glued-Gauge-Point System):*

9.2.1. Attach the gauge points to the specimen in accordance with the manufacturer's instructions.

9.2.2. Confirm that the gauge length is 70 mm ± 1 mm, measured center-to-center of the gauge points.

9.3. *Loading Platens and End-Friction Reducers:*

9.3.1. For the dynamic modulus test, the top platen shall be free to rotate.

9.3.2. Teflon end-friction reducers are made from 0.25-mm thick Teflon sheet, cut to a size slightly larger than the loading platen.

9.4. *Procedure:*

9.4.1. Place the specimens to be tested in the environmental chamber with the “dummy” specimen and monitor the temperature of the “dummy” specimen to determine when testing can begin.

9.4.2. Place platens and friction reducers inside the testing chamber. Turn on the AMPT, set the temperature control to the desired testing temperature, and allow the testing chamber to equilibrate at the testing temperature for at least 1 h.

9.4.3. When the “dummy” specimen and the testing chamber reach the target temperature, open the testing chamber. Remove a test specimen from the conditioning chamber and quickly place it in the testing chamber.

9.4.4. Assemble the specimen to be tested with platens in the following order from bottom to top: bottom loading platen, bottom friction reducer, specimen, top friction reducer, and top loading platen.

9.4.5. Install the specimen-mounted deformation-measuring system on the gauge points per the manufacturer’s instructions. Ensure that the deformation-measuring system is within its calibrated range. Ensure that the top loading platen is free to rotate during loading.

9.4.6. Close the testing chamber and allow the chamber temperature to return to the testing temperature.

9.4.7. Procedures in Sections 9.4.3 through 9.4.6, including the return of the test chamber to the target temperature, shall be completed in 5 min.

9.4.8. Enter the required identification and control information into the dynamic modulus software.

9.4.9. Follow the software prompts to begin the test. The AMPT will automatically unload when the test is complete and will display the test data and data quality indicators.

9.4.10. Review the data quality indicators as discussed in Section 9.5. Retest specimens with data quality indicators above the values specified in Section 9.5.

9.4.11. Once acceptable data have been collected, open the test chamber and remove the tested specimen. Repeat procedures in Sections 9.4.3 through 9.4.11 for the remaining test specimens.

9.5. *Computations and Data Quality:*

9.5.1. The calculation of dynamic modulus, phase angle, and the data quality indicators is performed automatically by the AMPT software.

9.5.2. Accept only test data meeting the data quality statistics given in Table 1. Table 2 summarizes actions that can be taken to improve the data quality statistic. Repeat tests as necessary to obtain test data meeting the data quality statistics requirements.

Table 1—Data Quality Statistics Requirements

Data Quality Statistic	Limit
Deformation drift	In direction of applied load
Peak-to-peak strain	50 to 75 μstrain
Load standard error	10%
Deformation standard error	10%
Deformation uniformity	30%
Phase uniformity	3°

Note 2—The data quality statistics in Table 1 are reported by the AMPT. If a dynamic modulus test system other than the AMPT is used, refer to the equipment specification for the Simple Performance Test (SPT) System, Version 3.0, for algorithms for the computation of dynamic modulus, phase angle, and data quality statistics.

Table 2—Data Quality Statistics Requirements

Item	Cause	Possible Solutions
Deformation drift not in direction of applied load	Gauge points are moving apart	Reduce LVDT spring force. Add compensation springs. Reduce test temperature.
Peak-to-peak strain too high	Load level too high	Reduce load level.
Peak-to-peak strain too low	Load level too low	Increase load level.
Load standard error >10%	Applied load not sinusoidal	Adjust tuning of hydraulics.
Deformation standard error >10%	1. Deformation not sinusoidal 2. Loose gauge point 3. Excessive noise on deformation signals 4. Damaged LVDT	1. Adjust tuning of hydraulics. 2. Check gauge points. Reinstall if loose. 3. Check wiring of deformation sensors. 4. Replace LVDT.
Deformation uniformity >30%	1. Eccentric loading 2. Loose gauge point 3. Sample ends not parallel 4. Poor gauge point placement 5. Non-uniform air void distribution	1. Ensure specimen is properly aligned. 2. Check gauge points. Reinstall if loose. 3. Check parallelism of sample ends. Mill ends if out of tolerance. 4. Check for specimen non-uniformity (segregation, air voids). Move gauge points. 5. Ensure test specimens are cored from the middle of the gyratory specimen.
Phase uniformity >3°	1. Eccentric loading 2. Loose gauge point 3. Poor gauge point placement 4. Damaged LVDT	1. Ensure specimen is properly aligned. 2. Check gauge points. Reinstall if loose. 3. Check for specimen non-uniformity (segregation, air voids). Move gauge points. 4. Replace LVDT.

9.6. *Reporting:*

9.6.1. For each specimen tested, report the following:

9.6.1.1. Test temperature,

9.6.1.2. Test frequency;

9.6.1.3. Confining stress level,

9.6.1.4. Dynamic modulus,

9.6.1.5. Phase angle, and

9.6.1.6. Data quality statistics.

9.6.2. Attach the AMPT dynamic modulus test summary report for each specimen tested.

10. KEYWORDS

10.1. AMPT; dynamic modulus; phase angle.

APPENDIXES

(Nonmandatory Information)

X1. USE OF ALTERNATIVE SMALL SPECIMEN GEOMETRIES

X1.1. *Alternative small specimen geometries*—Test specimens of geometries other than the one specified can be obtained from constructed pavement layers to measure the dynamic modulus for use in applications such as forensic investigations and field monitoring of test sections. Specimens with a diameter of 50 mm can be used where there are concerns about the use of 38-mm specimens. Prismatic specimens 25 mm by 50 mm by 110 mm have also been evaluated for thinner construction lifts; if diameter is needed for prismatic specimens, calculate the cross-sectional area and then calculate the effective circular diameter that yields the same cross-sectional area.

X1.2. *Alternative geometry test equipment*—The same gauge points, same gauge length, and same on-specimen deformation sensors are used. Alternate end plates should be designed or procured with to match the specimen geometry, as well as the end friction reducers.

APPENDIX C

Standard Method of Test for

Determining the Damage Characteristic Curve and Failure Criterion Using Small Specimens in the Asphalt Mixture Performance Tester (AMPT) Cyclic Fatigue Test

AASHTO Designation: TP XX-XX

American Association of State Highway and Transportation Officials
444 North Capitol Street N.W., Suite 249
Washington, D.C. 20001

Standard Method of Test for

Determining the Damage Characteristic Curve and Failure Criterion Using Small Specimens in the Asphalt Mixture Performance Tester (AMPT) Cyclic Fatigue Test

AASHTO Designation: TP XX-XX

1. SCOPE

1.1. This test method covers procedures for preparing and testing asphalt concrete mixture specimens to determine the damage characteristic curve and fatigue analysis parameters via direct tension cyclic fatigue test using the Asphalt Mixture Performance Tester (AMPT).

1.2. This standard is intended for dense-graded mixtures with nominal maximum size aggregate less than or equal to 25.0 mm (0.98 in.). Mixtures with a nominal maximum aggregate size greater than 25.0 mm (0.98 in.) should be tested following TP 107.

1.3. *This standard may involve hazardous material, operations, and equipment. This standard does not purport to address all safety problems associated with its use. It is the responsibility of the user of this procedure to establish appropriate safety and health practices and to determine the applicability of regulatory limitations prior to use.*

2. REFERENCED DOCUMENTS

2.1. *AASHTO Standards*:

- PP 61, Developing Dynamic Modulus Master Curves for Asphalt Mixtures Using the Asphalt Mixture Performance Tester (AMPT)
- PP XX, Preparation of 38-mm Diameter Cylindrical Performance Test Specimens Using the Superpave Gyratory Compactor (SGC)
- R 30, Mixture Conditioning of Hot Mix Asphalt (HMA)
- R 62, Developing Dynamic Modulus Master Curves for Asphalt Mixtures
- TP 79, Determining the Dynamic Modulus and Flow Number for Asphalt Mixtures Using the Asphalt Mixture Performance Tester (AMPT)
- TP XX, Determining the Dynamic Modulus for Asphalt Mixtures Using Small Specimens in the Asphalt Mixture Performance Tester (AMPT)

2.2. *ASTM Standards*:

- E 4, Standard Practices for Force Verification of Testing Machines

2.3. *Other Document*:

- NCHRP Report 629, *Equipment Specifications for the Simple Performance Test System, Appendix E*, October 16, 2007.
- FHWA Report, *Development of Asphalt Mixture Performance Related Specifications, Final Report of Project DTFH61-08-H-00005*, In Press, 2017.

3. TERMINOLOGY

3.1. *alpha term* (α)—value corresponding to the slope of the relaxation modulus master curve which is used in the accumulation of damage with time.

3.2. *average rate of dissipated pseudo strain energy per cycle* (G^R)—parameter used in the failure criterion for fatigue performance which is generated from a pseudo strain energy density function relating pseudo strain and damage.

3.3. *complex modulus* (E^*)—a complex number that defines the relationship between stress and strain for a linear viscoelastic material.

3.4. *cyclic pseudo secant modulus* (C^*)—the secant modulus in stress–pseudo strain space for a single cycle. This pseudo modulus differs from C because it is computed using a steady-state assumption and is used only with cycle-based data.

3.5. *damage* (S)—the internal state variable that quantifies microstructural changes in asphalt concrete.

3.6. *damage characteristic curve* (*C versus S curve*)—the curve formed when plotting the damage on the x-axis and the pseudo secant modulus on the y-axis. It defines the unique relationship between the structural integrity and amount of damage in a given mixture.

3.7. *dynamic modulus* ($|E^*|$)—the norm of the E^*, which is calculated by dividing the peak-to-peak stress by the peak-to-peak axial strain measured during the steady-state period.

3.8. *dynamic modulus ratio (DMR)*—the ratio between the dynamic modulus fingerprint and the dynamic modulus value from a master curve construction, both evaluated at the same temperature and frequency condition. This value is also used to characterize specimen-to-specimen variability.

3.9. *failure cycle* (N_f)—the cycle in which the measured phase angle drops sharply after a stable increase during cyclic loading.

3.10. *fatigue analysis coefficients* (K_1, K_2, K_3)—fitting coefficients to describe the classical stress (or strain) versus cycles to failure relationship.

3.11. *phase angle* (φ)—the angle, expressed in degrees, between an applied sinusoidal stress and the resulting sinusoidal strain measured during the steady-state period.

3.12. *pseudo strain* (ε_R)—a quantity that is similar to strain but does not include time effects. Pseudo strain is calculated by solving the convolution integral of the strain and $E(t)$.

3.13. *pseudo secant modulus* (C)—the secant modulus in stress–pseudo strain space.

3.14. *relaxation modulus* ($E(t)$)—the quotient of the stress response of a material with time to a constant step amplitude of strain.

4. SUMMARY OF METHOD

4.1. An actuator displacement-controlled and repeated cyclic loading is applied to a cylindrical asphalt concrete specimen until failure. The applied stress and on-specimen axial strain response are measured and used to calculate the necessary quantities. The relationship between the damage (S) and the pseudo secant modulus (C) is determined and expressed as the damage characteristic curve.

5. SIGNIFICANCE AND USE

5.1. The damage characteristic curve represents the fundamental relationship between damage and material integrity for asphalt concrete mixtures. This property is independent of temperature, frequency, and mode of loading. Combined with the linear viscoelastic properties of asphalt concrete, the damage characteristic curve can be used to analyze the fatigue characteristics of asphalt concrete mixtures.

5.2. Damage characteristic curves can also be combined with additional fatigue parameters and pavement response models to predict the fatigue behavior of in-service asphalt concrete mixtures.

6. APPARATUS

6.1. *Asphalt Mixture Performance Tester*—An AMPT or other system meeting or exceeding the requirements of Equipment Specifications for the Simple Performance Test System, NCHRP Report 629, Appendix E, with the additional capability to conduct direct tension testing, as shown in Figure 1.

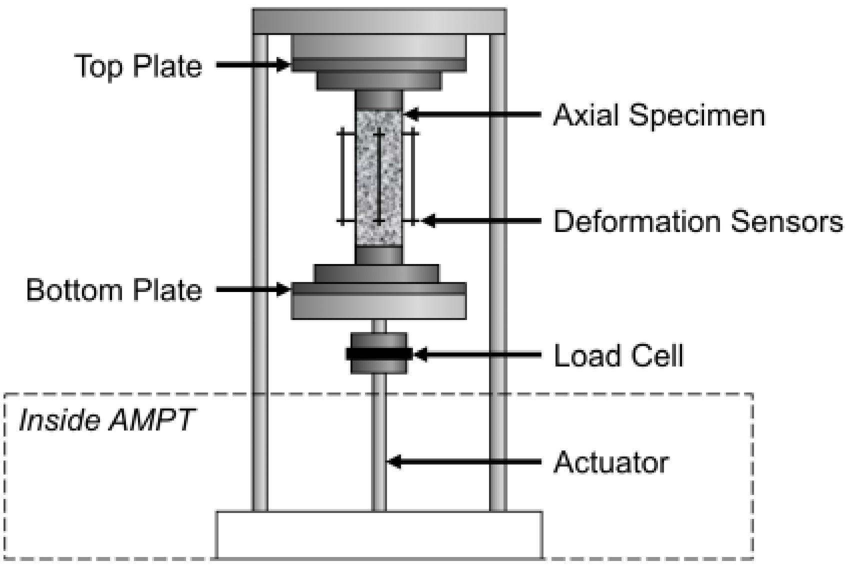

Figure 1—General Schematic of Direct Tension Test Setup

6.2. *External Conditioning Chamber (optional)*— An environmental chamber for conditioning the test specimens to the desired testing temperature. The chamber shall be capable of controlling the temperature of the specimen over a temperature range of 5 to 25°C (41 to 77°F) to within ±0.5°C (±1°F). The chamber shall be large enough to accommodate at least a single test specimen and a "dummy" specimen with a thermocouple or other calibrated temperature-measuring device mounted at the center for temperature verification.

6.3. *Loading Platens*—Are required above and below the specimen to transfer the load from the testing machine to the specimen. The diameter of the loading platens shall be 38±1 mm. These platens should be made of hardened or plated steel, or anodized high strength aluminum. Materials that have linear elastic modulus properties and hardness properties lower than that of 6061-T6 aluminum shall not be used. The face of each load platen shall be grooved to provide better adhesion between the glue and plate. The top loading platen shall be designed so that it can be mated to the test machine without inducing loading eccentricity.

6.4. *Ball Bearing (optional)* —Users may place a ball bearing between the platens and the top loading platform in an attempt to account for loading eccentricity. Extra care should be taken using the ball bearing because if the screws are not tightened evenly around then excessive tensile stresses will develop on one side of the specimen.

6.5. *End Plate Gluing Apparatus*—Should be available for gluing the end plates to the asphalt concrete specimen. The device should ensure that the end plates and specimen are all centered, that the two platens are held parallel, and that the specimen is standing perpendicular to the plates. The weight resting on the specimen during curing of the adhesive shall not exceed 0.02 kN (4.5 lb), otherwise it shall be possible to clamp or otherwise hold the gluing apparatus at a fixed height for a period of at least 4 h.

7. HAZARDS

7.1. Standard laboratory safety precautions must be observed when preparing and testing asphalt concrete specimens.

8. TESTING EQUIPMENT CALIBRATION

8.1. The guidelines provided in TP 79 shall be followed to ensure that the test equipment and on-specimen measurement devices are properly calibrated.

8.2. If any of the verifications yield data that do not comply with the accuracy specified, the problem shall be corrected prior to further testing.

8.3. The hydraulic machine shall be properly tuned in displacement control mode, to enable use of the strain selection guidance in this standard. In displacement control mode, the tuning shall be such that there is a sinusoidal actuator deformation shape and the actuator displacement returns close to the initial position on the first cycle, as this will ensure the cycles are uniform and the input strain closely matches the output strain. Consult the equipment manufacturer for guidance on the specific equipment. If the machine is not tuned properly, the strain selection guidance may need to be adjusted for the specific machine.

9. TEST SPECIMEN INSTRUMENTATION PROCEDURE

9.1. Test specimens, 38-mm diameter by 110-mm height, shall be fabricated in accordance with PP XX.

9.2. Attach the mounting studs for the axial sensors to the sides of the test specimen using epoxy cement. Take care to avoid placing mounting studs directly in-line with screw holes in the end plates, which will be used to attach the specimen to the testing machine. A spacing fixture may be used to facilitate the mounting of the axial deformation measuring hardware.

Note 1—Quick-setting steel putty, such as Devcon 10240, has been found to be satisfactory for attaching the studs.

9.3. Verify that the gauge length is 70 mm ± 1 mm, measured center to center of the gauge points.

9.4. Thoroughly clean all end plates by first heavily brushing the face of each platen using either a hand operated wire brush, sandpaper, or a wire brush attached to a standard electric drill. After cleaning the platen with the wire brush, wipe the surface clean of any dust by using a towel dipped in acetone or similar solvent.

9.5. Using the same towel, but with only a small amount of solvent, wipe the ends of the specimen clean of any residual dust.

9.6. Weigh out an appropriate amount of adhesive to adhere the end plates and specimen to one another. The gluing process will require approximately 5 minutes, so prepare an adhesive that is appropriate for this length of working time.

Note 2—Quick setting steel putty, such as Devcon 10240, has been found to be satisfactory for attaching the end plates, provided gluing can be completed within 5 minutes of blending.

Note 3—Approximately 6 grams of the Devcon 10240 has been found to be suitable for 38-mm diameter specimens.

9.7. Fill in any surface voids and pores in the top and bottom surfaces of the specimen with the adhesive.

9.8. Divide the remaining adhesive in half and spread evenly between the end plates, ensuring grooves are filled. Insert and secure the end plates into the gluing jig and gently place the specimen on top of the bottom end plate, as close as possible to the center. Engage the centering mechanism to center the specimen on the end plate. Lower the top plate into position, and secure if necessary. The final glue thickness should be approximately 1 mm (0.04 in.) thick. Allow the adhesive to reach its initial set before moving the specimen from the jig.

9.9. Remove the specimen from the gluing jig, taking special care to support the specimen from the bottom. Do not lift the specimen by the top end plate, so as not to put any tension stress on the specimen and adhesive.

Note 4— Users may attach mounting studs before or after the end plates, however the gluing jigs may require that the end plates and mounting studs are attached in a specific order.

9.10. Allow all adhesives to reach full cure before testing. Follow the manufacturer's recommendation to determine the time needed to reach full cure.

10. TEST INFORMATION

10.1. This test procedure is designed to first test the specimens, at a specific temperature and frequency in oscillation (cyclic) mode to obtain linear viscoelastic fingerprints and then at the desired frequency and temperature until failure.

10.2. A total of three tests need to be done at three different strain levels. This is sufficient for ranking of materials' sensitivity to fatigue damage. However, if pavement performance predictions are being done, a fourth test at a fourth strain level is strongly recommended. Guidance on selecting strain levels can be found in Appendix X1.

10.3. An appropriate testing temperature can be selected using Equation 1. The climatic Performance Grade (PG) for the location of interest at 98 percent reliability should be determined based on LTPPBind Version 3.1. The input depth in LTPPBind should be 20 mm and no traffic adjustment shall be used. For example, the testing temperature for the LTPPBind high temperature of 64°C and low temperature of –22°C is 18°C.

$$Test\ Temperature\ (°C) = \begin{cases} if\ \left(\frac{T_H+T_L}{2} - 3\right) \leq 21°C\ ,\ \left(\frac{T_H+T_L}{2} - 3\right) \\ otherwise,\ 21°C \end{cases} \qquad (1)$$

where:

T_H = High-temperature PG Grade from LTPPBind (ºC); and

T_L = Low-temperature PG Grade from LTPPBind (ºC), generally a negative number.

Note 5—This general temperature selection guidance may not be appropriate for all mixtures, such as mixtures from cold climates with recycled materials, which may need to be tested at a higher temperature than prescribed to account for the more brittle nature of mixtures with high recycled asphalt binder ratios. This brittleness is typically manifested through repeated end failures or a very low number of cycles to failure at a particular strain input.

11. PROCEDURE

11.1. *Test Setup:*

11.1.1. Spacers may be needed to compensate for the reduced size of the specimens. If so, attach the spacers to the machine according to the manufacturer's instructions.

11.1.2. If using a separate chamber to temperature-condition the specimens, continue to Section 11.1.3. If using the testing device to temperature-condition the specimens, skip to Section 11.1.5.

Note 6—Use of a separate chamber to temperature-condition specimens is advantageous only if the specimen can be secured to the testing machine quickly. Otherwise temperature conditioning in the machine may be more efficient.

11.1.3. Insert all specimens to be tested and the "dummy" specimen with the center-mounted temperature monitoring device into the external conditioning chamber, and start the temperature control of the testing machine.

11.1.4. Allow the test specimens to reach the specified testing temperature ±0.5°C (±1°F) by monitoring the temperature of the "dummy" specimen.

11.1.5. Insert the specimen into the testing machine, and tighten the specimen securely to the bottom support.

11.1.6. Bring the actuator into position and apply approximately 0.01 kN (2.2 lbs) of seating load. Quickly secure the upper loading platen, making sure not to overtighten any screws, which can shear the specimen.

Note 7—Feeler gauges may be placed between the specimen end plate and the top support of the testing machine to account for any small gaps. This is done at the user's discretion. Users should use the ball bearing for specimens which exhibit (after the seating load is applied) any gap between the specimen end plates and top support of the testing machine in excess of 1 mm (0.04 in.).

11.1.7. Reduce the load on the specimen to 0 kN ± 0.01 kN (0 lb ± 2 lb).

11.1.8. Attach the sensors to the specimen. Position the sensors in a location along its travel range where the elongation of the specimen as it undergoes damage will not exceed the range of the sensors, but the compression on the fingerprint can also be measured. This may not be the zero position; the exact position depends on the sensors.

11.1.9. Allow the specimen to reach the specified testing temperature ± 0.5°C (± 1°F). If the specimen is conditioned in a separate temperature-conditioning chamber and the steps presented in Sections 11.1.5 through 11.1.8 can be completed within 5 minutes, 30 minutes is enough to bring the specimen temperature back to the test temperature. If more than 5 minutes are needed, then calibrate the time for specific equipment. If temperature conditioning is done in the machine, calibrate this time by using a monitoring specimen alone in the machine chamber. To calibrate the conditioning time for testing without a monitoring specimen, record the temperature using a logger or other device with time to capture the equilibrium time needed for specimen to reach the appropriate temperature both before (i.e., conditioning) and after sensors (i.e., regaining temperature equilibrium before testing commences) are attached.

11.1.10. If the system does not automatically, adjust, balance, and zero the electronic measuring system.

11.2. *Dynamic Modulus Fingerprint Test:*

11.2.1. Input the required information for the dynamic modulus fingerprint test into the equipment control software. The fingerprint test shall be performed at the frequency of 10 Hz, at a target strain range of 50-75 microstrain, at the target test temperature, and in the tension-compression mode of loading.

Note 8—Some software may require input of an estimated dynamic modulus value to estimate the starting load amplitude. In this case, enter a value similar to the modulus obtained during frequency sweep testing (using TP XX) if available. If not available, enter a conservative value of dynamic modulus so that the initial load does not damage the specimen.

11.2.2. Start the fingerprint test. The machine shall calculate the load level necessary to achieve 50 to 75 microstrain using the results of these first few cycles and then apply this load level for 50 cycles. A minimum 50 data points per cycle shall be recorded using equipment control software.

11.2.3. Compute the dynamic modulus for the last five cycles according to the method recommended in T 342 or TP 79. If the peak-to-peak strain exceeds 150 microstrain, discard the specimen.

11.2.4. The specimen shall rest at a load of 0 kN ± 0.01 kN (0 lb ± 2 lb) for a minimum of 20 minutes following the fingerprint testing.

11.3. *Cyclic Fatigue Test:*

11.3.1. Perform a constant positive movement actuator oscillation (cyclic) fatigue experiment at a frequency of 10 Hz (e.g., a pull-pull actuator displacement test). Start the first cyclic fatigue test with the target peak-to-peak on-specimen strain amplitude of 300, 500, or 800 microstrain (ε_{os1}) based on the $|E^*|_{\text{fingerprint}}$ ranges in Table 3. For the first specimen, the target N_f shall be greater than 500 or the data shall be discarded.

Table 3—Target On-Specimen Strain Levels for the First Specimen

Case (units in MPa)	ε_{os1}
$\lvert E^*\rvert_{\text{fingerprint}} > 8{,}800$	300
$4{,}400 < \lvert E^*\rvert_{\text{fingerprint}} < 8{,}800$	500
$\lvert E^*\rvert_{\text{fingerprint}} < 4{,}400$	800

11.3.2. Stop the test when propagated micro-cracks form one clear macrocrack. This macrocrack can be visually seen on the specimen surface and will cause the specimen to break into two completely separate parts. If the macrocracks occur outside the on-specimen deformation sensors, the test data can only be used to construct the damage characteristic (C versus S) curve. However, for calculating other parameters such as G^R and N_f, a new specimen must be tested.

11.4. If the resultant number of cycles to failure of the first test (N_{f1}) is less than 500, the first test has to be discarded and redone with the target on-specimen peak-to-peak strain level (ε_{os1}) at the next lowest microstrain level in Table 3 (e.g., 300 microstrain instead of 500 microstrain). If the first specimen was done at 300 microstrain and failed before 500 cycles, discard the specimen and redo the testing at 250 microstrain. .

11.5. Repeat steps in Section 11.1 through 11.3 on the remaining two or more specimens. Recommended target on-specimen peak-to-peak strain levels in microstrain for the remaining tests can be found from Table X1.1 based on the resultant number of cycles to failure of the first test (N_{f1}).

12. CALCULATIONS

12.1. This section presents the equations used to calculate the pseudo strain, pseudo secant modulus, and damage parameter for the fatigue tests. All the calculations in this section can be automatically performed using a combination of the AMPT control software and the ALPHA-Fatigue software or the FlexMAT spreadsheet described in the FHWA PRS Report.

12.2. Determine the $E(t)$ Prony coefficients from the dynamic modulus and phase angle measured using TP XX and PP 61. It is assumed that the relaxation modulus can be represented by Equation 2.

$$E(t) = E_{\infty} + \sum_{m=1}^{N} E_m e^{-t/\rho_m} \qquad (2)$$

where:

$E(t)$ = relaxation modulus as a function of time, t, (kPa or psi);

E_{∞} = long-time equilibrium modulus, (kPa or psi);

E_m = modulus of Prony term number m, (kPa or psi);

ρ_m = relaxation time of Prony term m (s); and

N = number of Prony terms used.

12.3. Compute the storage modulus, E', for each temperature and frequency combination measured via Equation 3.

$$E' = |E^*| \times \cos\left(\frac{\theta \times \pi}{180}\right) \qquad (3)$$

where:

E' = storage modulus (kPa or psi);

$|E^*|$ = dynamic modulus determined via experiment (kPa or psi); and

θ = phase angle determined via experiment (degrees).

12.4. Because measured data contain some variability, a smoothing process is needed to obtain reliable coefficients. Optimizing the coefficients in Equation 4 and Equation 8 simultaneously.

$$\log\left(E'(\omega,T)\right) = \log\left(E'(\omega_R)\right) = \kappa + \frac{\log(\max E') - \kappa}{1 + e^{\delta + \gamma \log(\omega_R)}} \qquad (4)$$

where:

$E'(\omega,T)$ = storage modulus at a particular temperature and angular frequency (kPa or psi);

$E'(\omega_R)$ = storage modulus at a particular reduced angular frequency (kPa or psi);

ω_R = reduced angular frequency, Equation 7 (rad/s);

max E' = defined by Equation 5; and

κ, δ, γ = fitting coefficients.

$$\max E' = P_c\left[A\left(1-\frac{VMA}{100}\right)+B\left(\frac{VFA\ xVMA}{10{,}000}\right)\right]+\frac{1-P_c}{\left[\frac{\left(1-\frac{VMA}{100}\right)}{A}+\frac{VMA}{B(VFA)}\right]} \quad (5)$$

where:

P_c = defined in Equation 6 (kPa or psi);

VMA = voids in mineral aggregate, %;

VFA = voids filled with asphalt, %;

A = 4,200,000 for prediction in psi or 29,000,000 for prediction in kPa; and

B = 435,000 for prediction in psi or 3,000,000 for prediction in kPa.

$$P_c = \frac{\left(20+\frac{435{,}000(VFA)}{VMA}\right)^{0.58}}{650+\left(\frac{435{,}000(VFA)}{VMA}\right)^{0.58}} \quad (6)$$

$$\omega_R = \omega * a_T \quad (7)$$

where:

a_T = time–temperature shift factor at a given temperature, as shown in Equation 8.

$$a_T = 10^{\alpha_1\left(T^2-T_{ref}^2\right)+\alpha_2\left(T-T_{ref}\right)} \quad (8)$$

where:

T = temperature (°C or °F);

T_{ref} = reference temperature (°C or °F); and

α_1, α_2 = fitting coefficients.

12.5. Compute the total Storage modulus according to Equation 9.

$$E' = E_\infty + \sum_{m=1}^{N}\frac{E_m\omega_R^2\rho_m^2}{\omega_R^2\rho_m^2+1} \quad (9)$$

12.6. Compute the total Loss modulus according to Equation 10.

$$E'' = \sum_{m=1}^{N}\frac{E_m\omega_R\rho_m}{\omega_R^2\rho_m^2+1} \quad (10)$$

12.7. Compute the specimen-to-specimen normalization parameter using Equation 11 and denote this parameter as the DMR (Dynamic Modulus Ratio).

$$\mathrm{DMR} = \frac{|E^*|_{\text{fingerprint}}}{|E^*|_{LVE}} \quad (11)$$

where:

$|E^*|_{\text{fingerprint}}$ = dynamic modulus determined from Section 11. 16(kPa or psi) ;

$|E^*|_{LVE}$ = average representative dynamic modulus for the mixture of interest at the temperature and frequency of interest (kPa or psi), and computed by Equation 12; and

DMR = dynamic modulus ratio, which is the specimen variability compensation parameter.

$$|E^*|_{LVE} = \sqrt{\left[E_\infty + \sum_{m=1}^{N} \frac{E_m \omega_R^2 \rho_m^2}{\omega_R^2 \rho_m^2 + 1}\right]^2 + \left[\sum_{m=1}^{N} \frac{E_m \omega_R \rho_m}{\omega_R^2 \rho_m^2 + 1}\right]^2} \tag{12}$$

where:

ω = angular frequency used in the fingerprint experiment;

a_T = time–temperature shift factor for the fingerprint test temperature;

ω_R = reduced angular frequency, Equation 7, used in the fingerprint experiment; and

E_∞, E_m, ρ_m = Prony coefficient terms.

12.8. Separate the data into two parts. The first part, Dataset 1, comprises the data for the first half of the first loading path (from zero to first peak stress). The second part, Dataset 2, comprises the rest of the data.

12.9. For Dataset 1, average all sensor readings and compute the average strain for all data points.

12.10. Calculate the axial stress for each data point in Dataset 1.

12.11. Compute the reduced time for each data point in Dataset 1 using Equation 13.

$$t_R = \frac{t}{a_T} \tag{13}$$

where:

a_T = time–temperature shift factor at a given temperature;

t = time measured from the experiment (s), and

t_R = reduced time (s).

12.12. Compute the pseudo strain for each data point in Dataset 1 using the state variable formulation shown in Equation 13.

$$\varepsilon^{R(n+1)} = \frac{1}{E_R}\left[\eta_o^{n+1} + \sum_{m=1}^{N} \eta_m^{n+1}\right] \tag{14}$$

where:

$\varepsilon^{R(n+1)}$ = pseudo strain at the next time step;

E_R = reference modulus, a value of 1 should be chosen;

η = elastic component of the pseudo strain (Equation 15);

η_m = pseudo strain contribution of Prony element *m* (Equation 16);

n = time step used in the calculation;

ε	=	strain calculated for the current or subsequent time step;
Δt_R	=	duration of the reduced time step, t_R^{n+1}–t_R^{n}; and
t_R	=	reduced time.

$$\eta_0^{n+1} = E_\infty\left(\varepsilon^{n+1}\right) \tag{15}$$

$$\eta_m^{n+1} = e^{-\Delta t_R/\rho_m}\eta_m^{n} + E_m \times \rho_m\left(\frac{\varepsilon^{n+1}-\varepsilon^{n}}{\Delta t_R}\right)\left[1-e^{-\Delta t_R/\rho_m}\right]\ \eta_0^{n+1} = E_\infty\left(\varepsilon^{n+1}\right) \tag{16}$$

12.13. Compute the normalized pseudo secant modulus for each data point in Dataset 1 using Equation 17.

$$C = \frac{\sigma}{\varepsilon^R * DMR} \tag{17}$$

12.14. The continuum damage model power term, α, is related to the log-log slope of the relaxation modulus, $E(t)$. Its value is found numerically using the Prony series representation of the $E(t)$ in Equation 1. Determine m, the maximum value of the tangential slope of the relaxation modulus versus time relationship in log-log scale, and determine the α value using Equation 18.

$$\alpha = \frac{1}{m} + 1 \tag{18}$$

12.15. Compute the change in damage, ΔS, for each time step using Equation 19. Due to inherent electronic interference (data noise) during data acquisition, a few sequential data points may have positive ΔC values. A few of these spurious data points do not negatively affect the overall value of damage (S), but they do complicate the calculation. An efficient method that accounts for these spurious data points is the piecewise function shown in Equation 19.

$$\Delta S_i = \begin{cases} \left(-\frac{DMR}{2}\left(\varepsilon^R\right)^2\left(C_i - C_{i-1}\right)\right)^{\alpha/\alpha+1}\left(\Delta t_R\right)^{1/\alpha+1} & C_i \le C_{i-1} \\ 0 & C_i > C_{i-1} \end{cases} \tag{19}$$

where:

C_i	=	pseudo secant modulus at the current time step;
C_{i-1}	=	pseudo secant modulus at the previous time step;
Δt_R	=	change in the reduced time step; and
α	=	continuum damage power term related to material time dependence, Equation 18.

12.16. Determine the damage at each time step using Equation 20.

$$S_i = \sum_{i=1}^{N} \Delta S_i \tag{20}$$

where:

S_i = cumulative damage at the current time step; and

ΔS_i = incremental damage for all time steps to be summed from the initial time step, $i = 1$, to the current time step, N.

12.17. Define the damage at the final point in Dataset 1 as $S_{\text{Dataset 1}}$.

12.18. Compute the peak-to-peak strain for each sensor and each cycle in Dataset 2.

12.19. For each cycle in Dataset 2, average all sensor strains and denote this strain as the test peak-to-peak strain amplitude, ε_{pp}.

12.20. Compute the peak-to-peak stress for each cycle in Dataset 2.

12.21. Compute the phase angle for each sensor and average the values together for each cycle. Depending on the test equipment (e.g., an AMPT), phase angle may be automatically calculated per sensor and averaged.

12.22. Compute the peak-to-peak pseudo strain for each cycle in Dataset 2 using Equation 21.

$$\varepsilon_{pp}^{R} = \varepsilon_{pp} * |E^*|_{LVE} \tag{21}$$

where:

ε_{pp} = average peak-to-peak axial strain; and

ε^{R}_{pp} = peak-to-peak pseudo strain.

12.23. Compute the cyclic pseudo secant modulus for each cycle in Dataset 2 using Equation 22.

$$C^* = \frac{\sigma_{pp}}{\varepsilon_{pp}^{R} * DMR} \tag{22}$$

12.24. Compute the functional form factor, β, for each cycle in Dataset 2 using Equation 23.

$$\beta = \frac{F_{\text{peak}} + F_{\text{valley}}}{|F_{\text{peak}}| + |F_{\text{valley}}|} \tag{23}$$

where:

F_{peak} = peak axial force measured by the load transducer (kN or lb); and

F_{valley} = valley axial force measured by the load transducer (kN or lb).

12.25. Compute the tension amplitude pseudo strain for each cycle in Dataset 2 using Equation 24.

$$\varepsilon_{ta}^{R} = \frac{\beta + 1}{2} \varepsilon_{pp}^{R} \tag{24}$$

where:

ε^R_{ta} = tension amplitude pseudo strain.

12.26. Compute the time within a cycle when tensile loading begins, t_b, for each cycle in Dataset 2 by using Equation 25.

$$t_b = \frac{\cos^{-1}(\beta)}{62.83} \qquad (25)$$

12.27. Compute the time within a cycle when tensile loading ends, t_e, for each cycle in Dataset 2 by using Equation 26.

$$t_e = \frac{2\pi - \cos^{-1}(\beta)}{62.83} \qquad (26)$$

12.28. Compute the form adjustment factor for each cycle in Dataset 2 using Equation 27. Equation 27 should be solved for each cycle, but generally β does not change significantly after the first few cycles, and a constant value may be applied after this transient period. Values of K_1 have been tabulated for typical values of β and α in Table 4.

Table 4—Compiled K_1 Values for Typical Material and Test Conditions

	Alpha						
Beta	4.333	4.077	3.857	3.667	3.500	3.353	3.222
−0.5	0.277	0.285	0.293	0.300	0.306	0.312	0.318
0.0	0.263	0.271	0.278	0.285	0.291	0.297	0.302
0.2	0.256	0.264	0.271	0.277	0.284	0.289	0.295
0.4	0.248	0.256	0.262	0.269	0.275	0.280	0.286
0.6	0.238	0.245	0.252	0.258	0.264	0.269	0.274
0.8	0.225	0.231	0.238	0.243	0.249	0.254	0.259
1.0	0.189	0.195	0.200	0.205	0.209	0.214	0.218

$$K_1 = \frac{1}{t_e - t_b}\left[\left(\frac{1}{\beta+1}\right)^{2\alpha}\int_{t_b}^{t_e}\left(\beta - \cos(62.83 * t)\right)^{2\alpha} dt\right] \qquad (27)$$

Note 26—Equation 27 can be solved with sufficient accuracy using a suitable numerical technique with the number of time steps equal to 100.

12.29. Compute the average reduced time for each cycle in Dataset 2 using Equation 28.

$$t_R = \frac{1}{a_T}\left[\frac{N}{10}\right] \qquad (28)$$

where:

N = cycle number.

12.30. Compute the change in damage, ΔS, for each cycle in the Dataset 2 using Equation 29.

Note 27—Even with data reduction, a few sequential data points may have positive ΔC values. A few of these spurious data points do not negatively affect the overall value of S, but they do complicate the calculation. An efficient method that accounts for these spurious data points is to use the piecewise function shown in Equation 23.

$$\Delta S_n = \begin{cases} \left(-\frac{DMR}{2}\left(\varepsilon_{ta}^{R}\right)^2\left(C^*_n - C^*_{n-1}\right)\right)^{\alpha/\alpha+1}\left(\Delta t_R\right)^{1/\alpha+1}\left(K_1\right)^{1/\alpha+1} & C^*_n \le C^*_{n-1} \\ 0 & C^*_n > C^*_{n-1} \end{cases} \quad (29)$$

where:

C^*_n = the cyclic pseudo secant modulus at the current analysis cycle;

C^*_{n-1} = the cyclic pseudo secant modulus at the previous analysis cycle; and

Δt_R = the change in the average reduced time between analysis cycles.

12.31. Determine the damage at each analysis cycle using Equation 30.

$$S_n = S_{\text{dataset1}} + \sum_{n=1}^{N} \Delta S_n \quad (30)$$

where:

S_{Dataset1} = cumulative damage value at the end of Dataset 1;

S_n = cumulative damage at the current analysis cycle; and

ΔS_n = incremental damage for all analysis cycles to be summed from the initial analysis cycle step, n = 1, to the current time step, N.

12.32. Combine the damage and pseudo secant modulus from for each time step in the first cycle, Sections 12.13 and 12.16, with the cyclic pseudo secant moduli and damage values from Sections 12.23 and 12.31, into a single dataset.

12.33. Determine the damage characteristic relationship by fitting one of the following equations to the plot of the pseudo secant modulus and damage from all of the fatigue tests.

$$C = e^{aS^b} \text{ or} \quad (31)$$

$$C = 1 - yS^z \quad (32)$$

where:

a, b = the fitting coefficients for the exponential model; and

y, z = the fitting coefficients for the power model.

Note 28—The coefficients K_1, K_2, and K_3 can be fit using the N_f and ε_t for use in the AASHTOWare Pavement ME Design software with additional localized calibration coefficients. This can be calculated in the FlexMAT spreadsheet.

12.34. Determine the average released pseudo strain energy per cycle to aid in the fatigue assessment of the mixture.

$$W_C^R = \frac{1}{2}(\varepsilon_{ta}^R)_n^2(1 - C_n^*) \quad (33)$$

$$G^R = \frac{1}{2}\frac{\int_0^{N_f} W_C^R dN}{(N_f)^2} \qquad (34)$$

where:

W_C^R $\mathrm{W_C^R}$ = released pseudo strain energy per cycle;

G^R = average released pseudo strain energy per cycle; and

N_f = cycles to failure.

12.35. Using the data from all test specimens for the mixture, fit the G^R and N_f using the power law shown in Equation 35.

$$G^R = \gamma \cdot N_f^{\ \delta} \qquad (35)$$

where:

γ, δ = fitting parameters; and

N_f = cycles to failure.

13. REPORT

13.1. Report the following for each specimen tested:

13.1.1. Test temperature;

13.1.2. The fingerprint dynamic modulus, $|E^*|_{\text{fingerprint}}$;

13.1.3. DMR value;

13.1.4. The model term related to the log-log slope of the relaxation modulus master curve, α;

13.1.5. C versus S curve coefficients (a and b in Equation 31 or y and z in Equation 32); and

13.1.6. G^R and N_f for each test specimen.

14. KEYWORDS

14.1. AMPT; axial deformation; complex modulus; cyclic fatigue; damage characteristic curve; direct tension; DMR; dynamic modulus; failure cycle; fingerprint; modulus; phase angle; Prony coefficients; relaxation modulus; pseudo secant modulus; pseudo strain; specimen deformation; strain.

APPENDIXES

(Nonmandatory Information)

X1. PROCEDURE FOR ESTIMATING ON-SPECIMEN STRAIN LEVELS IN THE AMPT

X1.1. This appendix elaborates on the procedure for estimating strain levels for fatigue tests based upon the fingerprint dynamic modulus of the mixture, which is presented in Table 3. The approach is based on test performance from a large database of mixtures. This section is intended to provide guidance for selecting a programmed target on-specimen strain value for testing materials with unknown fatigue characteristics in the Asphalt Mixture Performance Tester (AMPT).

X1.2. Perform a fingerprint dynamic modulus test as prescribed in Section 11.3.

X1.3. Using the $|E^*|_{\text{fingerprint}}$, select the appropriate programmed target on-specimen strain level (ε_{os1}) for Specimen 1. Record the cycles to failure, N_f. Discard any specimens that do not fail between the gauge points.

X1.4. Based on the N_f for the first test specimen, use Table X1.1 to select a target on-specimen strain level for Specimens 2-4. Based on the database used to develop this approach, the mixture should lie on or between one of the families of curves in Table X1.1. Recall the intent of selecting different strain levels is to obtain a range of cycles to failure which are adequately spaced in log-log space for subsequent fatigue analyses. Due to the difficulty of obtaining specific N_f values, it is not possible to provide rigid guidance on strain selection processes. If this approach does not yield a sufficient range of N_f values, users are encouraged to adjust the strain inputs in increments of about 50 microstrain to achieve values in an acceptable range.

X1.5. As an example, Specimen A1 has a $|E^*|_{\text{fingerprint}}$ of 7,500 MPa. Using Table 3, the first specimen programmed actuator microstrain is 500 microstrain, which results in a N_f value of 4,900 cycles. The user could then use Table X6.1 and decide to test Specimen A2 at 450 microstrain to obtain an N_f around 10,000 cycles, Specimen A3 at about 550 microstrain to obtain an N_f of around 2,500 cycles, and Specimen A4 at around 600 microstrain to obtain an N_f of around 1,400 cycles. The values used in this example are underlined and italicized in Table X1.1.

X1.6. Table X6.1 was originally calibrated using $|E^*|$ values constructed from the master curve, such as in the PP 61 procedure. To simplify the strain selection process shown here, the values have been scaled to the fingerprint condition by using a DMR of 0.80. Users may choose to calibrate their own families of curves in a different fashion, but it is believed the $|E^*|_{\text{fingerprint}}$ is an easier approach for a testing laboratory.

X1.7. A family of curves is developed by plotting test data in the fashion shown in Figure X1.1. A power function is then fit to the data, which can be done in a spreadsheet application such as Microsoft Excel. The N_f can now be predicted based on the programmed actuator strain level.

X1.8. For users who wish to construct their own values for the first specimen target on-specimen strain level, a relationship between $|E^*|_{\text{fingerprint}}$ and N_f is developed. Typically, the mixtures with a higher $|E^*|_{\text{fingerprint}}$ will fail at a lower N_f value than mixtures with a lower $|E^*|_{\text{fingerprint}}$. Based on the correlation between $|E^*|_{\text{fingerprint}}$ and N_f, the user can identify ranges or categories of $|E^*|_{\text{fingerprint}}$ which best align with satisfactory performing and poorly performing materials.

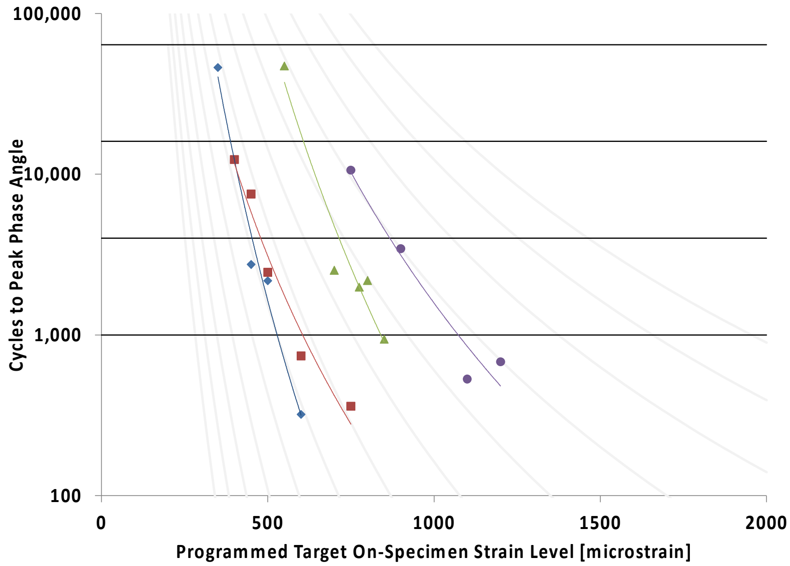

Figure X1.1-Example of Family of Curves Plot with Power Fit Trendlines to Predict Cycles to Failure

Table X1.1-Tool for Identifying Target On-Specimen Strain Levels for Second, Third, and Fourth Specimen of a Mixture Set.

Target On-Specimen Microstrain	$\|E^*\|_{fingerprint} \geq$ 8,800 MPa (ε_{os1} = 300 microstrain)				8,800 > $\|E^*\|_{fingerprint}$ > 4,400 MPa (ε_{os1} = 500 microstrain)					$\|E^*\|_{fingerprint}$ < 4,400 MPa (ε_{os1} = 800 microstrain)			
Estimated cycles to failure for test specimen													
200	62,500	129,000	258,700	503,800	-	-	-	-	-	-	-	-	-
250	4,200	11,000	27,200	64,500	145,900	315,000	-	-	-	-	-	-	-
300	**500**	**1,500**	**4,300**	**12,000**	31,500	77,500	180,000	-	-	-	-	-	-
350	-	-	900	2,900	8,600	23,700	60,800	144,800	-	-	-	-	-
400	-	-	-	850	2,800	8,500	23,700	61,000	144,500	-	-	-	-
450	-	-	-	-	1,000	3,400	*10,500*	28,500	71,400	163,500	-	-	-
500	**-**	**-**	**-**	**-**	**500**	**1,500**	***4,900***	**14,400**	**38,000**	91,000	-	-	-
550	-	-	-	-	-	750	*2,500*	7,800	21,500	53,500	119,600	-	-
600	-	-	-	-	-	-	*1,400*	4,400	12,800	33,000	75,850	155,700	-
650	-	-	-	-	-	-	800	2,600	7,900	21,000	49,900	104,600	-
700	-	-	-	-	-	-	-	1,600	5,100	14,000	33,900	72,400	136,400
750	-	-	-	-	-	-	-	1,000	3,400	9,500	23,600	51,400	98,000
800	**-**	**-**	**-**	**-**	**-**	**-**	**-**	700	2,300	**6,700**	**16,900**	**37,300**	**72,000**
850	-	-	-	-	-	-	-	-	1,600	4,800	12,300	27,600	53,900
900	-	-	-	-	-	-	-	-	1,200	3,500	9,100	20,800	41,000
950	-	-	-	-	-	-	-	-	800	2,600	6,900	15,900	31,600
1,000	-	-	-	-	-	-	-	-	-	1,900	5,300	12,300	24,700
1,050	-	-	-	-	-	-	-	-	-	1,500	4,100	9,700	19,600
1,100	-	-	-	-	-	-	-	-	-	1,100	3,200	7,700	15,700
1,150	-	-	-	-	-	-	-	-	-	900	2,500	6,200	12,700
1,200	-	-	-	-	-	-	-	-	-	-	2,000	5,000	10,300
1,250	-	-	-	-	-	-	-	-	-	-	1,600	4,100	8,500
1,300	-	-	-	-	-	-	-	-	-	-	1,300	3,300	7,000
1,350	-	-	-	-	-	-	-	-	-	-	1,100	2,800	5,900
1,400	-	-	-	-	-	-	-	-	-	-	900	2,300	4,900
1,450	-	-	-	-	-	-	-	-	-	-	750	2,000	4,200
1,500	-	-	-	-	-	-	-	-	-	-	-	1,700	3,600
1,550	-	-	-	-	-	-	-	-	-	-	-	1,400	3,000
1,600	-	-	-	-	-	-	-	-	-	-	-	1,200	2,600
1,650	-	-	-	-	-	-	-	-	-	-	-	1,000	2,300
1,700	-	-	-	-	-	-	-	-	-	-	-	900	2,000
1,750	-	-	-	-	-	-	-	-	-	-	-	750	1,700
1,800	-	-	-	-	-	-	-	-	-	-	-	-	1,500
1,850	-	-	-	-	-	-	-	-	-	-	-	-	1,300
1,900	-	-	-	-	-	-	-	-	-	-	-	-	1,150
1,950	-	-	-	-	-	-	-	-	-	-	-	-	1,000
2,000	-	-	-	-	-	-	-	-	-	-	-	-	900

APPENDIX D RESEARCH BRIEF

Program Steering Committee: NCHRP IDEA Program Committee

Month and Year: September 2017

Title: Development of Small Specimen Geometry for Asphalt Mixture Performance Testing

Project Number: N-181
Start Date: January 1, 2015
Completion Date: Month, Day, Year

Product Category:

Principal Investigator: Cassie Castorena, PhD Assistant Professor
E-Mail: cahintz@ncsu.edu

TITLE: Improving Asphalt Mixture Testing using Small Specimens

SUBHEAD: Investigation and optimization of small specimen geometries for dynamic modulus and cyclic fatigue asphalt mixture performance testing

WHAT WAS THE NEED?
Small specimen geometries have been gaining attention in recent years to enable the testing of as-built pavement layers. Performance testing of asphalt mixtures allows for evaluation of the material properties, which can be incorporated into pavement performance prediction models. The Asphalt Mixture Performance Tester (AMPT) was developed to allow for routine testing of asphalt mixtures using laboratory-fabricated cylindrical test specimens, 100 mm (4 in) diameter and 150 mm (6 in) tall. However, many pavement layers are less than 4 inches thick, which prevents forensic testing of as-built pavement layers. Several researchers have conducted preliminary studies evaluating various small specimen geometries, including 38 mm (1.5 in) and 50 mm (2 in) diameter cylinders and 25 mm by 50 mm (1 in by 2 in) prisms, with varying heights from 100 mm (4 in) to 140 mm (5.5 in). Although the initial trial results obtained from uniaxial small specimen testing are promising, further research was needed to more rigorously evaluate the effects of specimen geometry on the mechanical properties of asphalt concrete prior to the development of standard specifications for use in practice. While small specimens were initially developed to enable the testing of field cores, they also offer a significant opportunity to improve the efficiency of laboratory-fabricated specimen testing. Multiple small specimens can be extracted from a single laboratory-compacted sample. The smaller sample size also reduces the time required for thermal equilibration, which minimizes testing time and improves efficiency. However, there was a need to optimize the fabrication of small specimens from gyratory samples. In addition, the equipment used for small specimen preparation and testing by previous researchers was developed in house for their work, thus none was commercially available, limiting the use of the small specimen geometries.

WHAT WAS OUR GOAL?
The goal of this project was to rigorously evaluate 38-mm diameter cylindrical and the 25 mm by 50 mm prismatic small specimen geometries for AMPT dynamic modulus and cyclic fatigue performance testing to enable the development of standardized procedures.

WHAT DID WE DO?
This study developed the equipment necessary to enable small specimen testing in the AMPT and conducted an experimental program to inform the development standard procedures for small specimen testing of field cores and laboratory-fabricated samples. Initial experiments evaluated the effects of specimen geometry on dynamic modulus and fatigue results using five plant-produced mixtures. In addition, pavement structural analysis was conducted to assess the practical implications of material-level differences. These initial experiments identified the mixture and test conditions for which small specimen testing can provide representative results of bulk asphalt mixture behavior. Subsequent experiments evaluated the effect of small specimen coring direction on dynamic modulus and cyclic

fatigue testing results, which led to optimization of the procedure for the laboratory fabrication of small specimens. Dynamic modulus and cyclic fatigue testing was conducted to evaluate the specimen-to-specimen variability of small specimens prepared using the optimized procedure was evaluated using four plant-produced mixtures. In addition, the equipment needed for the preparation and testing of small specimens was developed with the assistance of IPC Global, Controls Group, Instrotek Inc., and the North Carolina State University Precision Machine Shop. Based on the equipment developed and experimental results, draft AASHTO standards for the preparation of small specimens, AMPT dynamic modulus testing of small specimens, and the AMPT cyclic fatigue testing of small specimens were developed. The draft standards and findings have been disseminated to the asphalt pavement community via presentations and workshops.

WHAT WAS THE OUTCOME?

The results demonstrate that small specimen geometries provide equivalent dynamic modulus and cyclic fatigue results to standard size specimens at the standard AMPT test temperatures. The horizontal extraction of small specimens from laboratory-compacted samples should be avoided because it leads to a peripheral air void gradient in the test specimens. The optimized laboratory fabrication procedure yields four small specimens per gyratory-compacted sample.

WHAT IS THE BENEFIT?

The small specimen fabrication and test procedures developed from this project will improve the efficiency of laboratory specimen fabrication, improve the efficiency of AMPT dynamic modulus and cyclic fatigue testing, and enable the AMPT testing of as-built pavement layers. Field core testing will enable performance based quality acceptance and forensic investigations of asphalt mixture properties of individual pavement layers throughout a pavement's service life.